Studies in Infrastructure and Control

Rabindra Nath Shaw
Nishad Mendis
Saad Mekhilef
Ankush Ghosh *Editors*

AI and IOT in Renewable Energy

Springer

Studies in Infrastructure and Control

The book series aims to publish top-quality state-of-the-art textbooks, research monographs, edited volumes and selected conference proceedings related to infrastructure, innovation, control, and related fields. Additionally, established and emerging applications related to applied areas like smart cities, internet of things, machine learning, artificial intelligence, etc., are developed and utilized in an effort to demonstrate recent innovations in infrastructure and the possible implications of control theory therein. The study also includes areas like transportation infrastructure, building infrastructure management and seismic vibration control, and also spans a gamut of areas from renewable energy infrastructure like solar parks, wind farms, biomass power plants and related technologies, to the associated policies and related innovations and control methodologies involved.

More information about this series at http://www.springer.com/series/16625

Rabindra Nath Shaw · Nishad Mendis ·
Saad Mekhilef · Ankush Ghosh
Editors

AI and IOT in Renewable Energy

Springer

Editors
Rabindra Nath Shaw
School of Electrical, Electronic
and Communication Engineering
Galgotias University
Greater Noida, Uttar Pradesh, India

Nishad Mendis
Senior Electrical Engineer
Wind, Solar and Energy Storage
DNV GL Docklands
Melbourne, VIC, Australia

Saad Mekhilef
Department of Electrical Engineering
University of Malaya
Kuala Lumpur, Malaysia

Ankush Ghosh
School of Engineering and Applied
Sciences
The Neotia University
Kolkata, West Bengal, India

ISSN 2730-6453 ISSN 2730-6461 (electronic)
Studies in Infrastructure and Control
ISBN 978-981-16-1010-3 ISBN 978-981-16-1011-0 (eBook)
https://doi.org/10.1007/978-981-16-1011-0

This Springer imprint is published by the registered company Springer Nature Singapore Pte Ltd.
The registered company address is: 152 Beach Road, #21-01/04 Gateway East, Singapore 189721, Singapore

Preface

This book presents the latest research on applications of artificial intelligence and the Internet of Things in renewable energy systems. Advanced renewable energy systems must necessarily involve the latest technologies like artificial intelligence and Internet of Things to develop low-cost, smart, and efficient solutions. Intelligence allows the system to optimize the power, thereby making it a power-efficient system; whereas, Internet of Things makes the system independent of wire and flexibility in operation. As a result, intelligent and IoT paradigms are finding increasing applications in the study of renewable energy systems. This book presents advanced applications of artificial intelligence and the Internet of Things in renewable energy systems development. It covers such topics as solar energy systems, electric vehicles, etc. In all these areas, applications of artificial intelligence methods such as artificial neural networks, genetic algorithms, fuzzy logic, and a combination of the above, called hybrid systems, are included. The book is intended for a wide audience ranging from the undergraduate level up to the research academic and industrial communities engaged in the study and performance prediction of renewable energy systems.

Greater Noida, India	Rabindra Nath Shaw
Melbourne, Australia	Nishad Mendis
Kuala Lumpur, Malaysia	Saad Mekhilef
Kolkata, India	Ankush Ghosh

Contents

Editors and Contributors

About the Editors

Rabindra Nath Shaw is a Senior Member of IEEE (USA), currently holding the post of Director, International Relations, Galgotias University India. He is an alumnus of the applied physics department, University of Calcutta, India. He has more than eleven years teaching experience in leading institutes like Motilal Nehru National Institute of Technology Allahabad, India, Jadavpur University and others in UG and PG level. He has successfully organised more than fifteen International conferences as Conference Chair, Publication Chair and Editor. He has published more than fifty Scopus/ WoS/ ISI indexed research papers in International Journals and conference Proceedings. He is the editor of several Springer and Elsevier books. His primary area of research is optimization algorithms and machine learning techniques for power systems, IoT Application, Renewable Energy, and power Electronics converters. He also worked as University Examination Coordinator, University MOOC's Coordinator, University Conference Coordinator and Faculty- In Charge, Centre of Excellence for Power Engineering and Clean Energy Integration.

Nishad Mendis is a Senior Engineer working in DNV. GL's Energy Advisory group in Melbourne, Australia. Before joining DNV GL, Nishad worked for Eltek as a Solutions Engineer working on the design of the implementation of energy storage-based applications, Alstom Grid as a Design and Commissioning Engineer for HV substations and Noratel as a transformer Design Engineer. Nishad has over 15 years of professional experience, including a Ph.D. from the University of Wollongong, Australia, and a Bachelor of Electrical Engineering with honors from the University of Moratuwa, Sri Lanka. Nishad also currently holds IEEE Senior membership and serves as Executive Board Member for the IEEE Industrial Application Society. Also, he is serving as an Honorary Fellow for the School of Electrical Engineering for Deakin University, Australia. He is experienced in engineering, project management, sales and tendering, research and development areas.

Saad Mekhilef is IET Fellow and IEEE Senior Member. He is Associate Editor of IEEE Transaction on Power Electronics and Journal of Power Electronics. He is Professor at the Department of Electrical Engineering, University of Malaya, since June 1999. He is currently Dean of the Faculty of Engineering and Director of Power Electronics and Renewable Energy Research Laboratory, PEARL. He is the author and the co-author of more than 400 publications in international journals and proceedings (253 ISI journal papers) and five books with more than 17000 citations and 64 H-index; 116 Ph.D. and master students have graduated under his supervision. He has six patents. He was frequently invited to give keynote lectures at international conferences. Prof. Saad listed by Thomson Reuters (Clarivate Analytics) as one of the Highly Cited (Hi Ci) engineering researchers in the world and included in the Thomson Reuters' The World's Most Influential Scientific Minds: 2018. He is actively involved in industrial consultancy for major corporations in the power electronics projects. His research interests include power conversion techniques, control of power converters, renewable energy and energy efficiency.

Ankush Ghosh is Associate Professor in the School of Engineering and Applied Sciences, The Neotia University, India and Visiting Faculty at Jadavpur University, Kolkata, India. He has more than 15 years of experience in Teaching, research as well as industry. He has outstanding research experiences and published more than 60 research papers in International Journal and Conferences. He was a research fellow of the Advanced Technology Cell- DRDO, Govt. of India. He was awarded National Scholarship by HRD, Govt. of India. He received his Ph.D. (Engg.) Degree from Jadavpur University, Kolkata, India in 2010. His UG and PG teaching assignments include Microprocessor and microcontroller, AI, IOT, Embedded and real time systems etc. He has delivered Invited lecture in a number of international seminars/conferences, refreshers courses, and FDPs. He has guided a large number of M.Tech and Ph.D. students. He is Editorial Board Member of seven International Journals.

Contributors

Sunil Agarwal Department of Electrical Engineering, Apex Institute of Engineering and Technology, Jaipur, India

Muhammad Naveed Akhter Power Electronics and Renewable Energy Research Laboratory (PEARL), Department of Electrical Engineering, Faculty of Engineering, University of Malaya, Kuala Lumpur, Malaysia;
Department of Electrical Engineering, Rachna College of Engineering and Technology (A Constituent College of University of Engineering and Technology Lahore), Gujranwala, Pakistan

Mandeep Singh Burdak Department of Electronics and Communication Engineering, G.B. Pant Government Engineering College, New Delhi, India

Debanjan Chatterjee Guru Nanak Institute of Technology, Sodepur, Kolkata, India

Rajeev Kumar Chauhan IMS Engineering College, Ghaziabad, Uttar Pradesh, India

Yogesh Kumar Chauhan Department of Electrical Engineering, Kamla Nehru Institute of Technology, Sultanpur, India

Poonam B. Dhabai Poornima University, Jaipur, India

Sakshi Gupta Department of Electrical Engineering, MNIT, Jaipur, India

Chetan Jain Department of Electrical Engineering, Apex Institute of Engineering and Technology, Jaipur, India

Kritika Khandelwal Department of Electrical Engineering, Apex Institute of Engineering and Technology, Jaipur, India

Anand Kishor School of Electrical, Electronics and Communication Engineering, Galgotias University, Greater Noida, India

Barnali Kundu Guru Nanak Institute of Technology, Sodepur, Kolkata, India

Ashok G. Matani Mechanical Engineering, Government College of Engineering, Amravati, MH, India

Gitanjali Mehta School of Electrical, Electronics and Communication Engineering, Galgotias University, Greater Noida, India

Saad Mekhilef Power Electronics and Renewable Energy Research Laboratory (PEARL), Department of Electrical Engineering, Faculty of Engineering, University of Malaya, Kuala Lumpur, Malaysia;
Center of Research Excellence in Renewable Energy and Power Systems, King Abdul-Aziz University, Jeddah, Saudi Arabia;
School of Software and Electrical Engineering, Swinburne University, Victoria, Australia

Hazlie Mokhlis Department of Electrical Engineering, Faculty of Engineering, University of Malaya, Kuala Lumpur, Malaysia

Munir Azam Muhammad Department of Electrical Engineering, Faculty of Engineering, University of Malaya, Kuala Lumpur, Malaysia

Swati Paliwal Department of Electrical and Electronics Engineering, Amity University, Noida, UP, India

Paras Patel School of Electrical, Electronics and Communication Engineering, Galgotias University, Greater Noida, India

Subharshi Roy Guru Nanak Institute of Technology, Sodepur, Kolkata, India

D. Saxena Department of Electrical Engineering, MNIT, Jaipur, India

Mukesh Kumar Shah Department of Electrical Engineering, MNIT, Jaipur, India

Manavi Shukla Department of Electronics and Communication Engineering, G.B. Pant Government Engineering College, New Delhi, India

Sanjay Kumar Sinha Department of Electrical and Electronics Engineering, Amity University, Noida, UP, India

Neeraj Tiwari Poornima University, Jaipur, India

Chapter 1
A Day-Ahead Power Output Forecasting of Three PV Systems Using Regression, Machine Learning and Deep Learning Techniques

Muhammad Naveed Akhter, Saad Mekhilef, Hazlie Mokhlis, and Munir Azam Muhammad

Abstract The forecasting of output solar power improves the quality, reliability and stability of power system. The aim of this research is day-ahead prediction of PV output power for 3 solar systems. The three PV systems are polycrystalline, monocrystalline and thin-film systems. A deep learning technique (RNN-LSTM) is proposed for day-ahead prediction of solar power output. The regression [GPR, GPR(PCA) and machine learning [SVR, SVR(PCA)] techniques are also developed. The forecasting accuracy is compared based on accuracy measurement parameters such as RMSE, MSE, correlation coefficient (R) and coefficient of determination (R^2). One-year data for 2016 is considered for analysis. 70% of data is utilized for training and 30% for validation and testing. It is found that deep learning technique has better forecasting accuracy than other developed techniques in terms of lower (RMSE, MSE) and higher (R, R^2), for day head forecasting of PV power output.

Keywords Deep learning · Forecasting · Day ahead · PV power output

---

M. N. Akhter · S. Mekhilef (✉)
Power Electronics and Renewable Energy Research Laboratory (PEARL), Department of Electrical Engineering, Faculty of Engineering, University of Malaya, 50603 Kuala Lumpur, Malaysia
e-mail: saad@um.edu.my

M. N. Akhter
Department of Electrical Engineering, Rachna College of Engineering and Technology (A Constituent College of University of Engineering and Technology Lahore), Gujranwala 52250, Pakistan

S. Mekhilef
Center of Research Excellence in Renewable Energy and Power Systems, King Abdul-Aziz University, Jeddah 21589, Saudi Arabia

School of Software and Electrical Engineering, Swinburne University, Victoria, Australia

H. Mokhlis · M. A. Muhammad
Department of Electrical Engineering, Faculty of Engineering, University of Malaya, 50603 Kuala Lumpur, Malaysia

R. N. Shaw et al. (eds.), *AI and IOT in Renewable Energy*,
Studies in Infrastructure and Control,
https://doi.org/10.1007/978-981-16-1011-0_1

1 Introduction

The demand for electrical energy has been increased due to world globalization and modernization. On the other hand, the prime fossil fuel sources of electrical energy are also being depleted from the earth [1]. Therefore, alternate sources of energy are under research for the past few decades. Among these alternate sources, PV sources have a major impact as renewable and sustainable energy sources. PV energy has benefits like low maintenance cost, more robust, enhanced lifespan, and fixed payback period [2].

The PV energy is utilized in both urban and rural areas for electrification [3, 4]. The installed PV capacity is enhanced from 2 GW in 2007 to 130 GW in 2019 [5]. Furthermore, it will be increased to 1700 GW by the end of 2030 according to report of International Energy Agency (IEA) [6]. Figure 1 describes the PV power output rise for the duration (2007–2019). The PV systems are mainly installed in China, Germany, the USA, and Japan.

The PV power output production is strictly dependent upon the climate factors such as humidity, wind speed, solar radiation and temperature. It has a strong correlation with solar radiation. Due to fluctuation in the weather, the solar radiation varies abruptly and alters the PV power output consequently. This variability output solar power affects the quality of power system. Therefore, forecasting of solar power output is necessary in order to maintain the power system's stability and reliability. Having the forecasted information, remedial measures are taken to maintain the power system stability.

Various forecasting techniques have been used for the prediction of PV power output such as regression, machine learning (SVM, ANN, ANFIS), physical, remote sensing and sky image methods [8–11]. Table 1 elaborates the benefits and drawbacks of these existing forecasting techniques.

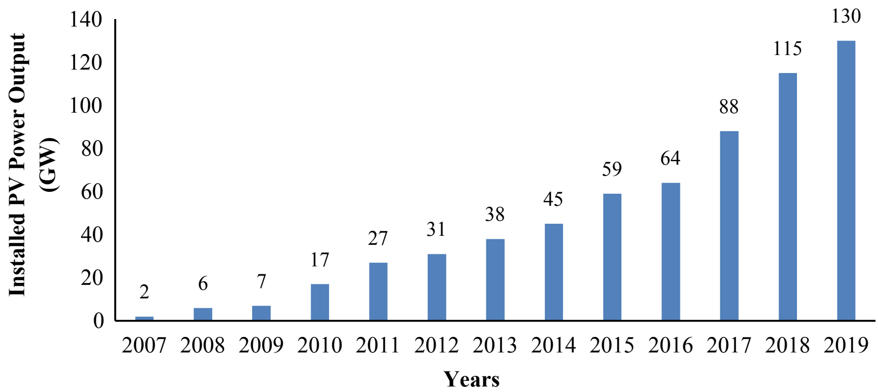

Fig. 1 PV power output rise from 2007 to 2019 [5, 7]

Table 1 Benefits and limitations of the existing forecasting techniques

Techniques	Benefits	Limitations
Persistence model [6]	Linear data	Nonlinear data
Statistical methods [6]	Linear data	Nonlinear data
ANN, ANFIS [12]	Nonlinear data	Random initial data, local minima, overfitting, and complex multilayered structure
SVM [13]	No local minima	Highly sensitive to kernel function, tube radius (ε) and penalty factor (C)
ELM [6]	Faster convergence	Random choice of input weights and hidden node biases
Physical methods (NWP) [14]	Medium-term forecast	Restriction on meteorological data from local departments
Remote sensing [15]	No need for ground sensors	Low-resolution satellite data
Sky images [15]	Very short-term prediction for future cloud patterns	Limited coverage from ground

To overcome the limitations of existing techniques, a deep learning technique (RNN-LSTM) is proposed. The forward pass of RNN is similar to MLP-ANN with a lone hidden layer, except the activations in hidden layer from the current inputs and preceding time steps. RNN has an issue of gradient vanishing. When weights are adjusted by backpropagation, the network is optimized in a negative direction. As a result, the network is not updated.

The objective of this study is to develop an LSTM-RNN technique for a day-ahead forecasting of PV power output for 2016 data. Secondly, a day-ahead prediction of power output is also performed annually using GPR, SVR, GPR (PCA), SVR (PCA). Finally, a comparative analysis is performed for all these techniques. The main contributions of the study are described as follows:

The contributions of this research are as follows:

(1) A (RNN-LSTM) method for day before prediction of PV power output of three different PV systems.
(2) The regression [GPR, GPR(PCA)] and machine learning [SVR, SVR(PCA)] techniques are also developed for a day-ahead prediction of PV power output.
(3) A comparative analysis of deep learning method is performed with the regression and machine learning techniques.

The remaining paper is structured as follows; Sect. 2 describes the site, data collection and methodology are described in Sect. 3. While results and discussions are presented in Sect. 4. The conclusions are summarized in Sect. 5.

Table 2 Description of different PV systems

PV system type	No of PV modules	Capacity of each module (W)	Total capacity (KW)
Polycrystalline	16	125	2
Monocrystalline	25	75	1.875
Thin-film	20	135	2.7
Combined system			6.575

2 Description of Site and Data Preprocessing

PEARL's grid-linked PV system was commissioned for use in October 2015. Table 2 describes the types of PV systems and their capacity. The results calculated in this study are based on data measured between January 2016 and December 2016. A 5-min data is recorded by a webserver. The solar irradiance, wind speed, ambient and PV module temperature are the four recorded parameters [16]. Data is divided into two segments, 70% for training and 30% for testing in order to compare all the applied techniques equally.

3 Methodology

3.1 Gaussian Process Regression

This is the nonparametric probabilistic model based on some kernel functions. It represents that the joint Gaussian distribution is followed by a finite set of values. GP model provides a way of indicating prior distributions over functions. For a training data set D, $= \{x_n, y_n\} for\, n = 1, 2, \ldots, N$, where the input is $x_n \in R^{dx}$ and output $y_n \in R$, the output in yn ∈ R. Suppose the observation model is

$$y = f(x) + \varepsilon \tag{1}$$

where f is the latent function and ε is Gaussian noise with zero mean and variance σ_n^2, i.e. $\varepsilon \sim N(0, \sigma_n^2)$. While y is the actual target value $y - \left[y_1 \ldots y_n\right]^T$ and x is the input features as $x - [x_1 \ldots x_n]^T$.

For the new sample X_{test}, prediction is the average of prediction results for all models

$$y_{\text{predicted}} = \frac{1}{P}\sum_{P=1}^{P} M_p(X_{\text{test}}) \tag{2}$$

where $M_p(X_{\text{test}})$ is the prediction result for new test data set.

3.2 Support Vector Regression (SVR)

It is used to enhance the generalization ability by minimizing the empirical risk and confidence interval using the hypothesis of structural risk minimization [17]. In addition to classification, SVM can also be applied for successfully for regression problems known as support vector regression (SVR).

The general mathematical function for SVM is given as

$$y = f(x) = \sum_{n=1}^{M} \propto_n . \varphi(x) = w\varphi(x) \tag{3}$$

where $\varphi(x)$ perform the nonlinear transformation and out is the linearly weighted sum of M. The decision function of SVM is described as

$$y = f(x) = \left\{ \sum_{n=1}^{N} \propto_n . k(x_n, x) \right\} - b \tag{4}$$

where k is kernel function. Proper choice of kernel function is necessary to make the data separable in feature space. While N, $\propto_n$ and b are the number of training data, objective function parameter and bias values, respectively.x and x_n are independent vector and vector used in the training.

3.3 Principal Component Analysis (PCA)

It transforms the group of correlated variables into small sets of variables that are not correlated and preserves most of the information of original data. The orthonormal transformation z can be used to transform w to new space y as follows:

$$Y = ZW \tag{5}$$

The Y matrix elements are derived from linear combination of W matrix elements, which translates the pattern of linkage between the samples. The Y covariance matrix is defined as:

$$C_Y = ZC_W Z^Y \tag{6}$$

C_W is the covariance of matrix W. The loading matrix Z can be found from the eigenvalue equation shown as

$$(C_Y - \lambda I)e_i = 0 \tag{7}$$

The corresponding eigenvalues will determine the magnitude of these principal components. Putting all the eigenvectors and eigenvalues in descending order, the covariance of the first principal component is maximum. It should be considered that there is no correlation between the resulting principal components, even though input variables are correlated due to the orthogonality of the decomposed eigenvectors [18].

3.4 *Deep Learning Technique (RNN-LSTM)*

In training of RNN both forward and backward passes are involved. The weights of RNN are adjusted by backward pass, known as backpropagation through time (BPPT). BPPT consists of frequent application of the chain rule like standard backpropagation.

The RNN has an important feature of using related mapping information between input and output. However, the range of context is limited for standard RNN architectures. The LSTM improves the accuracy of basic RNN model. The basic LSTM neuron is shown in Fig. 2. The subnets in LSTM-RNN are known as memory blocks. Three gates are there in each memory block, namely, input, output, and forget gates. These gates perform the operation of write, read and reset for memory cells. The input gate saves and transfers the information towards output on its activation. Then, the data is shifted to the next neuron on the activation of output gate. The forget gate deletes the information in memory cell on its activation. Therefore, the activation of these gates realizes the long short-term memory of input data sequence [19]. The

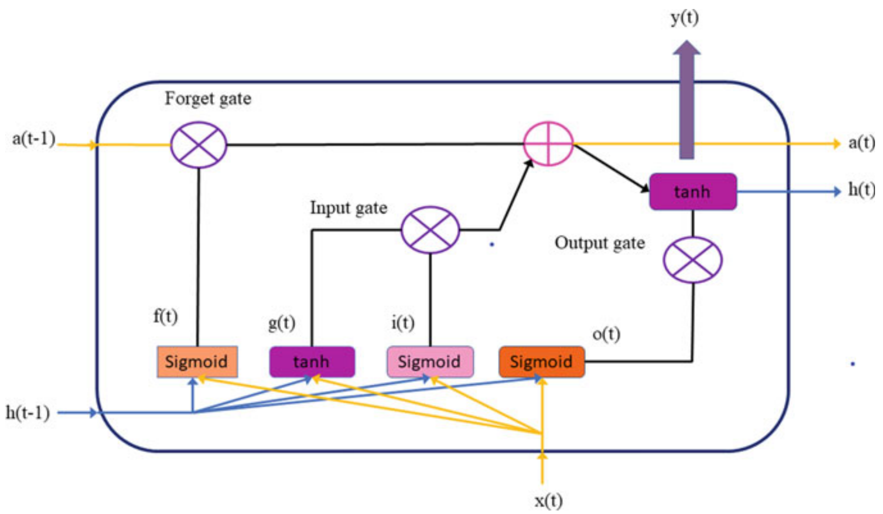

Fig. 2 LSTM-based neuron

training of LSTM neurons is also performed by forward and backward passes. The BPTT method is used for updating the neuron weight.

3.5 Performance Parameters to Measure Forecasting Accuracy

The parameters used for the evaluation of the prediction model are given as follows:

(a) Root mean square error (RMSE)

$$\mathrm{RMSE} = \sqrt{\frac{1}{N}\sum\nolimits_{i=1}^{N}(X-Y)^2} \tag{8}$$

(b) Mean square error (MSE)

$$\mathrm{MSE} = \frac{1}{N}\sum\nolimits_{i=1}^{N}(X-Y)^2 \tag{9}$$

(c) Correlation coefficient (r)

$$r = \frac{\sum_{i=1}^{N}\left[\left(X-X_{\mathrm{avg}}\right)*\left(Y-Y_{\mathrm{avg}}\right)\right]}{\sqrt{\sum_{i=1}^{N}(X-X_{\mathrm{avg}})^2 * \sum_{i=1}^{N}(Y-Y_{\mathrm{avg}})^2}} \tag{10}$$

(d) Coefficient of determination (R^2)

$$R^2 = 1 - \frac{\sum_{i=1}^{N}(X-Y)^2}{\sum_{i=1}^{N}(Y-Y_{\mathrm{avg}})^2} \tag{11}$$

4 Results and Discussion

Figure 3 describes the training RMSE and MSE values for day-ahead forecasting of power output for polycrystalline PV system in the year 2016. It is obvious from the figure that the deep learning technique (RNN-LSTM) has the lowest training RMSE and MSE values of 8.33 and 69.4, respectively, in comparison with other techniques. While GPR (PCA) is second to deep learning technique. In Fig. 4, DL(LSTM) has also performed better for day-ahead prediction of PV power output lowest testing RMSE and MSE of 23.09 and 532.94 as compared to other techniques.

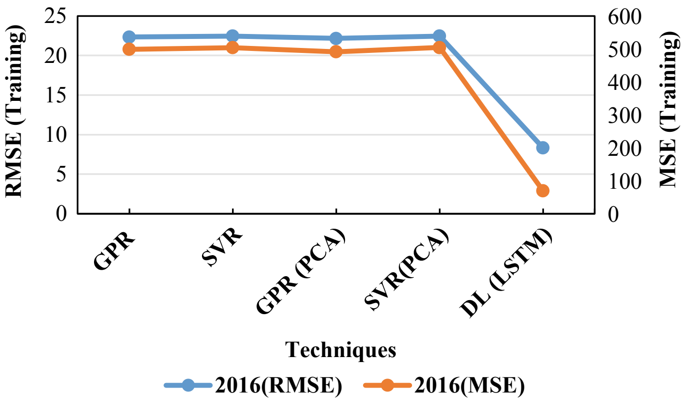

Fig. 3 Training RMSE and MSE for polycrystalline PV system for the year 2016

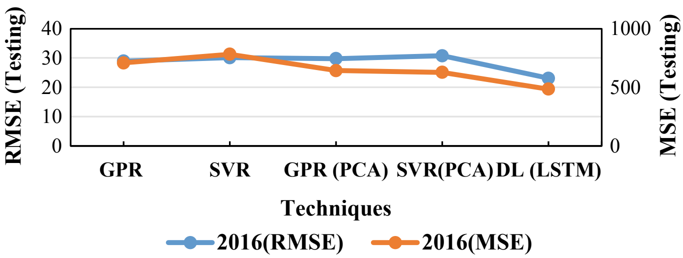

Fig. 4 Testing RMSE and MSE for polycrystalline PV system for the year 2016

Figure 5 describes the training RMSE and MSE for day-ahead prediction of Monocrystalline PV system power output for 2016 data. It is shown that the deep learning technique (RNN-LSTM) has the lowest training RMSE and MSE values of 3.27 and 10.66, respectively, in comparison with other techniques. While GPR is at the second position to deep learning technique with training RMSE and MSE of 19 and 360.7, respectively. In Fig. 6, GPR(PCA) has performed better than DL(LSTM)

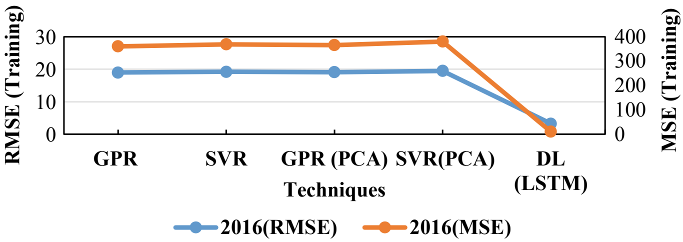

Fig. 5 Training RMSE and MSE for monocrystalline PV system for the year 2016

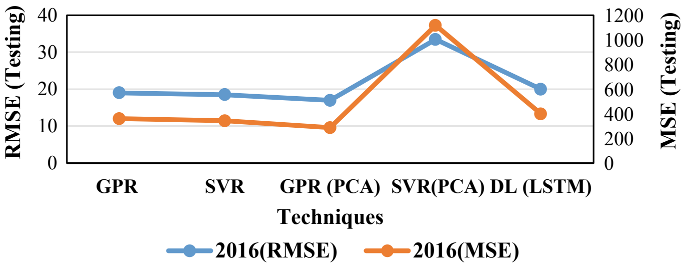

Fig. 6 Testing RMSE and MSE for monocrystalline PV system for the year 2016

with lowest testing RMSE and MSE of 16.94 and 287.12. However, the DL (LSTM) has RMSE and MSE values of 19.97 and 278.3, respectively.

Figure 7 describes the training RMSE and MSE values for day-ahead prediction of thin-film PV power output for the year 2016. It is obvious from the figure that the deep learning technique (RNN-LSTM) has the lowest training RMSE and MSE values of 3.58 and 12.84, respectively, in comparison with other techniques. While SVR (PCA) is second to deep learning technique with RMSE and MSE values of 23.5 and 552.5, respectively. In Fig. 8, DL(LSTM) has also performed better for day-ahead prediction of PV power output with the lowest testing RMSE and MSE of 22.014 and 484.6 as compared to other techniques.

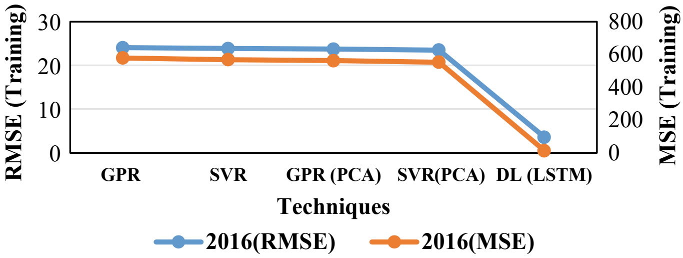

Fig. 7 Training RMSE and MSE for thin-film PV system for the year 2016

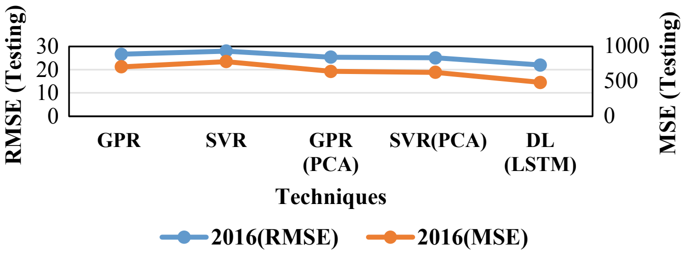

Fig. 8 Testing RMSE and MSE for thin-film PV system for the year 2016

Figure 9 describes the training R and R^2 values for day-ahead prediction of power output for polycrystalline PV system in the year 2016. It is obvious from the figure that the deep learning technique (RNN-LSTM) has the highest training R and R^2 values of 0.9976 and 0.9953, respectively, in comparison with other techniques. In Fig. 10, DL (LSTM) has also performed better for day-ahead forecasting of PV power output with highest testing R and R^2 of 0.9851 and 0.9704 as compared to other techniques.

Figure 11 describes the training R and R^2 values for day-ahead forecasting of power output for monocrystalline PV system in the year 2016. It is obvious from the figure that the deep learning technique (RNN-LSTM) has the highest training R and R^2 values of 0.9988 and 0.9977, respectively, in comparison with other techniques. In Fig. 12, GPR (PCA) has performed better for day–ahead prediction of PV power output with the highest testing R and R^2 values of 0.9763 and 0.9531 as compared to other techniques. However, DL (LSTM) has also a comparative performance with testing R and R^2 of 0.967 and 0.935, respectively.

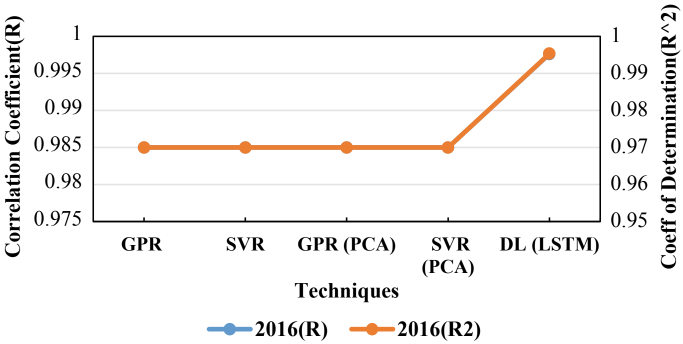

Fig. 9 Training R and R^2 for polycrystalline PV system for the year 2016

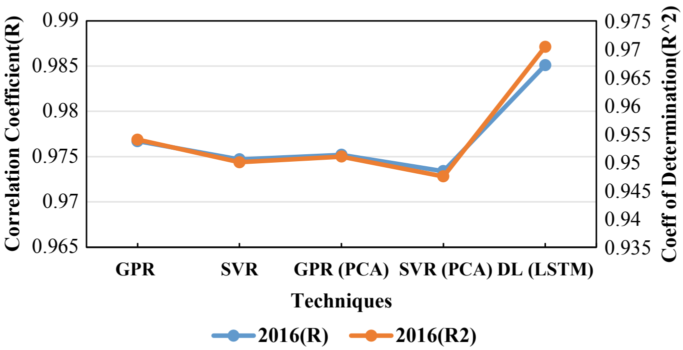

Fig. 10 Testing R and R^2 for polycrystalline PV system for the year 2016

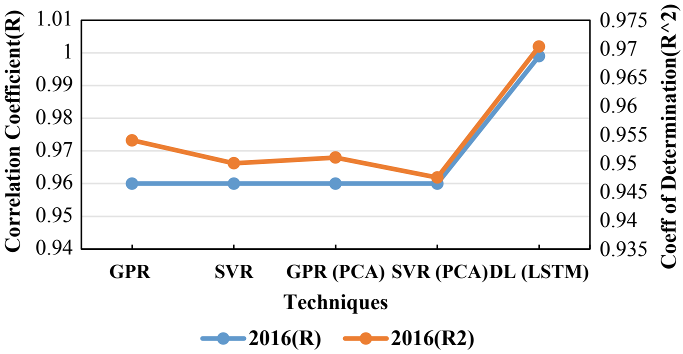

Fig. 11 Training R and R^2 for monocrystalline PV system for the year 2016

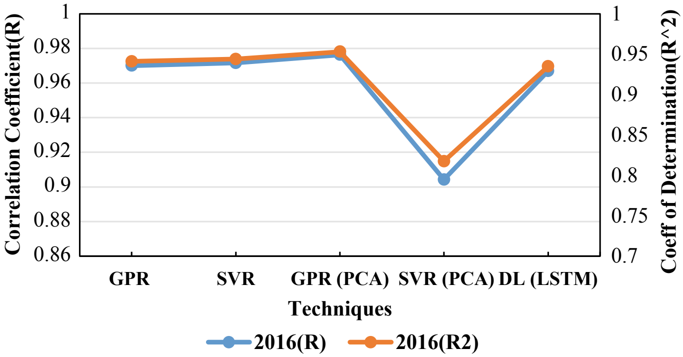

Fig. 12 Testing R and R^2 for monocrystalline PV system for the year 2016

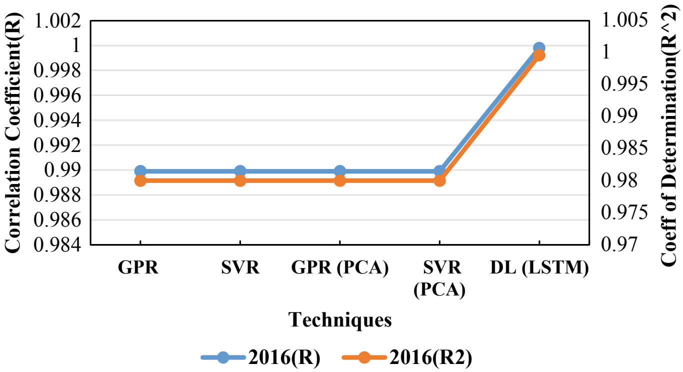

Fig. 13 Training R and R^2 for thin-film PV system for the year 2016

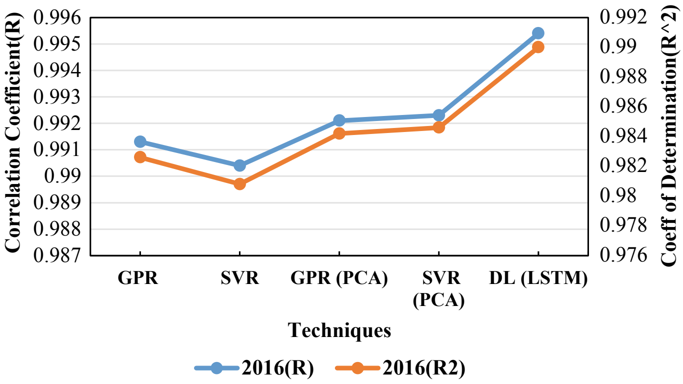

Fig. 14 Testing R and R^2 for thin-film PV system for the year 2016

Figure 13 describes the training R and R^2 values for day-ahead forecasting of power output for thin-film PV system in the year 2016. It is obvious from the figure that the deep learning technique (RNN-LSTM) has the highest training R and R^2 values of 0.9997 and 0.9996, respectively, in comparison with other techniques. In Fig. 14, DL (LSTM) has also performed better for day-ahead prediction of PV power output with higher testing R and R^2 values of 0.9940 and 0.9881 as compared to other techniques.

5 Conclusion

This research proposed a deep learning technique (RNN-LSTM) for a day-ahead forecast of output solar power for three different PV systems installed in the faculty of engineering, UM, Kuala Lumpur, in comparison with regression [GPR, GPR (PCA)] and machine learning [SVR, SVR (PCA)] techniques. The data for the year 2016 is considered to compare the forecasting results of these techniques. The considered performance parameters are RMSE, MSE, R, and R^2. For the training phase, 70% of data is used. While remaining 30% of data is used for the testing phase.

It is found that the DL (LSTM) has better prediction performance in terms of lowest (RMSE and MSE) and highest (R and R^2) for polycrystalline and monocrystalline PV systems compared with regression and machine learning methods. However, for monocrystalline PV system DL (LSTM) has comparative performance with GPR (PCA) for testing (RMSE and MSE) and with SVR (PCA) for testing (R and R^2).

Therefore, it is concluded that the deep learning technique (RNN-LSTM) is the best technique for day-ahead prediction of output solar power for three different systems. The forecasting performance can be evaluated for more than one-year data. The ANN and ANFIS methods can also be incorporated for future work.

Acknowledgements The authors would like to thank the Ministry of Higher Education, Malaysia under the Large Research Grant Scheme (LRGS): LRGS/1/2019/UKM/01/6/3 and the University of Malaya, Malaysia, for providing financial support under the research Grant RU-SATU Joint Research 2020: ST009-2020.

References

1. Akhter MN, Mekhilef S, Mokhlis H, Olatomiwa L, Muhammad MA (2020) Performance assessment of three grid-connected photovoltaic systems with combined capacity of 6.575 kWp in Malaysia. J Clean Prod 277:123242
2. Akhter MN, Mekhilef S, Mokhlis H, Shah PG (2019) Review on forecasting of photovoltaic power generation based on machine learning and metaheuristic techniques. IET Renew Power Gener 13(7):1009–1023
3. Halabi LM, Mekhilef S, Olatomiwa L, Hazelton J (2017) Performance analysis of hybrid PV/diesel/battery system using HOMER: a case study Sabah, Malaysia. Energy Convers Manage 144:322–339
4. Hossain M, Mekhilef S, Olatomiwa L (2017) Performance evaluation of a stand-alone PV-wind-diesel-battery hybrid system feasible for a large resort center in South China Sea, Malaysia. Sustain Cities Soc 28:358–366
5. Jäger-Waldau AJE (2020) Snapshot of photovoltaics—February 2020. Energies 13(4):930
6. Das UK et al (2018) Forecasting of photovoltaic power generation and model optimization: a review. Renew Sustain Energy Rev 81:912–928
7. Bugała A et al (2018) Short-term forecast of generation of electric energy in photovoltaic systems. Renew Sustain Energy Rev 81:306–312
8. Olatomiwa L, Mekhilef S, Shamshirband S, Petković D (2015) Adaptive neuro-fuzzy approach for solar radiation prediction in Nigeria. Renew Sustain Energy Rev 51:1784–1791
9. Olatomiwa L, Mekhilef S, Shamshirband S, Mohammadi K, Petković D, Sudheer C (2015) A support vector machine–firefly algorithm-based model for global solar radiation prediction. Sol Energy 115:632–644
10. Hossain M, Mekhilef S, Danesh M, Olatomiwa L, Shamshirband S (2017)Application of extreme learning machine for short term output power forecasting of three grid-connected PV systems. J Clean Prod 167:395–405
11. Halabi LM, Mekhilef S, Hossain MJAE (2018) Performance evaluation of hybrid adaptive neuro-fuzzy inference system models for predicting monthly global solar radiation. Appl Energy 213:247–261
12. De Giorgi M, Malvoni M, Congedo P (2016) Comparison of strategies for multi-step ahead photovoltaic power forecasting models based on hybrid group method of data handling networks and least square support vector machine. Energy 107:360–373
13. Wolff B, Kühnert J, Lorenz E, Kramer O, Heinemann D (2016) Comparing support vector regression for PV power forecasting to a physical modeling approach using measurement, numerical weather prediction, and cloud motion data. Sol Energy 135:197–208
14. Lima FJL, Martins FR, Pereira EB, Lorenz E, Heinemann D (2016) Forecast for surface solar irradiance at the Brazilian Northeastern region using NWP model and artificial neural networks. Renew Energy 87:807–818
15. Wang F et al. (2018)Image phase shift invariance based cloud motion displacement vector calculation method for ultra-short-term solar PV power forecasting. Energy Conv Manage 157:123–135
16. Halabi LM, Mekhilef SJE (2018) Performance analysis of multi-photovoltaic (PV)-grid tied plant in Malaysia. vol 164, no 1, p 012013.

17. Quej VH, Almorox J, Arnaldo JA, Saito L (2017) ANFIS, SVM and ANN soft-computing techniques to estimate daily global solar radiation in a warm sub-humid environment. J Atmos Solar Terr Phys 155:62–70
18. Adar M, Najih Y, Gouskir M, Chebak A, Mabrouki M, Bennouna A (2020)Three PV plants performance analysis using the principal component analysis method. Energy 207:118315
19. Wang F, Xuan Z, Zhen Z, Li K, Wang T, Shi M (2020)A day-ahead PV power forecasting method based on LSTM-RNN model and time correlation modification under partial daily pattern prediction framework. Energy Conv Manage 212:112766

Chapter 2
Internet of Things and Internet of Drones in the Renewable Energy Infrastructure Towards Energy Optimization

Ashok G. Matani

Abstract A significant growth in implementing various renewable energy systems is observed throughout the world. Variable renewable electricity (VRE) sources such as solar PV and wind power have gained attractive investments in many countries, resulting in rapid growth in the installed capacity of these green sources of energy. The contribution of these variable renewable electricity energy sources had produced around 8.7% of global electricity as compared to 27.3% of all renewable energy sources at the world level. Therefore, there is an urgent need to improve the power system flexibility as the progress of the integration of variable renewable electricity energy sources. International efforts to meet renewable energy deployment and energy efficiency measures are resulting in a safe and reliable manner of renewable energy, thereby, resulting in minimized environmental, climate impacts, air quality improvement, good public health, and increased jobs and economic growth, increased grid reliability as well as lower energy costs on a household, corporate and national levels, The joint efforts by various institutions, corporations, governments, and non-governmental organizations (NGOs) has resulted in enhancing world level energy efficiency highlighting the potential to significantly minimization of greenhouse gas emissions on the earth. This paper highlights the latest developments in implementing Internet of Things (IoT) GPS and GIS tools and applications in energy sector in various parts of the world.

Keywords Sensor-based technology and data science · Efficiency and automation of wind farms and solar fields · Remotely regulate and control tracking systems

1 Introduction

The practicality, applicability and flexibility of drones offer are widely acknowledged throughout the world, be it any field of application. Drones are now being used in the energy sector for various applications in both the generation and distribution side

A. G. Matani (✉)
Mechanical Engineering, Government College of Engineering, Amravati 444604, MH, India
e-mail: ashokgm333@rediffmail.com; dragmatani@gmail.com

R. N. Shaw et al. (eds.), *AI and IOT in Renewable Energy*,
Studies in Infrastructure and Control,
https://doi.org/10.1007/978-981-16-1011-0_2

of the sector. Reference [1] Major areas where drones can be employed include, but are not limited to.

1. Power plant mapping and inspection,
2. Corridor Mapping,
3. Corona Detection,
4. Substation Static Line Inspection,
5. Intermittent Power [2].

Timeline of drones and exploration of drone-based applications.

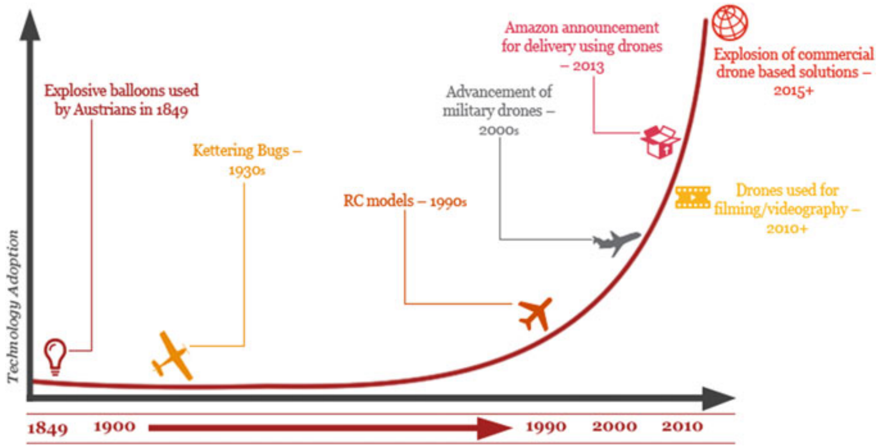

2 Latest Emerging Innovative Trends in Renewable Energy

2.1 Optimizing Offshore Wind in the U.S.

Wind turbines are commissioned on ocean vistas in Northern Europe. A major offshore wind farm in the Netherlands is providing power to one million households. The United States is planning to optimize the incredible potential of offshore wind. Several states along the Eastern Seaboard have projects in the works, including Virginia, New York, Rhode Island and New Jersey. Atlantic Shores wind farm financed by the oil and gas company Royal Dutch Shell is planning to provide power to about one million homes [3].

2.2 More Number of Electric Vehicles Running on Roads

More and more electric vehicles (EVs) have been appearing on the roads in recent years. According to estimates, there were only around 17,000 electric cars globally in 2010. In 2020 more than over seven million EVs are being sold every day. The new models "tidal wave" of new EV models, including the Rivian truck, Ford's electric Mustang, an affordable Volkswagen and Volvo's electric SUV [4].

2.3 Utilities and Corporations Investing in Solar Energy at Record Levels

Despite the upheaval caused by the COVID-19 pandemic, large-scale solar installations have not been much affected. According to a new report, solar installations are expected to grow by 43 percent in the year 2021 and are expected to install a total of 19 Gigawatts—for providing power to nearly four million homes. In addition to activity from utilities, corporations continue to invest in clean energy sources at record levels. With Amazon's latest investments in 26 solar and wind projects, the company is now investing in 6.5 Gigawatts of renewable energy for providing power to about 1.7 million homes for a year and has surpassed Google as the largest corporate buyer of renewable [5].

2.4 Energy Efficiency Encouragement from Governments

Energy efficiency is an essential part of creating a clean energy economy—it saves money, increases comfort and improves air quality. The energy plan includes a considerable focus on energy efficiency. The plan looks to upgrade and weatherize millions of homes and businesses and incentivize efficient-appliance manufacturing. According to a report, consumers and businesses could save more than $1 trillion on utility bills through 2050 when the new efficiency standards for many types of appliances and products will be implemented [6].

2.5 Energy Storage Becoming a Significant Part of the Power Grid

Energy storage, namely, battery storage is increasingly utilized homes, businesses and power grid at record levels as prices for these technologies continue to drop. A new report found that the cost of lithium-ion battery storage has reduced from $1,200 per kilowatt-hour in 2010 to just $137 per kilowatt-hour in the year 2020.

Table 1 Renewable energy capacity (GW)—for the year 2018

	BRICS	EU-28	China	US	Germany	India	Japan	UK	World total
Geotechnical power	0.1	0.9	0.0	2.5	0.0	0.0	0.5	0.0	13.3
Bio power	44	42	17.8	16.2	8.4	10.2	4.0	7.7	130
Hydro power	519	130	322	80	5.6	45	22	1.9	1132
Solar power	214	115	176	62	45	33	56	13	505
Ocean power	0.0	0.0	0.2	0.0	0.0	0.0	0.0	0.0	0.5
Wind power	262	179	210	96	59	35	3.7	21	591
Concentrating solar thermal power	0.8	2.3	0.2	1.7	0.0	0.2	0.0	0.0	5.5
Total renewable energy capacity	1040	469	727	250	119	124	86	44	2378
Per capita capacity	0.2	0.7	0.3	0.6	1.4	0.05	0.5	0.6	0.2

**BRICS countries include Brazil, Russian Federation, India, China, South Africa

Energy storage is essential for increasing the amount of clean energy on the grid, and it has proven to save utilities and consumers money, while preventing blackouts. A massive Tesla battery in Australia has already saved more than $100 million in two years, and U.S. power companies are implementing the same [7] (Tables 1 and 2).

3 IoT Applications Areas in Renewable Energy

3.1 Automation to Improve Overall Production

Solar and wind energy are the most popular renewable energy sources due to their abundance availability and reliability as compared to any other renewable energy sources. In 2019, Germany sufficed a quarter of its energy demands from its windmill farms. The cost associated with energy production through these resources has also decreased significantly. From the year 1977 onwards, the cost of solar panels has reduced by 99%. Japan, Germany and China are the global leaders in using solar energy [8].

The assimilation of Artificial Intelligence (AI) and Internet of Things (IoT) systems along with sensors in solar and wind energy systems application had increased their reliability. In order to maximize energy production, most of the solar panels use dual-axis trackers. These tracking systems calibrate the angle of solar panels and assist to receive the maximum solar radiation throughout the day [9].

Table 2 Comparison of renewable energy indicators in 2018 and 2019

		Year 2019	Year 2018
INVESTMENT [in billion USD]			
Annual value of investment in renewable power and fuels	billion USD	301.7	296.0
POWER [in GigaWatts]			
Capacity of renewable energy (including hydropower)	GigaWatts	2,588	2,387
Capacity of renewable energy (excluding hydropower)	GigaWatts	1,437	1,252
Capacity of hydropower	GigaWatts	1,150	1,135
Capacity of wind power	GigaWatts	651	591
Capacity of solar PV	GigaWatts	627	512
Capacity of bio power	GigaWatts	139	131
Capacity of geothermal power	GigaWatts	13.9	13.2
Capacity of concentrating solar thermal power (CSP)	GigaWatts	6.2	5.6
Capacity of ocean power	GigaWatts	0.5	0.5
HEAT			
Approximated modern bio heat demand	Exajoules (EJ)	14.1	13.9
Approximated solar hot water demand	Exajoules EJ	1.4	1.4
Approximated geothermal direct-use heat demand	Petajoules (PJ)	421	384
TRANSPORT			
Annual ethanol production	billion liters	114	111
Annual fatty acid methyl esters (FAME) biodiesel production	billion liters	47	41
Annual hydrotreated vegetable oil (HVO) biodiesel production	billion liters	6.5	6.0

Artificial Intelligence (AI) and Internet of Things (IoT) systems can be used to remotely regulate and control these tracking systems to ensure maximum energy production efficiency. By using analytics solutions, the movement of the sun and solar radiation is tracked which is used to automatically adjust the angle of solar panels. Also, Artificial Intelligence (AI) and Internet of Things (IoT) systems in wind energy systems are used to monitor operating parameters affecting power generation [10].

3.2 Smart Grids for Elevated Renewable Implementation

The growth of renewable energy is restricted due to less reliability of transmission and distribution systems. The traditional energy grids were built to support the one-way transmission of uniform energy from power plants and bill the customers once a month. Hence nowadays these grids are not applied to support the varying electricity supply from renewable sources. Artificial Intelligence (AI) and Internet of Things (IoT) systems have enabled the creation of smart grids supporting manual switching between renewable and long-established power plants to ensure an uninterrupted power supply. This switching in smart grids is supporting the varying nature of renewable energy and facilitates non-stop energy supply to the consumers [11].

3.3 IoT Increasing the Adoption of Renewable Systems

The development of smart grids through Artificial Intelligence (AI) and Internet of Things (IoT) systems has escalated the growth of renewable energy sources. Because they offer benefits of power consumption monitoring and real-time alerting which allows energy utilities to include renewable sources for energy distribution [12].

3.4 Contribution from End Consumers

Even the end consumers are now utilizing renewable energy sources to reduce their electricity bills and become self-dependent. Many countries and India are providing solar subsidies to citizens to increase the adoption of renewable energy systems. Countries are assisting the renewable energy users to develop solar stations on their rooftop and use them for personal electricity needs. Moreover, consumers can also discharge the excess electricity into the smart grids in exchange for money. This is helping countries to increase the overall adoption of renewables and create a greener environment for citizens to live in [13].

3.5 Balancing Supply and Demand

Smart grids allow energy utilities to provide consumers with a consistent power supply. The integration of Artificial Intelligence (AI) and Internet of Things (IoT) systems in renewable energy assists the energy suppliers to accommodate electricity from renewable sources and suffice the end-consumer demands. The use of smart energy meters on a commercial level gives real-time consumption data to electricity suppliers [14]. By using analytics and data processing solutions, they can also develop trends and patterns related to peak load conditions. Therefore, by using manual switching techniques, energy utilities have reduced the use of power plants during normal off-peak timings and run them when the electricity demand is extreme, resulting in synchronizing the demand and supply conditions in addition to reducing the emission limits of toxic substances in the environment [15].

3.6 Cost-Effectiveness

As per estimates, the global energy demands can be fulfilled by harnessing 1.2% of solar energy from the Sahara desert (around 110,400 km^2) thereby reducing losses linked with the transmission and distribution of electricity from such a remote location. Power losses in transmission lines can reach up to 10% for long distances thereby creating complications and challenges which are preventing the escalated growth of solar and renewable energy as a whole. Moreover, the implementation of Artificial Intelligence (AI) and Internet of Things (IoT) systems in solar energy will also reduce the cost of building and managing solar stations significantly [16]. Real-time monitoring and predictive analytics features of Artificial Intelligence (AI) and Internet of Things (IoT) systems are used to monitor parameters that can reduce the efficiency of the power station or result in unexpected breakdowns. Hence, utilities can cut some costs related to inspection and repairs; and improve their efficiency [17].

4 Significant Role of Big Data Analytics in the Renewable Energy Sector

Data analytics and machine learning are assisting in data-driven decisions-making for predicting of weather conditions and weather forecasting, maintaining the supply chain, improving productivity, increasing affordability as well as fulfilling various shortcomings in the energy sector infrastructure. This has resulted in implementation of these intelligent technical interventions and technologies has resulted in the modernization of the energy sector [18].

4.1 Data Forecasting

Predictive analytics is the primary requirement of the energy sector for data forecasting. Hence, upgrading predictive analysis methods are assisting in the reduction of costs, conserve energy, offering adaptability to changing conditions, and improving final user experience is to be performed immediately towards enhancing forecasting of power. The cost of mismanagement and errors in the renewable energy industry is marginal and in this situation, forecasting helps to avoid that and accurately predicts changes in demand, overloads, and potential failure of systems [19].

4.2 Efficient Resource Management

Optimum utilization and resources management of available energy infrastructure is considered significant for the energy and power sector. By implementing data analytics and predictive mechanisms, renewable energy suppliers are preparing demand schedules before actual dates, predicting problems at the initial level, dispatching energy resources comparatively in good situation and conserving saving resources to the best possible levels resulting in low energy utilization and energy tariffs bills for customers [20].

4.3 Intelligent Storage of Resources

There is an emerging need to conserve and store renewable energy. Therefore, new capacity addition and new management systems are of significant importance and big data and analytics assist in efficient renewable energy storage towards optimizing energy storage [21].

4.4 Improving Safety and Reliability

By implementing data analytics and big data tools, it is possible to achieve improved safety, efficiency and reliability to estimate usage patterns, identify energy leakage and the health of the energy infrastructure systems.

4.5 Predicting Transformer Breakdowns and Prevention

Mismanagement of energy is very much hazardous and uneconomical. Artificial Intelligence (AI) predicts system overloads and gives awareness to users about potential transformer breakdowns. Hence, it is essential to implement data intelligence to forecast and prevent deadly disasters so that energy systems infrastructure is protected [22].

5 Maharashtra Using Drones in EHV Power Transmission Lines and Towers

Maharashtra in India has become the first state to use drones for aerial surveillance and inspection of extra-high voltage (EHV) power transmission lines and towers to reduce risk to staff, slash maintenance costs and minimize losses from outages. The Union Ministry of Home Affairs and the Director-General of Civil Aviation have permitted the Maharashtra State Electricity Transmission Company Ltd. (MSETCL) to utilize drones to inspect faulty lines, reducing the risk posed to operating staff of MSETCL [23, 24]. Up till now, workers are using ladders and chairs to inspect transformers which are very risky in the hilly areas of the State. Maharashtra State Electricity Transmission Company Ltd., is planning to provide a drone equipped with ultra HD cameras to capture high-resolution close-up photographs and videos of EHV lines and towers in each zone. This will allow a better assessment of faults. In addition to zonal offices, the head office in Mumbai will be monitoring the drones to guide engineers and operators in case of any failure and guidance required. The proposed drones will assist in slashing maintenance costs and reducing various losses from outages. These drones have the potential to revolutionize the inspection of power lines and transmission towers. It will also allow aerial surveillance, which is more efficient than manually surveying power lines. Drones will also help to detect defects at the incipient stage. The Maharashtra State Electricity Distribution Company Limited (MSEDCL) is planning for the electrification of remote and inaccessible tribal areas in Melghat and Gadchiroli of Maharashtra, which presently do not have electricity due to geographical hurdles due to forest clearances [25].

6 Long-Distance Drones Used for Surveillance to Avoid Network Failures

Energy generating and transmission companies in Europe and other developed economies are utilizing drones used for surveillance of long-distance grids for identification of damage and leaks to avoid network failures to avoid losses of billions of dollars being incurred per year. Italy's Snam, one of the biggest gas utilities in Europe, is utilizing BVLOS drones in the Apennine hills around Genoa for scouting a 20 km stretch of the pipeline because they fly beyond the visual line of sight of operators. France's RTE—a subsidiary of Snam and EDF's network has tested prototypes of long-distance drones which are flying at low altitudes over pipelines and power lines. The company also tested a long-distance drone inspecting 50 km range of transmission lines and sent data to virtually model a section of the grid. For the coming two years, in drone technology, the company has planned a budget for investing 4.8 million Euros ($5.6 million). France's RTE—a subsidiary of Snam and EDF's network has recently tested prototypes of long-distance drones flying at low altitudes for surveillance of pipelines and power lines [26].

According to Navigant Research reports, various power grid companies are planning to spend from about $2 billion in the year 2020 to more than $13 billion/year on drones and robotics by 2026 globally. At present due to network failures and forced shutdowns, the energy sector incurs a loss of about $170 billion every year. For controlling these losses, flying robots traveling dozens of kilometers without stopping are now utilized by power companies. New advanced technology drones which are 100 times faster than manual measurement, more accurate than helicopters and with artificial intelligence devices on board are now utilized by renewable energy companies in various sectors to monitor and link solar and wind parks to grids [27].

7 Conclusions

Considering continuous exposure to weather, moisture intrusion and dust, solar panels are easily damaged and hence their efficiency is affected. With programmed waypoints, drone surveys are performed and replicated to pinpoint damage and provide operators with up-to-date imagery of damage, cracks or shading. A drone easily detects damage on a solar panel, monitors the panel's efficiency also. With an infrared camera, defects and temperature imbalances on solar panels are identified to allow operators to quickly order repairs, and keep operations running at maximum efficiency. Therefore, drone surveys are a fast and economical way for regular maintenance, and maintaining solar farms functioning at optimal efficiency. A drone also conducts a complete thermal inspection by using an IR camera to identify sub-module hotspots that manual inspections did not consider. Drone data is uploaded into an interactive, online web map and sent to a Smartphone App for use by maintenance and repair personnel in the field.

Considering mergers and rapid advancement in radio communication and smartphone technologies, consumer and commercial drones have grown at an exponential rate. Radio communication assists in governing the aircraft movement, and smartphones had resulted in steep minimization of the prices of various equipment such as chips, microcontrollers, cameras, accelerometers and other sensors. These have resulted in capturing of data with better computing capabilities. Data analytics and machine learning assist in making data-driven decisions for predicting weather conditions, increasing affordability and improving shortcomings maintaining the supply chain, thereby enhancing productivity.

References

1. Woldeyohannes AD, Woldemichael DE, Baheta AT (2016) Sustainable renewable energy resources utilization in rural areas. Renew Sustain Energy Rev 66(12):1–9
2. Aydin NY, Kentel E, Duzgun S (2010) GIS-based environmental assessment of wind energy systems for spatial planning: a case study from Western Turkey. Renew Sustain Energy Rev 14(1):364–373
3. Ahmadi A, Tiruta-Barna L, Benetto E, Capitanescu F, Marvuglia A (2016) On the importance of integrating alternative renewable energy resources and their life cycle networks in the eco-design of conventional drinking water plants. J Clean Prod 135(11):872–883
4. Javed A, Kasi BK, Khan FA (2019) Predicting solar irradiance using machine learning techniques. In: 15th international wireless communications & mobile computing conference (IWCMC)

5. Ingole AN (2016) Arduino based solar tracking system. In: Satellite conference ICSTSD 2016 international conference on science and technology for sustainable development, pp 61–66
6. Revathi B, Soundharya M, Swathihaa DK, Umamaheshwari R, Vinotha P (2017) Design of solar remote monitoring using raspberry pi. South Asian J Eng Technol 3(3):139–147
7. Nadpurohit B, Kulkarni R, Matager K, Devar N, Karnawadi R, Carvalho E (2017) IOT enabled smart solar PV system. Int J Innov Res Comput Commun Eng 5(6):97–98
8. Freitas S, Catita C, Redweik P, Brito MC (2015) Modeling solar potential in the Urban environment: State-of-the-art review. Renew Sustain Energy Rev Renew Sustain Energy Rev 41, 915–931
9. Fumo N, Biswas MR (2015) Regression analysis for prediction of residential energy consumption. Renew Sustain Energy Rev 47, 332–343
10. Gadsden S, Rylatt M, Lomas K (2003) Putting solar energy on the urban map: a new GIS-based approach for dwellings. *Sol Energy* 74(5):397–407
11. Sasajima H, Ishikuma T, Hayashi H (2015) Future IIOT in process automation—Latest trends of standardization in industrial automation, IEC/TC65. In: 54th annual conference of the society of instrument and control engineers of Japan (SICE), pp 963–967
12. Pan J, Paul RJS, Tam Vu, Saifullah A, Sha Mo (2015) An internet of things framework for smart energy in buildings: designs. Prototype Exp, IEEE Internet Things J 2(6):527–537
13. Das K, Ghosh H, Sengupta M (2016) Single axis solar tracking system using microcontroller (atmega328) and servo motor. Int J Sci Res Publ 6(6):24–29
14. Pathak KS, Darbari M, Yagyasen D, Ahmed H (2014) Making renewable energy SMART using internet of things (IOT). In: 2014 International conference on advances in engineering & technology research (ICAETR—2014), Unnao, pp 1–4. https://doi.org/10.1109/ICAETR.2014.7012862
15. Barazane L, Rouibah N, Mellit A, Hajji B, Rabhi A (2019) A low-cost monitoring system for maximum power point of a photovoltaic system using IoT technique. In: International conference on wireless technologies embedded and intelligent systems (WITS)
16. Deshmukh NS, Bhuyar DL (2018) A smart solar photovoltaic remote monitoring and controlling. In: 2018 second international conference on intelligent computing and control systems (ICICCS). Madurai, India, pp 67–71. https://doi.org/10.1109/ICCONS.2018.8663127
17. Sun Q, Li H, Ma Z, Wang C, Campillo J, Zhang Qi, Wallin F, Guo J (2015) A comprehensive review of smart energy meters in intelligent energy networks. IEEE Internet Things J 3(4):464–479
18. Batcha RR, Geetha MK (2020) A survey on IOT based on renewable energy for efficient energy conservation using machine learning approaches. In: 3rd international conference on emerging technologies in computer engineering: machine learning and internet of things (ICETCE). Jaipur, India, pp 123–128. https://doi.org/10.1109/ICETCE48199.2020.9091737
19. Vignesh R, Samydurai A (2016) A survey on IOT system for monitoring solar panel. Int J Sci Dev Res 1(11):114–116
20. Reddy SS, Bijwe PR (2016) Day-ahead and real time optimal power flow considering renewable energy resources. Int J Electr Power Energy Syst 82(11):400–408
21. Shaw RN, Walde P, Ghosh A (2020) IOT based MPPT for performance improvement of solar PV arrays operating under partial shade dispersion. In: 2020 IEEE 9th power india international conference (PIICON), SONEPAT, India, pp 1–4.https://doi.org/10.1109/PIICON49524.2020.9112952
22. Gurav U, Patil C (2016) IOT based interactive controlling and monitoring system for home automation. Int J Adv Res Comput Eng Technol 5(9):2392–2397
23. Krey VL (2011) Clarke Role of renewable energy in climate mitigation: a synthesis of recent scenarios. Clim Policy 11(4):1131–1158
24. Various reports published in The Times of India Mumbai edition (2020)
25. Various reports published in The Indian Express Mumbai edition (2020)
26. Various reports of Government of India (2020)
27. Various reports of Government of Maharashtra (2020)

Chapter 3
Reinforcement Learning Algorithm to Reduce Energy Consumption in Electric Vehicles

Manavi Shukla and Mandeep Singh Burdak

Abstract This chapter consists of the analysis, design and testing of a reinforcement learning algorithm that is used to monitor the fuel efficiency in different environmental and terrain conditions to provide an optimized velocity, which if driven upon can improve the energy consumption behavior of an electric vehicle. To monitor the effects of the algorithm, a Simulink Electric Vehicle Model is used with parameters of a normal Sedan Size car with a lithium-ion battery energy source. First, the various factors that contribute to energy losses in an electric vehicle are defined. Then, the model-free Q-learning technique is explained. Finally, the tested energy consumption results are discussed, and further scope of this algorithm is mentioned.

Keywords Reinforcement learning · Electric vehicle · Energy optimization

1 Introduction

The upcoming technology of electric vehicles brings us the freedom to use batteries as the fuel, making it a clean and feasible energy source. But unlike normal gas vehicles, EVs may not particularly have a huge tank for the gas. It uses a huge amount of battery power to overcome external conditions like air drag, extra weight, inclination, and temperature. Also, since the battery is being used for powering the complete vehicle, air conditioner usage causes a major power drain [1]. All these factors ultimately affect the range that you can get out of your EV in one full charge. We propose an algorithm to monitor and optimize the range of the EV. The algorithm uses the monitored data from different APIs to process the information and maximizes the cost function of the total power required for given trip details, and on the basis of the power required, power consumed and battery charge it assists the driver to follow certain driving patterns for improving the range of the vehicle.

M. Shukla (✉) · M. S. Burdak
Department of Electronics and Communication Engineering, G.B. Pant Government Engineering College, Okhla Phase – III, New Delhi 110017, India

R. N. Shaw et al. (eds.), *AI and IOT in Renewable Energy*,
Studies in Infrastructure and Control,
https://doi.org/10.1007/978-981-16-1011-0_3

1.1 Overview

For the development of the project, we collect data from the working electric vehicle models in the market [2]. We make sure that the latest technologies and optimization techniques have been incorporated into our project to make it more effective, cheap and less time-consuming. The optimization algorithm is a machine learning technique called reinforcement learning.

Reinforcement Learning. Unlike supervised learning, it does not contain labeled training dataset to learn from. It works on the idea of exploiting and exploring given information to find the optimal solution even for the situations that occur outside the problem. It can be either model-based or model-free [7].

The model-based method is used when the actions to be taken can be planned beforehand by predicting future outcomes and building a probability distribution matrix for sets of states and actions in our environment.

The model-free method learns by trial and error. Therefore, for optimization of an indefinite environment, where it's impossible to predict all outcomes, this approach is favored.

2 Literature Review

The use of reinforcement learning (RL) for energy management has been around for a very long time. In real-life situations where the dynamics are always changing, RL plays a crucial role in helping to find a strategy to manage the parameters that help increase or decrease the cost function. Some researchers have also worked on other core algorithms to solve the problem of optimal usage of battery/power utilization without machine learning. Although, research is definitely tending toward ML because of its sensitivity to unknown scenarios. With better methods, having greater accuracy, ML has become dependable unlike ever before.

- In the past, researchers have proposed reinforcement-learning-based real-time system for energy management for a plug-in HEV (Hybrid Electric Vehicle) [3] in which the power supply is distributed between the battery and IC engine or battery and ultracapacitor.
- In 2014, a system was proposed that optimizes vehicle's fuel consumption where cars are moving behind each other automatically. And the designed system was able to work at the starting level of V2V (Vehicle to Vehicle) communications. The system is developed based on Model Predictive Control (MPC) [4].
- In 2015, research was done for a hybrid electric tracked vehicle using reinforcement-based energy management techniques. Two optimal control solutions: Dyna Algorithm and Q-learning method were applied and it was concluded that the computational cost of Dyna algorithm is substantially lesser than that of the stochastic dynamic programming [5].

3 Design and Analysis of Q-Learning-Based Algorithm

The energy requirements of a vehicle can be understood by the various forces applied to it.

$$F_{total} = F_i + F_s + F_r + F_a \tag{1}$$

where

$F_i = Initial\ Force$

$F_s = Road\ Slope\ Force$

$F_r = Road\ Load\ Force$

$F_a = Aerodynamic\ drag\ force$

As all these factors are predominantly depend on weight, velocity, and acceleration of the vehicle and as weight optimization was not the intention of our research, the velocity was taken as the primary action parameter of our algorithm [6]. For optimization of an indefinite environment, where it is impossible to predict all outcomes, model-free approach is favored. The equation that correctly defines the learning approach is as follows.

$$Q(S_t, A_t) \leftarrow Q(S_t, A_t) + \alpha\left[R_t + 1 + \gamma max_a Q(S_{t+1}, A_t) - Q(S_t, A_t)\right] \tag{2}$$

where $Q(S_t, A_t) = current\ state\ and\ action\ Qmatrix,$

$\alpha, \gamma =$ learning rate, discount rate,

$R_t = Reward\ for\ the\ current\ action\ maxa,$

$Q(S_{t+1}, A_t) = Maximum\ expected\ future\ reward$ (Fig. 1).

We obtain various long natural driving schedules containing data for acceleration, charge requirements, external factors such as wind speed, temperature, road gradient 4 from online datasets. The power request for the respective driving schedule is calculated (Fig. 2).

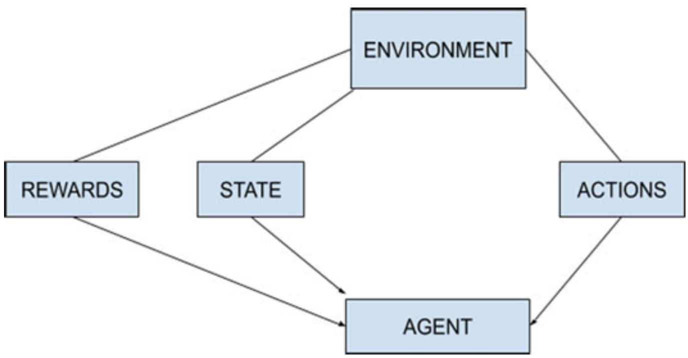

Fig. 1 Block diagram of reinforcement learning algorithm

	F	G	H	I	J	K	L
1	Power Base	Distance (m)		Inclination	Inclination_	Inclination_y	
2	-0.35	0		-0.00872	0.999962	-0.00872	
3	-80.8685	32.752047		0.006564	0.999978	0.006564	
4	3.28927	10.648512		1.156367	0.402668	0.915346	
5	4.25408	10.46411		0.704599	0.761871	0.647728	

Fig. 2 Sample trip data used for training the algorithm

Table 1 Table captions should be placed above the tables

Q-learning parameters	Real-life dependent variables
Environment	Location, road gradient, wind speed, fuel available
Agent	Driving schedule (velocity, acceleration)
State	Value of environmental parameters at next location
Rewards	Ratio of distance upon power drawn in each iteration
Actions	Velocity change corresponding to driving, accelerating, braking, coasting, traction drive

We will use Web APIs to get traffic data, weather data and make environment simulation in Simulink and also, the expected vehicle output data from the vehicle manufacturer to build the algorithm. Then we assign these real-time data to the equation variations (see Table 1).

In order to study the effects of our algorithm on a vehicle, we added a few blocks in a default Simulink electric vehicle model to simulate its behavior in accordance with more realistic environmental data points. This model simulates a vehicle driving on different terrains with variable elevation. In this model, we have made different blocks for simulating different systems in a vehicle in order to simplify the working and making it easier to understand. The model takes in as input a series of velocity, wind speed, temperature and road inclination angle which it experiences at any given time interval. And as output this model gives us the value of various vehicle parameters such as acceleration, velocity, distance covered, energy consumed, different energy losses, torque produced, net tractive force experienced, state of charge of the battery, etc., at any given time during the journey. These parameters are then automatically exported to MATLAB workspace, where we have used them in our code to get power requirement results, and then input suggestive velocity to optimize the same. The output of the algorithm thus is a matrix [1 $\times$ N], with optimal velocity in the row for different state parameters in n columns.

Finally, a sample trip from real electric vehicle drive schedules was taken for testing the algorithm. The power required with respect to the time graph when the car is driven on optimal velocity versus the velocity with which it was initially driven is plotted (Fig. 3).

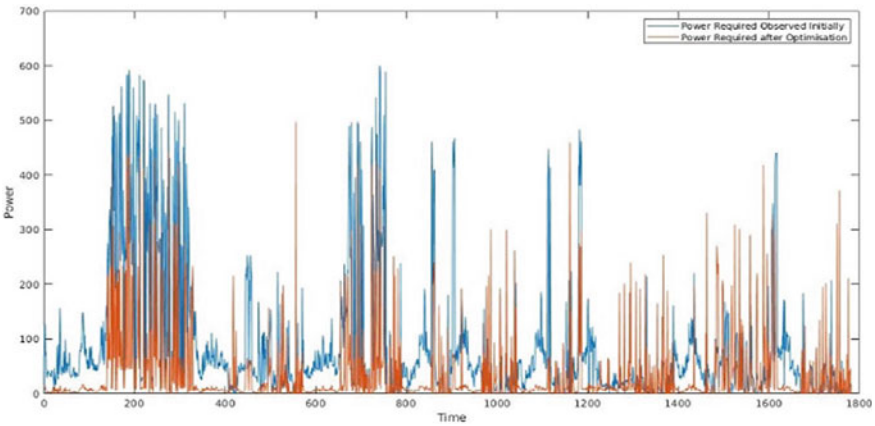

Fig. 3 Power requirement as observed initially versus after the optimized velocity has been assigned

4 Result

We sampled the data in multiple time intervals to calculate the average power-saving efficiency (Fig. 4).

Therefore, after testing our algorithm on a simulated vehicle of a normal size sedan vehicle having vehicle parameters of a TATA Tigor car, we found that the power consumed after optimization is 79.33% of the power consumed initially.

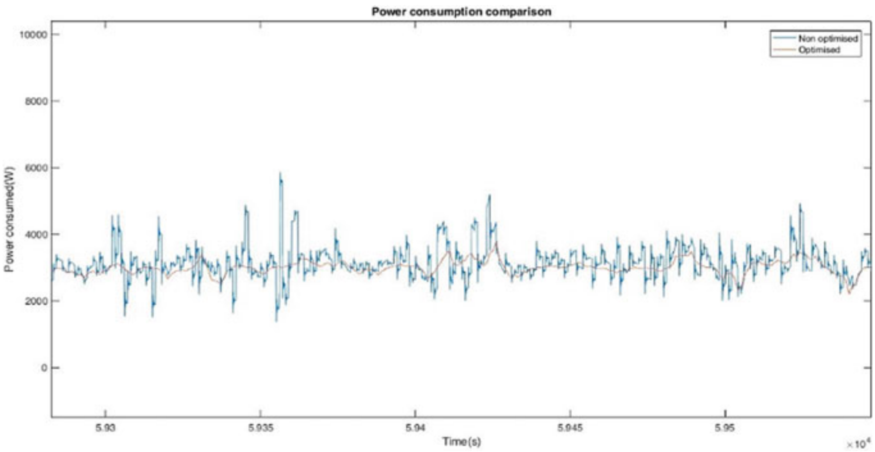

Fig. 4 A sampled graph for clear representation of power consumption variations of initial velocity versus optimized velocity

5 Conclusions

We can apply our reinforcement learning algorithm in any type of fuel-consuming vehicle to increase fuel sustainability but mainly it is a new and efficient approach to improve battery consumption in electric-charging-based vehicle because it is a comparatively new area of research and not much has been done or implemented to assure optimization of batteries. For example, a more personalized driver assistance model will only be possible by partnering with a vehicle company to get day-to-day user data to develop compatible hardware that can be attached to the vehicle to extract all the data by the permission of the user.

This algorithm is not only restricted to land-borne vehicles; it can re-learn given the parameters of any vehicle. For example, airplanes, ships, drones and even smart home appliances. Our product is a tool to assist all battery backing devices, either as an extension to the hardware the user is engaging with, or as a standalone software with packaged embedded systems.

References

1. Zeng X, Li M, Abd El-Hady D, Alshitari W, Al-Bogami AS, Lu J, Amine K (2019) Commercialization of lithium battery technologies for electric vehicles. Adv Energy Mater 9:27, 1900161. Online publication date: 6-Jun-2019
2. Musk E, Straubel JB (2012) Model S efficiency and range. Tesla. https://www.tesla.com/blog/model-s-efficiency-and-range. Accessed 9 May 2012
3. Xiong R, Cao J, Yu Q (2017) Reinforcement learning-based real-time power management for hybrid energy storage system in the plug-in hybrid electric vehicle. Appl Energy 211:538–548. https://doi.org/10.1016/j.apenergy.2017.11.072
4. Alsabaan M, Naik K, Khalifa T (2013) Optimization of fuel cost and emissions using V2V communications. IEEE Trans Intell Transp Syst 14:1449–1461. https://doi.org/10.1109/tits.2013.2262175
5. Liu T, Zou Y, Liu D, Sun F (2015) Reinforcement learning-based energy management strategy for a hybrid electric tracked vehicle. Energies 8:7243–7260. https://doi.org/10.3390/en8077243
6. Wu X, He X (Sean), Yu G, Harmandayan A, Wang Y (2015) Energy-optimal speed control for electric vehicles on signalized artrials. IEEE Trans Intell Transp Syst 16:2786–2796. https://doi.org/10.1109/TITS.2015.2422778
7. Sutton RS, Barto AG (2015) Reinforcement learning: an introduction, 2 ed. MIT Press. ISBN 9780262039246

Chapter 4
Simulation and Performance Analysis of Standalone Photovoltaic System with Boost Converter Under Irradiation and Temperature

Kritika Khandelwal, Chetan Jain, and Sunil Agarwal

Abstract Renewable energy technology is the advanced technology capable of satisfying the problems of energy crisis that the world is facing as well as meeting the future energy demands due to the availability of energy source in infinite quantity in the atmosphere. This chapter presents a simulation and performance survey of the standalone photovoltaic (PV) system with boost converter under irradiation and temperature and in order to seize the utmost power at output Perturb and Observe (P&O) Maximum Power Point Tracking Algorithm (MPPT) is used. The output results are obtained and analyzed at different irradiations and temperature parameters. The proposed model is outlined and simulated in MATLAB/SIMULINK R2015a software.

Keywords PV system · DC-DC boost converter · MPPT

1 Introduction

Solar Energy is the most ubiquitous, sustainable and inexhaustible source of energy. These renewable sources of energy can be utilized for power generation as these are easily available, non-polluted, optimal cost and an inexhaustible option for human kind. Hence as a fuel of choice for power generation, solar energy has emerged as a safe and comfortable energy solution [1–5]. Therefore, the energy generation through the solar photovoltaic (PV) technology converting solar energy into electrical energy offers distinctive advantages in comparison with coal, oil and nuclear energy.

K. Khandelwal (✉) · C. Jain · S. Agarwal
Department of Electrical Engineering, Apex Institute of Engineering and Technology, Jaipur, India
e-mail: kritikakhandelwal8696@gmail.com

C. Jain
e-mail: cjchetan91@gmail.com

S. Agarwal
e-mail: hodee@apexcollege.in

R. N. Shaw et al. (eds.), *AI and IOT in Renewable Energy*,
Studies in Infrastructure and Control,
https://doi.org/10.1007/978-981-16-1011-0_5

A group of many cells electrically connected together either in the series to give a rise in output voltage or in parallel to give a rise in output current as per requirement is known as solar module. A group of the number of modules forms a solar array or panel. These PV modules and arrays are used for PV power generation projects to generate electricity [6–9]. The PV-based systems are accommodated in grid-connected systems and are also employed in standalone applications such as street lighting, water pumping, etc. [10]. A system for energy storage, control mechanism, converter and a measuring equipment are required for the balance of the PV system to be connected to the grid. This chapter highlights the layout of the DC-DC boost converter and its combination with the PV module with the application of the MPPT algorithm using MATLAB software. To comprehend, simulink models, mathematical equations, figures, flowcharts and tables have been provided for optimal designs.

2 Circuit Model of PV Module

The PV module's fundamental element is the PV cell that directly converts the sun's energy (light energy) into low output direct current (DC) voltage electrical energy. These cells are semiconductor devices, generally made up of silicon material, forming a p-n junction. This conversion from light energy to electrical energy takes place through the phenomenon called "photovoltaic effect". For understanding the behavior of solar photovoltaic cells under various operating and atmospheric conditions, the modeling of solar cells is to be studied. Because of its non-linear characteristics, accuracy is difficult. Hence the proper mathematical modeling of the PV module is necessary. Through this, the performance of its current-voltage (I-V) and power-voltage (P-V) properties are also studied at distinct irradiation and temperature, respectively. The single-diode model circuit is employed for the modeling of the PV module, also termed as five-parameter model (I_s, n, R_s, R_p, I_{pv}), where I_s = diode saturation current (A), n = diode factor ($1 \leq n \leq 2$), R_s = series resistance (Ω), R_p = parallel resistance (Ω) and I_{pv} = photocurrent (A). Figure 1 demonstrates the electrical equivalent circuit of the PV cell. The working task of the series and parallel resistances connected with the diode is represented as follows:

- To account for the drop-in voltage and internal dissipation (due to the flow of current), the series resistance R_s is introduced.
- When the diode is in reversed biased condition, the parallel resistance R_p takes the leakage current to the ground into consideration.

This model consists of current source I_{pv} in anti-parallel connection with Diode D, parallel resistance R_p and series resistance R_s. From the figure, the output current equation is

$$I = I_{pv} - I_d \tag{1}$$

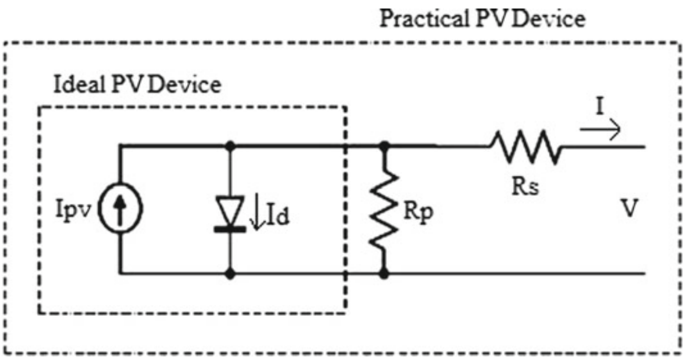

Fig. 1 PV cell's general model

where I_{pv} = Current (Amp) generated through light energy, directly proportional to solar irradiation and I_d = diode current or Shockley equation (Amp).

I_{pv} is determined as

$$I_{pv} = [I_{sc} + K_i(T_c - T_r)] \cdot G \tag{2}$$

where V_{oc}= open-circuit voltage (V), I_{sc} = short-circuit current (Amp) at 25 °C and G = 1, K_i = temperature coefficient of cell's short-circuit current (0.0032), T_c = operating temperature (K), T_r = reference temperature (298 K) and G = solar irradiation (W/m^2).

The Shockley equation is

$$I_d = I_s\{\exp(q/nkT_c) - 1\} \tag{3}$$

where I_s = leakage current of diode (Amp), q = electron charge (1.60×10^{-19} C), n = ideality factor of diode (1.2 for monocrystalline Si and 1.3 for polycrystalline Si) and k = Boltzmann constant (1.38×10^{-23} J/K).

The equation derived for the solar cell's output current on the basis of the practical model is expressed as

$$I = I_{pv} - I_d - I_p \tag{4}$$

$$I = I_{pv} - I_s\{[\exp\left(\frac{q}{nkTcNs}\right)(V + IR_s)] - 1\}\frac{V + IR_s}{R_p} \tag{5}$$

where I_p = shunt branch current, Ns = No. of cells connected in the series, V = output voltage (V) and I = input current (Amp).

The saturation current of diode is expressed as

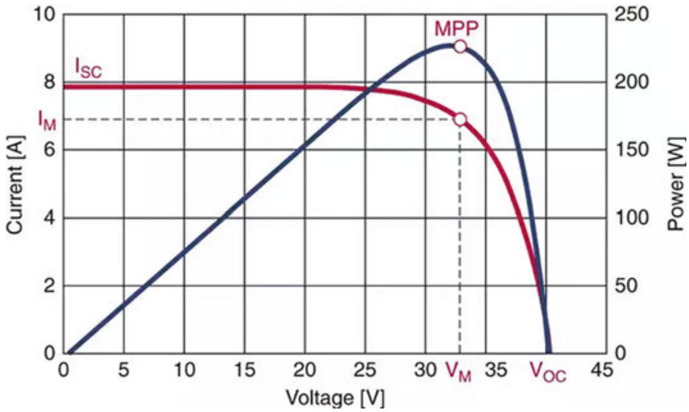

Fig. 2 I-V and P-V characteristics of PV module

$$I_s = I_{rs}(\frac{T_c}{T_r})^3 \exp\left[\frac{qE_{g0}}{nk}\left(\frac{1}{Tc} - \frac{1}{Tr}\right)\right] \tag{6}$$

where I_{rs} = Reverse saturation current (Amp) at STC and E_{g0} = Energy band gap of semiconductor (1.1 eV for poly-crystalline Si at STC).

From Eq. (6), the reverse saturation current I_{rs} is determined as

$$I_{rs} = I_{sc}/\exp\left(\frac{qVoc}{nkTcNs}\right) - 1 \tag{7}$$

Here, in PV cell, the temperature and irradiation are two factors affecting its output. Therefore, the Standard Test Conditions (STC), i.e., on 25 °C temperature and 1000 W/m^2 solar irradiation at air mass (AM) of 1.5 is taken as the nominal operating condition for the PV module. The attributes of PV cell (I-V and P-V characteristics) are demonstrated in Fig. 2.

Here, the Maximum Power Point (MPP) is defined as the point of operation or the only point where the maximum power is generated by the PV cell, having coordinates (V_{MPP}, I_{MPP}). V_{MPP} stands for maximum power point voltage and I_{MPP} for the maximum power point current. The P_m, I_m and V_m in the graph denotes the maximum power, maximum current and maximum voltage value.

3 Circuit Model of DC-DC Boost Converter

DC-DC boost converter is used to step up the value of the voltage from low input to the high output voltage. An inductor (L), a diode (D), capacitor (C), load resistor (R_L) and high-frequency switch (S) are the basic components of the boost converter. The low output from the PV module is used as an input to the boost converter. The duty

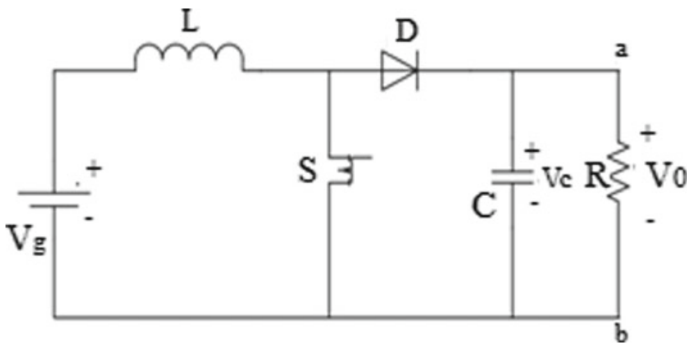

Fig. 3 Circuit model of DC-DC boost converter

cycle (D) of the high-frequency power switch is a controlling mechanism deciding its optimal operating point by causing the variation in the voltage. Figure 3 shows the equivalent circuit of the DC-DC boost converter [11, 12].

The mean output voltage for the duty cycle (D) by fluctuating the ON time of the button (switch) can be determined as

$$\frac{V_o}{V_{in}} = \frac{1}{(1 - D)} \tag{8}$$

where V_{in} = converter's input voltage, V_o = converter's output voltage and D = duty cycle of converter.

Using Eqs. (9) and (11), the value of inductor and capacitor can be computed as follows:

3.1 *Choice of Inductor*

Boost converter's inductor (L) value is obtained from

$$L = V_{in} D/(f_s \Delta I_L) \tag{9}$$

where f_s = switching frequency and ΔI_L = input current ripple.

The correlation between the input current ripple to output current is defined as Current Ripple Factor (CRF) [1]. CRF should be within 30% for good prediction of inductor value.

$$\Delta I_L / I_o = 0.3 \tag{10}$$

The maximum value of output current should always be less than the current rating of the inductor.

3.2 Choice of Capacitor

Boost converter's capacitor (C) value is obtained from

$$C = I_{out}D/(f_s \Delta V_o) \tag{11}$$

where ΔV_o = Ripple in output voltage.

The ratio between the output voltage ripple to output voltage is defined as Voltage Ripple Factor (VRF). VRF should be within 5% for good prediction of capacitor value.

$$\Delta V_o/V_o = 5\% \tag{12}$$

Using $V_{in} = 16.85$ V, $V_{out} = 33.26$ V, $I_{out} = 1.663$ amp and switching frequency as 100 kHz values for designing converter, the calculated values of components are as follows: R = 0.1 Ω, L = 10 mH, C1 = 1000 μF and R = 20 Ω.

4 Simulation Results

Hereinafter, the simulation results of the PV system are briefed in Sects. 4.1 and 4.2. The result after the simulation of the PV module is discussed in Sect. 4.1, while the following section discusses the results obtained after the overall simulation of MPPT DC-DC boost converter with the PV module.

4.1 Simulation of PV Module

The mathematical model of the PV module is modeled in MATLAB/Simulink software using blocks of Simscape library tools. These library tools are obtained from the Simulink library present in the MATLAB toolbar. The PV current (I) generated at the output of the PV module is the function of I_s, I_{rs}, I_{sh} and I_{pv}. The input parameters of the PV module are substituted in the dialog box (properties) of the subsystems of the PV module as shown in Fig. 4. The final circuit for PV (by the interconnection of distinct subsystems) is shown in Fig. 5. The final Simulink model has a temperature (T) in kelvin (K) and solar irradiation (G) in Weber per square meter (W/m^2) as input parameters in order to return the output current (I) and voltage (V) value of the PV module. The Solarex MSX60 PV type is taken as the reference model for the modeling of the PV module [13, 14].

The MSX60 module provides a nominal maximum power of 60 W, consisting of 36 poly-crystalline silicon cells connected in the series (N_s) having $V_{oc} = 21.1$ V and $I_{sc} = 3.8$A, respectively. I-V and P-V attributes of the PV module at a constant

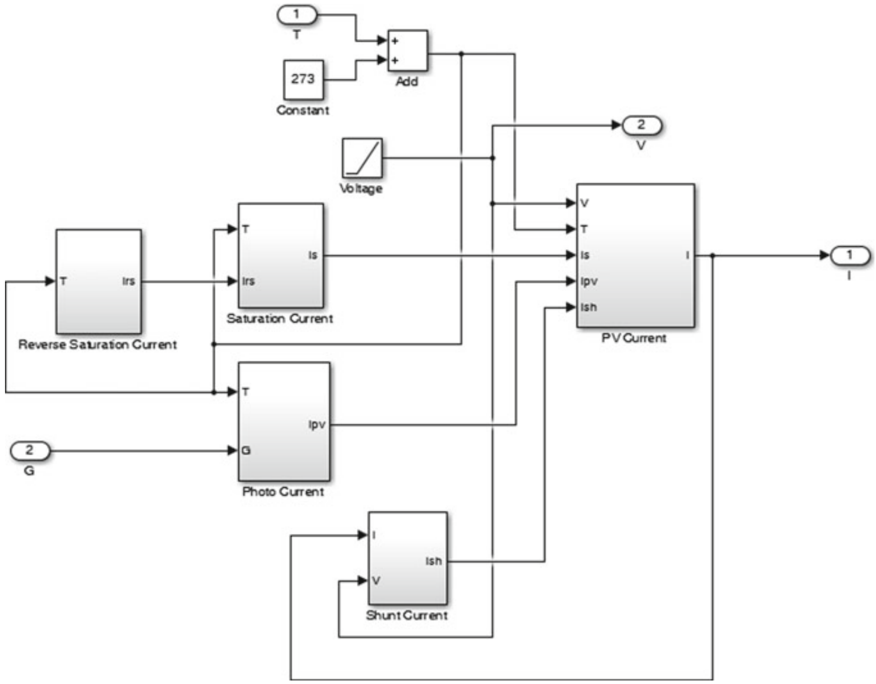

Fig. 4 Subsystems of the PV module

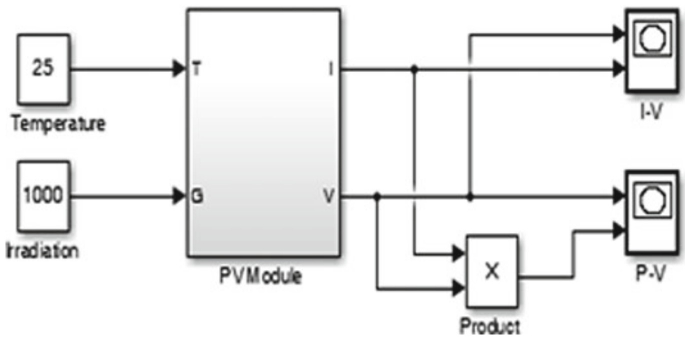

Fig. 5 Final Simulink circuit of the PV module

solar irradiation (G = 1000 W/m^2) and different temperature at 20, 40, and 60 °C is shown in Fig. 6a, b while characteristics at a constant temperature (T = 25 °C) and varying solar irradiation at 900, 1000, and 1100 W/m^2 is shown in Fig. 7a, b.

The Fig. 6a, b results that the increment in the temperature value leads to the decrement in the values of voltage and power while Fig. 7a, b results that on increasing the solar irradiation, the value of voltage and power increases.

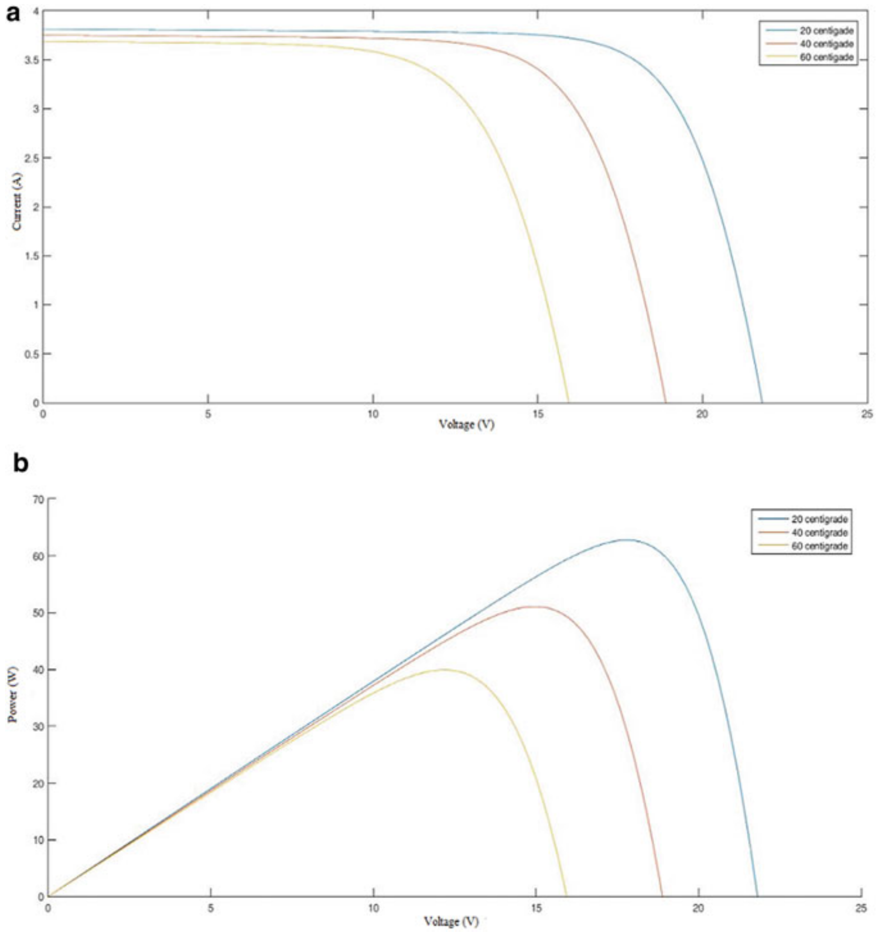

Fig. 6 **a** I-V curve at a constant irradiation of 1000 W/m2 and varying temperature. **b** P-V curve at a constant irradiation of 1000 W/m^2 and varying temperature

4.2 Simulation of MPPT DC-DC Boost Converter

MPPT method acquires the maximum point by controlling the DC-DC converter output voltage by disrupting this system and then scrutinizing the impact on the PV power output [15, 16]. The detailed diagram of perturb and observe (P&O) MPPT algorithm is demonstrated in Fig. 8. It is observed that the increase in power P ($dP/dV > 0$) due to the disturbance of the operating voltage V in the defined direction leads to a shifting of the operating point toward the Maximum Power Point (MPP).

This disturbance in the voltage due to perturb and observe algorithm will be continued in the same direction until the MPP is reached. Here, the reference point (V_{ref}) is referred to as the corresponding voltage at which MPP is reached [17–20].

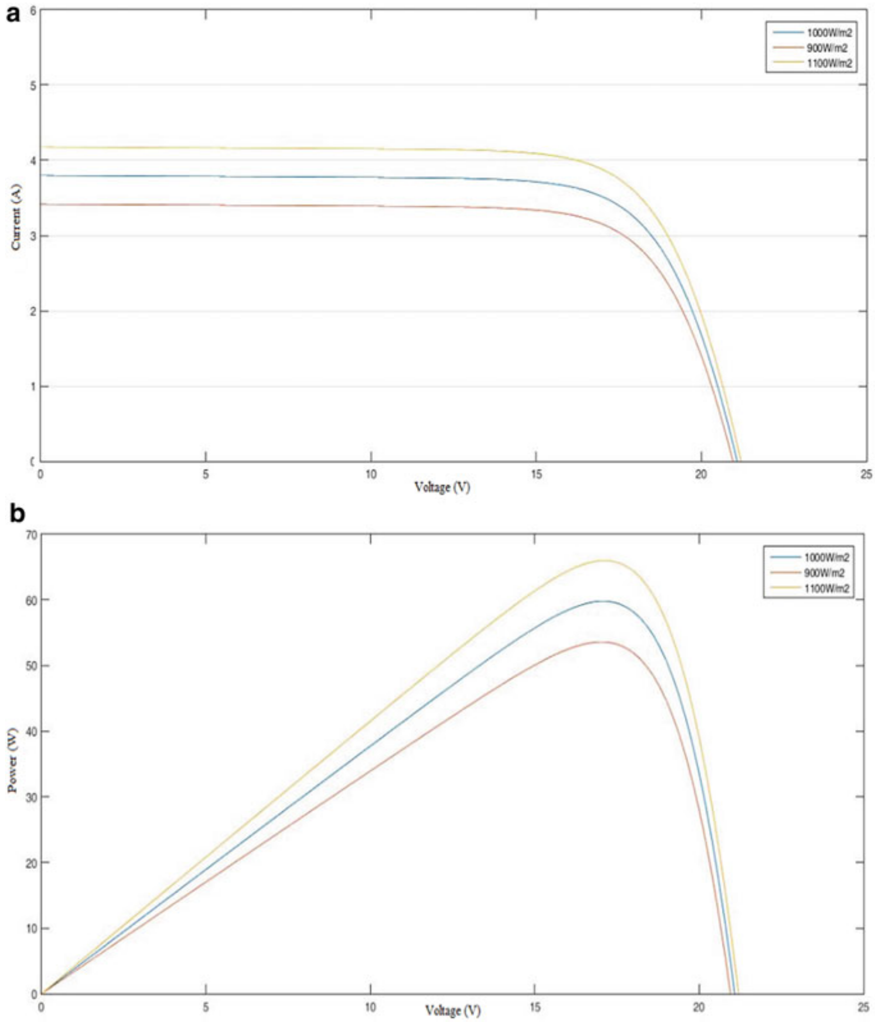

Fig. 7 **a** I-V curve at a constant temperature of 25 °C and varying solar irradiation. **b** P-V curve at a constant temperature of 25 °C and varying solar irradiation

On the contrary, the disturbance in the operating voltage causes the decrement in the power ($dP/dV < 0$) that will move the operating position apart from MPP. Hence, the direction of the subsequent disturbance will be reversed by this algorithm.

The output voltage, current, and power waveforms of boost converter fed with PV using P&O algorithm are analyzed at constant 1000 W/m^2 solar irradiation and different temperatures are represented in Fig. 9a–c.

Figure 10a–c shown are at constant 25 °C temperature and different solar irradiations. Here, the MPPT technique is extracting the utmost power from the PV system

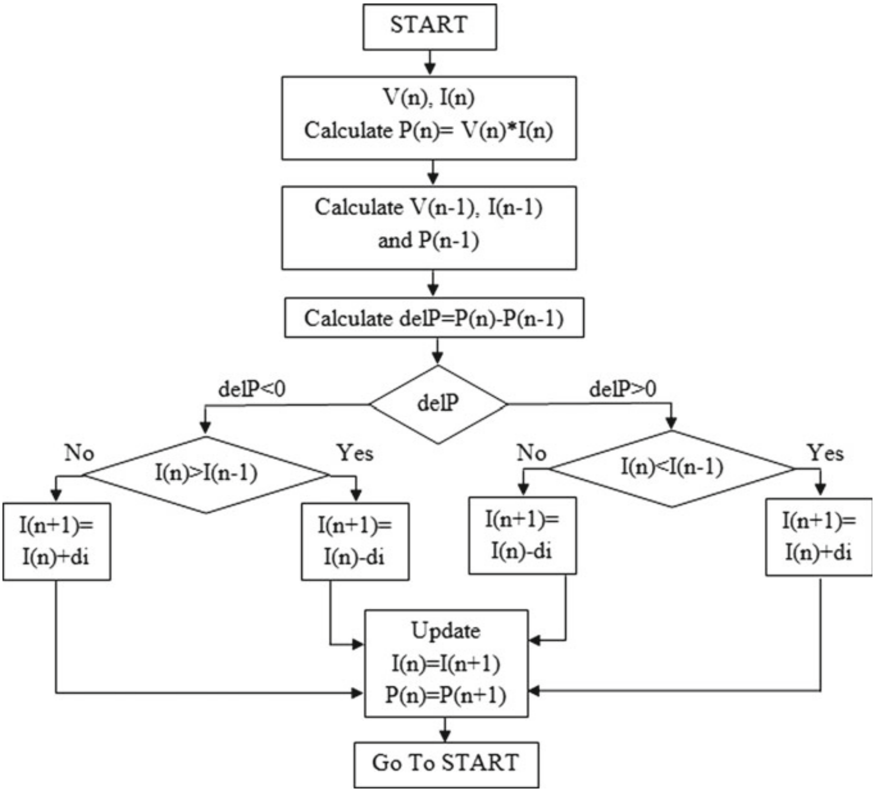

Fig. 8 Flowchart of perturb and observe algorithm

at 51.8% of the duty cycle. This can be done by matching the source impedances with that of a load impedance through varying the duty cycle of converters.

The output power under consistent solar irradiation (G = 1000 W/m^2) and distinct temperatures as well as distinct solar irradiations and consistent temperature (T = 25 °C) is represented in tabular form in Table 1 [11].

It is perceived that, as the temperature value rises, the value of output power decreases whereas it increases with an increase in the solar irradiations. The ripple in the designed boost converter is approximately 2%. Hence, the boost converter is working with an efficiency of 92.6%. The output power of the boost converter shows it has reached MPP at 0.47 sec at 55.31 W.

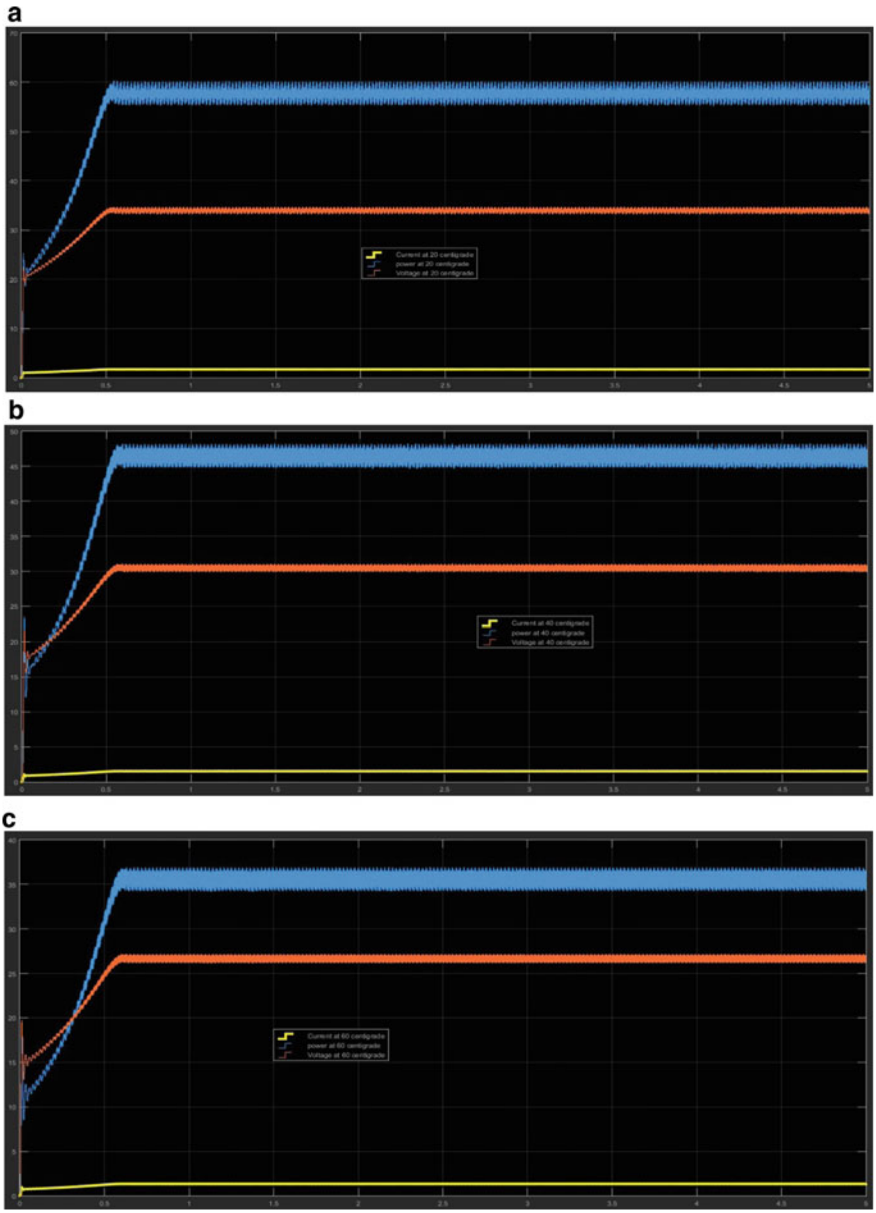

Fig. 9 **a** Performance characteristic of boost converter at 20 °C. **b** Performance characteristic of boost converter at 40 °C. **c** Performance characteristic of boost converter at 60 °C

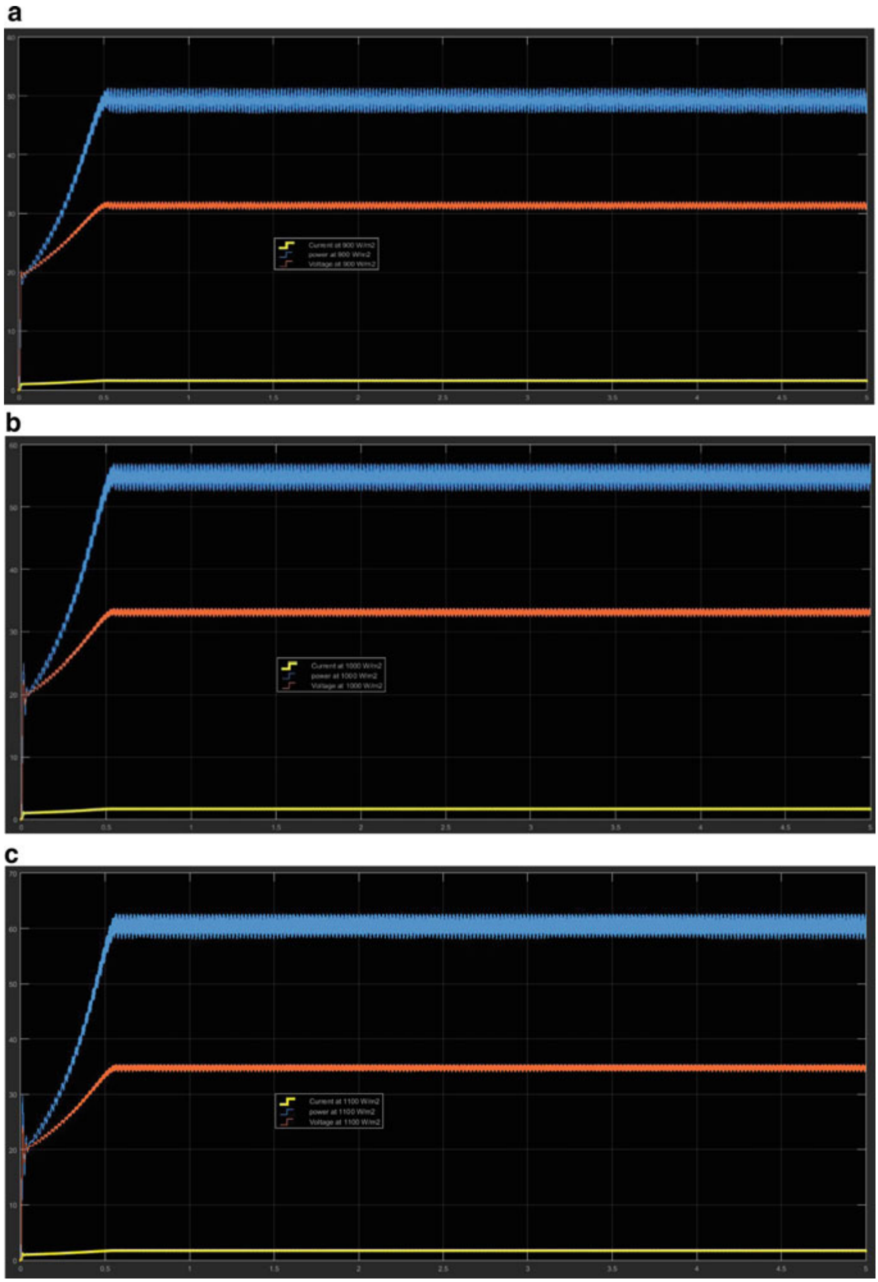

Fig. 10 **a** Performance characteristic of boost converter at 900 W/m^2. **b** Performance characteristic of boost converter at 1000 W/m^2. **c** Performance characteristic of boost converter at 1100 W/m^2

Table 1 Power output at operating parameters

Parameters	Values	PV module power (W)	Boost converter power (W)
Constant solar irradiation (G = 1000 W/m^2)	20 °C	62.57	57.65
	40 °C	51.07	46.38
	60 °C	39.92	35.4
Constant temperature (T = 25 °C)	900 W/m^2	53.38	49.3
	1000 W/m^2	59.72	55.31
	1100 W/m^2	65.84	60.8

5 Conclusions

From the above simulation outcomes, it is seen that the output power of the boost converter fed with photovoltaic module using perturb and observe maximum power point tracking algorithm varies depending on the solar irradiation and temperature. With the analysis of output results, it has been proved that the rise in the value of temperature assist the decrease in the output power whereas for solar irradiations, output power increases with an increase in solar irradiations. Many research have been done in designing the boost converter but very few researchers were reported considering ripple parameter in the inductor current. In the chapter, the ripple parameter is the main criteria in the designing of boost converter. Hence, the achieved output result shows that the DC-DC boost converter is operating at 92.6% efficiency within the operation range having approximately 2% ripple. Analyzing and observing the variation in results, we conclude that the practical execution of the work is reasonable.

Acknowledgements The authors would like to thank the Department of Electrical Engineering, Apex Institute of Engineering and Technology for their support and assistance for this work.

References

1. Devi SL, Nagarajan S, Vaishali R (2019) Design, analysis and comparison of suitable converters for photovoltaic system. Int J Recent Technol Eng (IJRTE) 7:205–211
2. Sudha K, Premkumar K, Sowmiya A (2019) Design and simulation of enhanced adaptive perturbation and observe MPPT algorithm for PV fed dc to dc boost converter system. Int J Innov Technol Explor Eng (IJITEE) 9:1715–1719. https://doi.org/10.35940/ijitee.b7618.129219
3. Koca YB, Aslan Y, Yonetken A, Oguz Y (2019) Boost converter design and analysis for photovoltaic systems. Int Con Eng Technol Applied Sci (ICETAS):384–389 (Kiev, Ukraine)
4. Pasha A, Jayakumar N, Thiruvonasundari D (2017) Performance analysis of DC-DC converters and comparative study of buck-boost with SLLB converter by using SPV based INC MPPT technique. Int Res J Eng Technol (IRJET) 4:1158–1164
5. Matias CA, Medeiros GP, Moraes PHF, Fernandes B de A, Alves AJ, Calixto WP, Furriel GP (2017) Simulation and analysis of an isolated full bridge DC-DC boost converter operating with a modified perturb and observe maximum power point tracking algorithm. Trans Environ Electri Eng, IEEE 2(2). https://doi.org/10.1109/eeeic.2016.7555846 (Florence, Italy)

6. Shaw RN, Walde P, Ghosh A (2020) Review and analysis of photovoltaic arrays with different configuration system in partial shadowing condition. Int J Adv Sci Technol 29(9s):2945–2956
7. Sahu P, Verma D, Nema S (2016) Physical design and modelling of boost converter for maximum power point tracking in solar PV systems. Int Con Electri Pow Energy Sys (ICEPES) IEEE:10–15. https://doi.org/10.1109/icepes.2016.7915898 (Bhopal, India)
8. Nguyen XH, Nguyen MP (2015) Mathematical modeling of photovoltaic cell/module/arrays with tags in Matlab/Simulink. Environ Sys Res:1–13. https://doi.org/10.1186/s40068-015-0047-9
9. Tamrakar V, Gupta SC, Sawle Y (2015) Single diode PV cell modeling and study of characteristics of single and two diode equivalent circuit. Electri Electron Eng Int J (ELELIJ) 4(3):13–24. https://doi.org/10.14810/elelij.2015.4302
10. Shaw RN, Walde P, Ghosh A (2020) Enhancement of power and performance of 9x4 PV arrays by a novel arrangement with shade dispersion. Test Eng Manage:13136–13146. ISSN: 0193-4120
11. Keshavani K, Joshi J, Trivedi V, Bhavsar M (2014) Modelling and simulation of photovoltaic array using Matlab/Simulink. Int J Eng Develop Res (IJEDR) 2:3742–3751
12. Shaw RN, Walde P, Ghosh A (2020) IOT based MPPT for performance improvement of solar PV arrays operating under partial shade dispersion. 9th Pow India Int Con (PIICON) IEEE: 1–4. https://doi.org/10.1109/piicon49524.2020.9112952 (Sonepat, India)
13. Mohammed SS, Devaraj D (2014) Simulation and analysis of standalone photovoltaic system with boost converter using Matlab/Simulink. Int Con Circuit Pow Comput Technol (ICCPCT), IEEE: 814–821. https://doi.org/10.1109/iccpct.2014.7054991 (Nagercoil, India)
14. Shaw RN, Walde P, Ghosh A (2019) Effects of solar irradiance on load sharing of integrated photovoltaic system with IEEE standard bus network. Int J Eng Adv Technol 9(1)
15. Sahu TP, Dixit TV, Kumar R (2014) Simulation and analysis of perturb and observe MPPT algorithm for PV array using ĊUK converter. Adv Electron Electric Eng 4(2):213–224
16. Shaw RN, Walde P, Ghosh A, A new model to enhance the power and performances of 4x4 PV arrays with puzzle shade dispersion. Int J Innov Technol Explor Eng 8(12)
17. Chermitti A, Boukli-Hacene O, Mouhadjer S (2012) Design of a library of components for autonomous photovoltaic system under Matlab/Simulink. Int J Comput Appl (0975–8887) 53(14). https://doi.org/10.5120/8488-2434
18. Bialasiewicz JT (2008) Renewable energy systems with photovoltaic power generators: operation and modeling. IEEE Trans Indus Electron, IEEE 55(7):2752–2758. https://doi.org/10.1109/tie.2008.920583
19. Desai HP, Patel HK (2007) Maximum power point algorithm in PV generation: an overview. Int Con Pow Electron Drive Sys (PEDS), IEEE: 624–630. https://doi.org/10.1109/peds.2007.4487766
20. Enslin JHR, Wolf MS, Snyman DB, Swiegers W (1997) Integrated photovoltaic maximum power point tracking converter. IEEE Trans Indus Electron, IEEE 44(6):769–773. https://doi.org/10.1109/41.649937

Chapter 5
Analysis of Variation in Locational Marginal Pricing Under Influence of Stochastic Wind Generation

Poonam B. Dhabai and Neeraj Tiwari

Abstract This chapter presents an approach for analysis of variation in Locational Marginal Pricing (LMP) due to integration of stochastic wind generation in stabilized grid network by using Probabilistic Optimal Power Flow (P-OPF) in MATPOWER environment. The competitive market led to the assessment of the nodal price values for bidding the next MW charges. Consequently, the precise estimation and analysis of LMP values become a challenging task in the presence of dubious wind generation. LMP at any power transport bus 'z' constitutes of: base LMP, LMP due to losses at bus z and LMP due to congestion at the same bus. As LMP itself is composed of congestion cost factors at an individual bus, it not only aids in the determination of Network Rental (NR), yet in addition, has a significant part in the determination and management of congestion from an economical perspective within the system. Therefore presented work underscores a methodology to analyze the variation in LMP values highlighting the congestion scenario. The analysis is carried out statistically and power flow run. This analysis is performed on the wind data set obtained from Indian Meteorological Department (IMD) section, Pune, India, on a standard IEEE 30 bus test system.

Keywords Uncertainty · Locational marginal pricing · MATPOWER · Congestion management

1 Introduction

Year-to-year increment in demand for electrical energy, urbanization, increased global warming have turned us into grid modernization. The existing power grid has the self-characteristic promoting the integration of uncertain and stochastic environmentally friendly renewable energy sources (RES). Grid integration is the put into practice of enhancing the methods to deliver higher penetration intensity of variable RES in the stabilized power system without violating any of the system constraints.

P. B. Dhabai · N. Tiwari (✉)
Poornima University, Jaipur, India

R. N. Shaw et al. (eds.), *AI and IOT in Renewable Energy*,
Studies in Infrastructure and Control,
https://doi.org/10.1007/978-981-16-1011-0_6

The power insertion into the power system may hamper the power flow into the transmission lines. Due to continuous variation in power input due to stochastic wind, congestion scenarios may occur within the system. The congestion occurrence introduces the congestion cost factor into the nodal price at each bus. Computing the LMP values at each bus, gives the per MW transfer charge. LMP computation can be carried out in many different ways depending upon the observation required. The LMP values can be utilized for determining the transmission zones of the system, calculating the reliability margins of the system. The congestion link can be derived by observing the variation in the values from the corresponding base values. The LMP values mainly depend upon generator, transmission margin and load through the network. The computation of LMP is a crucial task in presence of uncertain wind, as it not only depends upon the varying cost of power transfer between any two points in the system but also on the load flow pattern, variation in generation and load. Post integration of wind source into the system changes the grid power flow pattern which in hand includes the congestion cost factor in LMP computation depending upon the penetration level of the source.

Yu [1] addressed the challenges and issues associated with current LMP operations and proposed nodal LMP system. Ge et al. [2] calculated the LMP values for East China power market by analyzing the three components that constitute the formation of LMP assuming the two different scenarios of the market. Albadi et al. [3] present a manuscript investigating the effect of solar power plant on LMP in an interconnected system in Oman through simulations. Umale and Warkad [4] approached ACOPF considering losses for LMP model with real bus data system on 765 kV/400 kV MSETCL; they also analyzed variation in the LMP based on transmission constraints of transmission lines. Nnamdi et al. presents a decision tree model with different power system variables for predicting the LMP values concluding better performance of decision tree under certain circumstances [5]. Umale and Warkad [6] reflected the importance of LMP in transmission congestion management and market operations based on financial transmission rights. Variation in LMP with the change of load into the system was focused by Jain and Mahajan [7] for PJM 5 bus transmission system for peak load period with and without transmission constraints. A new methodology P2P for local energy market algorithm based on multi-phase low voltage distribution system was proposed by Mortysn et al. [8]. Post integration of RES into the transmission system changes the power flow of the system; this analysis was presented by Poonam. Dhabai and Tiwari utilizing the linear sensitivity factors [9]. This work is an extension of the analysis done in [9].

The chapter is alienated into the following subsections: Sect. 1 notifies the literature work on LMP. Section 2 speaks on problem formulation. Section 3 presents the test case and related data along with assumptions. Section 4 showcases the algorithm used for the computation of LMPs. Section 5 includes the results of the analysis. Section 6 provides a discussion on the results obtained. Eventually, Sect. 7 concludes the chapter with concluding notes on the work presented and potential future scope.

2 Problem Formulation

2.1 Problem Description

The presented work is based on analyzing the variation in LMP from its base value post integration of uncertain wind energy into the system with the change in its location. To compute LMP, calculations of three factors are required: base LMP values in presence of only conventional generation, LMP contributed due to losses and LMP due to congestion. Mathematically, LMP formulation at any bus z can be expressed as

$$LMP_z = LMP_{base(Conventional)} + LMP_{Loss(z)} + LMP_{congestion(z)} \tag{1}$$

2.2 Methodology

The computation of LMP in real time is estimated using MATPOWER [10] programming by DC-P-P-OPF [12] algorithm. Considering the real-time based wind data from Pune, India, (uncertainties) are mapped as input to the system with 1000 random samples generated from the data after meticulous analysis of PDF and CDF (in the obtained data, distribution followed is lognormal). These samples are then used as uncertain input to standard IEEE 30 bus system and finally validated.

3 Test Case, Data, and Assumptions

3.1 Test Case

The IEEE 30 bus system consists of totally six conventional generators. Out of all these, the minimum generation (19.2 MW) is at bus number 23 and the maximum generation (60.97 MW) is at bus number 2. The transmission system consists of a total of 41 transmission lines and 30 power busses. Table 1 shows the conventional generator data of the system.

Table 1 Conventional generator data IEEE 30 bus system

Bus number	Generation (MW)
Bus-1	23.54
Bus-2	60.97
Bus-22	21.59
Bus-27	26.91
Bus-23	19.2
Bus-13	37.0

Table 2 Wind speed data

Parameter	Value
Wind speed-maximum	28.789 (m/s)
Wind speed-minimum	14.248 (m/s)
Mean wind speed-4 years	24.358 (m/s)
Variance-σ	10.654

3.2 Data Analysis

The collection of data is done for a window of four years, i.e., 1st January 2014–31st December 2018. The wind data is collected and assessed at an interval of 3 h for each day. After obtaining the data, meticulous analysis is done on it. PDF and CDF are obtained in the MATH WAVE environment. Statistical analysis is presented in [9]. The wind speed data follows a lognormal distribution. The wind speed is then converted into the required power input samples [9]. These power input samples are distributed normally. The most variable month for wind speed accounted for was the month of June. Most of the uncertainties in input were supplemented by this month. Table 2 gives the maximum and minimum wind speed limit from the accessible data.

The 1000 random samples are generated in MATLAB environment from the mean and variance followed by the wind speed.

3.3 Assumptions

For the computation of LMP, bus number 1 is considered to be the slack bus and kept untouched. The wind plant is integrated into the grid firstly at bus number 23 as the generation at this bus is minimum i.e. 19.2 MW. To match the practical aspect of the wind plant, wind generator data of 'GE 1.5 SLE' [11] is considered. The output power of the wind plant is scaled to this generator. Table 3 represents the technical data for GE 1.5 SLE.

One generator of GE 1.5 SLE is rated to 1.5 MW and the wind farm integrated into the transmission network is of 19.2 MW. Hence, the wind farm consists of 13

Table 3 Technical data-GE 1.5 SLE

Parameter	Value
Cut-in-speed	3.5 m/s
Cut-out-speed	30 m/s
Rated wind speed	12 m/s
Swept area	4567 m^2
Rotor diameter	77 m
Output power	1.5 MW

Table 4 Test cases

Base case	Conventional generator
Cases	Wind farm integration at
1	Bus-23
2	Bus-2
3	Bus-22
4	Bus-27
5	Bus-13

GE 1.5 SLE generators [$13 \times 1.5 = 19.5$ MW]. To study the variation in LMP 5 different cases where the wind farm is integrated at different locations are considered for the analysis. Table 4 gives the details for all the cases.

4 LMP Algorithm

To compute the LMP values at every node within the system, the following steps were approached:

1. Run DC-P-OPF in MATPOWER environment with all conventional generators into the system.
2. Obtain the base LMPs for every bus representing the non-congestion scenario.
3. Integrate the wind farm as per case 1, with uncertain generation record the new LMPs for case 1.
4. Run DC-P-OPF for all the remaining cases to record the variation in LMPs.

4.1 Mathematical Calculation

The optimized mathematical equation of LMP is

$$\begin{aligned} \text{Minimize}: \ & C^T * P_g = b^T P_L \\ \text{Subject to}: \ & P_{gmin} \le P_g \le P_{gmax} \end{aligned}$$

$$P_{Lmin} \leq P_L \leq P_{Lmax} \quad (2)$$

c = bid of generator zone,
b = bid of load zone,
P_{gmin}, P_{gmax} = lower and upper limit of energy for generation,
P_{Lmin}, P_{Lmax} = lower and upper limit of energy for load.

5 Results

DC-P-OPF run for the base case provided the base LMP value for comparison of the LMP values post wind integration. The LMP values recorded are in $/MWh. The base case LMP for conventional generation obtained is 3.635 and considered as reference LMP for comparison of remaining cases. Table 5 presents the nodal price values for all 5 cases with wind generation.

The congestion occurrence into the transmission lines is calculated using the performance index for all 5 cases shown in Table 6.

Figure 1 is the graphical representation of base LMP and new LMP values.

6 Discussion

From Table 5, the base LMP value indicates the non-congestion scenario with a system operating without violating any transmission constraint. In base case LMP, the congestion cost factor accounts to be zero. Post integration it can be clearly seen that for all 5 cases the LMP varies along with the variation in wind plant input. The LMP varies to a greater extent over different buses for all the cases considered. On observing keenly, the LMP variation indicates the congestion scenario for different cases. The LMP values above the base LMP indicate a violation of system constraints. Table 6 gives the performance index for all 5 cases. It can be understood from the values that for any case the system undergoes congestion increasing the LMP under the worst-case scenario of wind plant. From the PI it can be understood that if the wind plant is integrated at bus-13 and 23 it gives the higher congestion within the system, whereas when the wind farm is integrated at bus-27 gives minimum congestion and hereby reducing the congestion cost factor in the LMP. The graph resembles the same. Later on, the bids can be allotted from producers and consumers upon the minimum LMP values. The variation in the LMP and violation of transmission congestion is due to uncertain wind input and location of the wind farm.

Table 5 LMP values for all 5 cases for all 30 buses

Bus number	Base LMP	Case 1	Case 2	Case 3	Case 4	Case 5
1	3.635	3.347	4.393	4.565	4.766	2.324
2	3.635	4.675	4.522	2.112	4.545	4.567
3	3.635	4.878	4.572	4.678	3.876	4.666
4	3.635	3.662	4.561	5.123	3.982	4.867
5	3.635	4.234	4.572	4.332	2.980	3.435
6	3.635	2.345	4.531	4.567	4.991	1.237
7	3.635	4.364	4.664	3.443	4.785	8.432
8	3.635	5.332	4.664	4.665	2.764	1.323
9	3.635	4.121	4.614	1.234	2.975	3.456
10	3.635	4.454	5.132	4.675	3.331	4.120
11	3.635	6.556	5.489	1.234	4.768	8.675
12	3.635	5.122	5.122	8.456	4.567	9.876
13	3.635	4.213	4.911	5.123	4.218	8.345
14	3.635	0.908	2.626	6.778	2.564	7.776
15	3.635	5.353	4.265	3.111	4.121	6.545
16	3.635	8.487	4.881	5.454	4.098	6.089
17	3.635	2.764	5.221	1.120	4.001	1.223
18	3.635	3.699	4.765	2.334	2.335	8.767
19	3.635	6.638	4.983	7.898	3.435	4.546
20	3.635	8.831	5.071	4.456	2.349	9.675
21	3.635	3.864	8.101	1.128	2.459	3.345
22	3.635	7.505	0.997	0.876	3.114	8.886
23	3.635	5.069	3.422	2.347	4.536	7.668
24	3.635	8.811	2.864	1.354	2.111	6.123
25	3.635	3.604	3.168	10.871	3.431	5.436
26	3.635	3.324	3.693	3.478	4.087	7.789
27	3.635	3.873	3.598	4.568	4.576	4.567
28	3.635	0.805	4.554	2.348	4.098	7.341
29	3.635	7.034	3.535	0.111	3.121	7.347
30	3.635	2.704	3.542	6.343	3.121	4.331

Table 6 Performance Index (PI) reflecting congestion scenario

Case	Case 1	Case 2	Case 3	Case 4	Case 5
Mean	4.707	4.317	3.959	3.673	5.759
Median	4.429	4.574	4.394	3.929	5.763
Variance	4.215	1.499	6.193	0.737	6.596
PI (%)	−30	−19	−9	−1	−58

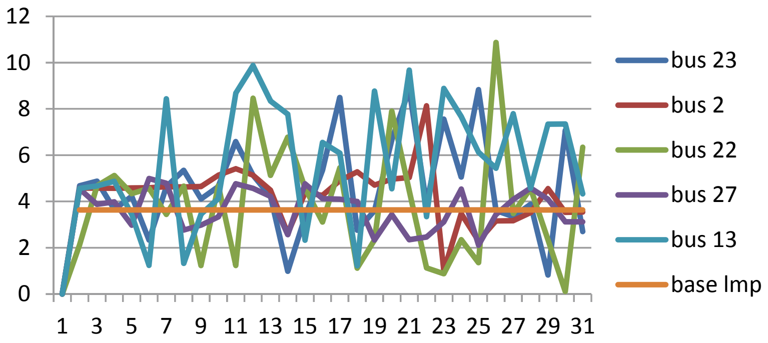

Fig. 1 LMP variation with uncertain wind generation of all 5 cases with respect to base LMP

7 Conclusion and Future Scope

7.1 Conclusion

Owing to suspicions at hand in renewable energy sources, it is indispensable to have former awareness of system performance under these circumstances. This requires a comprehensive revision, for instance, made in this work. The incorporation of wind farms into the accessible system not only affects the power flow in the network but also varies the LMPs foremost to the congestion state of affairs and inclusion of congestion cost. Moreover, it is obvious that it is not straightforwardly predictable devoid of this kind of extended analysis that which of the bus node is gravely exaggerated due to uncertainties miscellaneous with a contingency. This analysis provides a trouble-free and accessible methodology for the computation of LMPs of every node under the influence of uncertainty in wind generation. Computation and analysis of LMP is an imperative pace to estimate the network rental, system reliability margins, congestion cost and manage the system congestion. The analysis indicates that LMP depends mainly upon the location of the solar farm. The larger the difference between the base and new LMP, the higher is the congestion introduced into the system increasing the congestion cost, which increases the burden on the generation companies. By analyzing the different locations prior, we can be able to manage the congestion into the system. This analysis gives the commercial aspect to manage the congestion from an economical aspect; consequently, it can also be expanded to a practical system incorporated with an uncertain wind farm.

7.2 Future Scope

This analysis can be willingly mitigated to a realistic and real-time-based system integrated with wind farms. The most favorable and optimized location can be thought of to utilize most of the available wind power without jeopardizing the system security. Linear Sensitivity factors and LMPs are cooperative in shaping the factors like Transmission Reliability Margin (TRM), Available Transfer Capability (ATC), reliability margins, and congestion cost burden which forms a base building block in congestion management.

Acknowledgements The authors would like to thank the Indian Meteorological Department, Pune, and Poornima University, Jaipur, India, for their precious hold up in providing the data points for research and analysis purposes, facilities. Devoid of their continuous support this analysis possibly may not have been progressed.

References

1. Yu J (2006) Locational marginal pricing in ERCOT market. In: 2006 IEEE Power Engineering Society General Meeting, Montreal, Que., 3 pp. https://doi.org/10.1109/pes.2006.1708980
2. Ge Z, Ge M, Yang L, Wang D (2008) Locational marginal price of East China Electric Power Market. In: 2008 Third international conference on electric utility deregulation and restructuring and power technologies, Nanjing, pp 214–217. https://doi.org/10.1109/drpt.2008.4523405
3. Albadi MH, El-Rayani YM, El-Saadany EF, Al-Riyami HA (2017) Effect of large solar power plant on locational marginal prices in Oman. In: 2017 IEEE 30th Canadian conference on electrical and computer engineering (CCECE), Windsor, ON, pp 1–4. https://doi.org/10.1109/ccece.2017.7946741
4. Umale VG, Warkad SB (2017) Locational marginal transmission pricing for 765 kV transmission line. In: 2017 IEEE international conference on circuits and systems (ICCS), Thiruvananthapuram, pp 40–42. https://doi.org/10.1109/iccs1.2017.8325959
5. Nwulu NI (2017) Modelling locational marginal prices using decision trees. In: 2017 international conference on information and communication technologies (ICICT), Karachi, pp 156–159. https://doi.org/10.1109/icict.2017.8320181
6. Umale VG, Warkad SB (2017) Locational marginal pricing based financial transmission right. In: 2017 IEEE international conference on circuits and systems (ICCS), Thiruvananthapuram, pp 459–462. https://doi.org/10.1109/iccs1.2017.8326042
7. Jain R, Mahajan V (2017) Computation of locational marginal price in power market in different load and system conditions. In: 2017 14th IEEE India council international conference (INDICON), Roorkee, 2017, pp 1–6. https://doi.org/10.1109/INDICON.2017.8487527
8. Morstyn T, Teytelboym A, Hepburn C, McCulloch MD (2020) Integrating P2P energy trading with probabilistic distribution locational marginal pricing. IEEE Trans Smart Grid 11(4):3095–3106. https://doi.org/10.1109/TSG.2019.2963238
9. Dhabai P, Tiwari N (2020) Effect of stochastic nature and location change of wind and solar generation on transmission lattice power flows. In: 2020 international conference for emerging technology (INCET), Belgaum, India, pp 1–5. https://doi.org/10.1109/INCET49848.2020.9154035
10. Kristiansen T. Utilizing matpower in optimal power flow
11. Wind data sheet, GE Energy. www.ge-energy.com/wind (2009) (Online)
12. Burke DJ, Malley MJO. Optimal wind power location on transmission system—a probabilistic load flow approach. Member IEEE

Chapter 6
Optimal Integration of Plug-in Electric Vehicles Within a Distribution Network Using Genetic Algorithm

Sakshi Gupta, D. Saxena, Mukesh Kumar Shah, and Rajeev Kumar Chauhan

Abstract This chapter mainly discusses and analyzes two smart charging approaches with objective functions as optimization of total daily cost (TDC) acquired by the charging facilitator and peak to average ratio (PAR), in that order to examine the effect on electric vehicle (EV) charging from both commercial and technical aspects. The proposed approaches are then executed on the industrial nodes of an 11 kV 37-bus distribution system to study the impacts as we increase the percentage penetration. Any system can accommodate a limited amount of EV penetration into it after which voltage and loading limits start to exceed. In this manner, here we are attempting to assess the most extreme conceivable PEV penetration by which the distribution system can entertain relating to both procedures.

Keywords Plug-in electric vehicle · Optimization · Charging strategies · State-of-charge · Genetic algorithm · Load flow

1 Introduction

In last years, electric vehicles have seen a stable increment in proving itself as a sustainable alternative to commercial cars used from years running on petrol and diesel. Due to various environmental boons such as decreased fossil fuel consumption, reduced greenhouse gas releases, etc., many administrations of various countries

S. Gupta · D. Saxena (✉) · M. K. Shah
Department of Electrical Engineering, MNIT, Jaipur, India
e-mail: dsaxena.ee@mnit.ac.in

S. Gupta
e-mail: 2018psm5424@mnit.ac.in

M. K. Shah
e-mail: mkshah.ee@mnit.ac.in

R. K. Chauhan
IMS Engineering College, Ghaziabad, Uttar Pradesh, India
e-mail: mmmec.rkc@gmail.com

R. N. Shaw et al. (eds.), *AI and IOT in Renewable Energy*,
Studies in Infrastructure and Control,
https://doi.org/10.1007/978-981-16-1011-0_7

are trying various measures to increase the integration and development of EVs in the distribution framework. One of the key concerns of using electric vehicles (EVs) is their charging time and places. Most of the EVs are charged using a wired connection between the low voltage (LV) distribution system and the vehicle. Such types of EV, having the likelihood to be associated with the infrastructure, are called plug-in electric vehicle (PEV). Turker and Bacha [1] Proposed a contemporary vehicle to grid (V2G) methodology called Optimal Logical Control (V2G-OLC) based upon logical command series and compared it with classical optimal charging methodologies available with the main aim to minimize the charging cost incurred. Wei et al. [2] Designed an operating model for cost minimization to discuss the issue of EV charging in a park-and-charge arrangement. A system for ongoing charging the executives of an electric vehicle aggregator (EVA) taking an interest in electric vitality and guideline markets was presented in [3]. Tan and Wang [4] Considered the influence of EV charging process on both, transportation system and power system. For this purpose, an integrated real-time EV charging navigation framework was developed, modeling the struggle between electric vehicle charging stations (EVCSs) with a non-cooperative game approach. Jeong et al. [5] Used a dynamic wireless charging (DWC) technology which lets the batteries to get charged automatically while the electric vehicles (EVs) are in motion. Kong and Karagiannidis [6] Presented a review of all the plug-in hybrid electric vehicle (PHEV) battery charging techniques prevailing in the system. Wu et al. [7] Centres on the difficulties of energy planning for places of business incorporated with photovoltaic frameworks and work environment EV charging. Crow [8] Discussed the issues of overloading the distribution line due to EV charging and mitigating them through real-time (dynamic) and day-ahead (static) frameworks, using continuous and discrete charging rates. Zheng [9] Discusses an aggregation charging model for vast number of EVs employing GA to reduce the variations in power levels due to electric vehicle charging characteristics. There is a noteworthy increase in the EV penetration in urban areas. In such situation, power outages may occur if uncoordinated charging is done. Therefore, productive EV charging the board is required for overseeing and assigning scant charging station assets [10]. Different charging procedures, considering just the G2V framework, have likewise been suggested in the writing which might lessen the effects of PEVs on the energy framework [11–14].

Due to advancement in technology, immediate charging of PEVs is possible by directly plugging them into the electrical power supply. Thus, this may lead to uncontrolled charging of a certain number of PEVs which may result in increased demand thus leading to various problems such as peak power, overload issues, increment in energy losses, reduction of distribution transformer (DT) lifetime, and voltage deviations. These problems concerning the distribution system depend on various other factors like number of PEVs integrating the system, their charging power, connection and disconnection time, energy demand, charging and discharging efficiency, etc. Therefore, it is required to develop some charging methodologies to find out and compare the effects of the integration of PEVs at various penetration rates. The objective of this chapter is to formulate smart charging methodologies for PEVs integration in the distribution network optimally taking into account a unified G2V and V2G charging scheme. For this purpose, two smart charging strategies have been implemented using Genetic Algorithms with heuristic initialization. Later on, the proposed smart charging strategies were tested on 37-node distribution network using backward forward load flow to identify the most extreme conceivable PEV penetration by which the distribution system can entertain relating to both the procedures in the lateral.

2 Problem Overview

The principle focus of this chapter is workplace automobile parking lots where vehicles are parked in the day time in the industrial framework of a distribution network.

The industrial area where the study is done is expected to have a parking space for thousand vehicles including conventional and PHEVs both. The cars are parked in specifically allotted areas in the car park which have charging slots for PEVs armed with V2G and G2V both the functionalities. Every parking lot in the industrial lateral is thought to be undertaken by a charging facilitator which performs PEVs smart charging.

As PEVs arrive in the car parking lot, the owners of PEV provides their STD, initial SOC (i.e., current State of Charge), PEV specifications (Battery capacity of PEV and driving range of automobile known as all electric range (AER)), and predicted duration of parking to the charging facilitator. PEV specifications need not be submitted by the PEV owner daily. It can just be entered once (at the time of arrival) for the record and used in future. On the basis of information collected from the PEV owner, the charging facilitator calculates the total required energy by PEVs and then an optimized and effective charging schedule of PEV is generated utilizing a smart charging methodology. Accordingly, the charging load of PEVs is included ideally into the total industrial lateral's load demand on half-hourly basis. The charging methodology used by the charging facilitator is chosen relying on the prerequisites which may be financial or technical. Here, two smart charging methodologies, which depend on optimization of total daily cost (TDC) and peak to average ratio (PAR), individually, are executed for optimal penetration of PEVs, and a systematic investigation is then carried to assess the most extreme conceivable PEV penetration that the presented techniques can incorporate inside the current distribution framework.

2.1 Modeling PVE's Driving Pattern

To optimally integrate the PEVs into the distribution network, the total energy demand which requires to be managed and controlled intelligently is important to be estimated. Thus, modeling of energy requirement of PEVs is important.

PEV charging happens during the daytime in the car parking lots. During the daytime, cost of power is high so the charging of PEVs to its maximum value of SOC is kept away from and the charging as indicated by PEVs' next tour is executed [15]. For the examination, the data identifying with the following mentioned characteristics is embraced from reads which led for Singapore [16–18].

2.2 Distance Travelled Per Trip and Daily Mileage

The typical Daily Mileage traveled by a person is the aggregate number of miles traveled over in a given time by a private automobile. Normal distribution data is generated for daily mileage from data taken from [15]. It is expected that automobiles reach the parking lot toward the finish of the 1st trip of the day. In this way, the first trip distance is characterized as the separation which a PEV goes before reaching the vehicle parking area. Figure 1 and Fig. 2 show the pdf (probability density function) and normal distribution curve obtained for the daily mileage and first trip distance traveled, respectively.

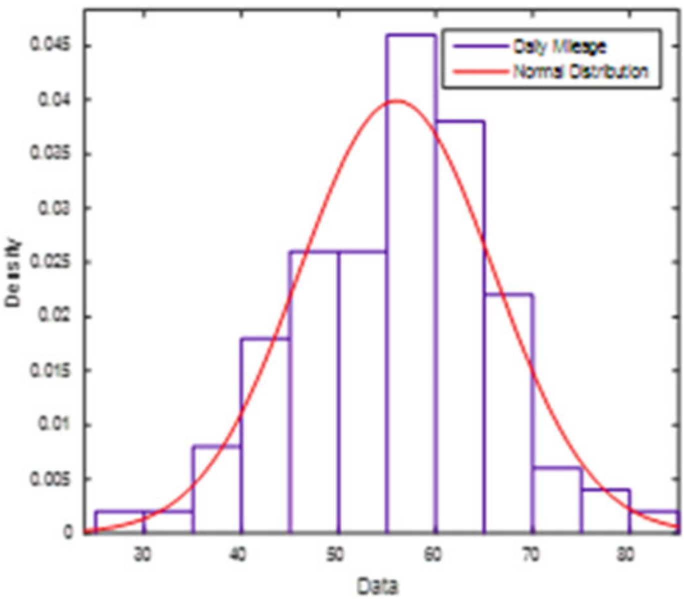

Fig. 1 Average daily mileage

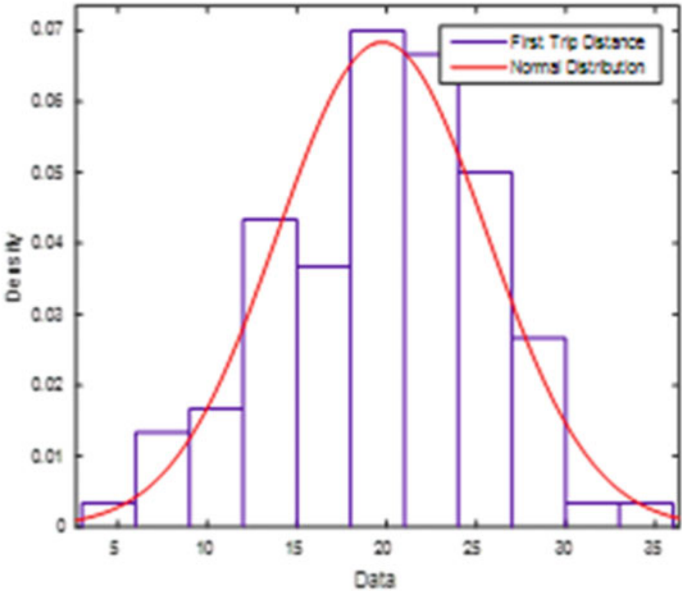

Fig. 2 First trip distance

3 Subsequent Trip Distance (STD)

The assessment of desired SOC at the departure time is subject to the assessment of length to be gone for the following outing, which is a feasible errand for anyone driving a PEV. Subsequent Trip Distance is characterized as mileage of all the resulting tours that are taken by a PEV in the wake of leaving from car parking lot and before at long last showing up at home. Here, STD is determined utilizing the normal distribution for the distance traveled per trip and daily mileage. Hereinafter, we have discussed PEVs arrival and departure times in Sect. 3.1. Sections 3.2 and 3.3 provide initial SOC and desired departure time SOC of PEVs and PEVs energy requirement (Figs. 3 and 4).

3.1 PEVs Arrival and Departure Times

In this chapter, the charging car park is assumed to be situated in the industrial lateral which is active from 9:00 a.m. to 6:00 p.m. using the attributes of the normal distribution provided in Table 1, and a normally distributed pdf of arrival and departure time values are created. Combining the pdfs (probability density functions) of A_t (Arrival Time) and D_t (Departure Time), the combined pdf of $D_t - A_t$ can be created,

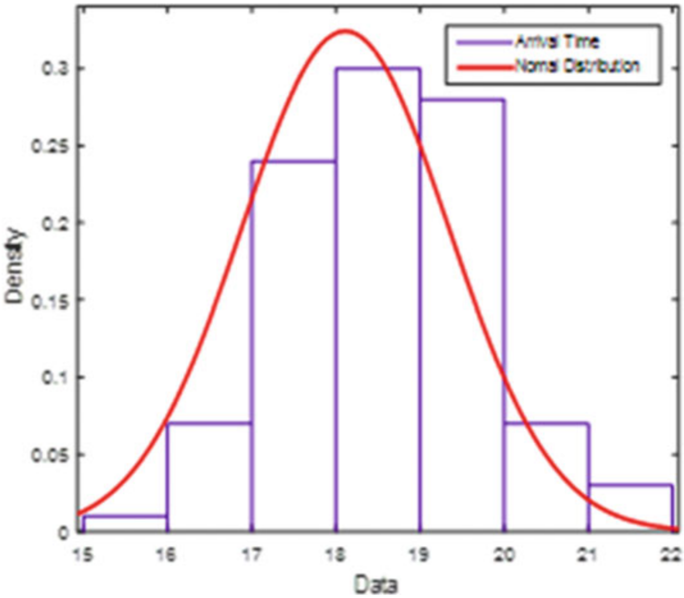

Fig. 3 Arrival time

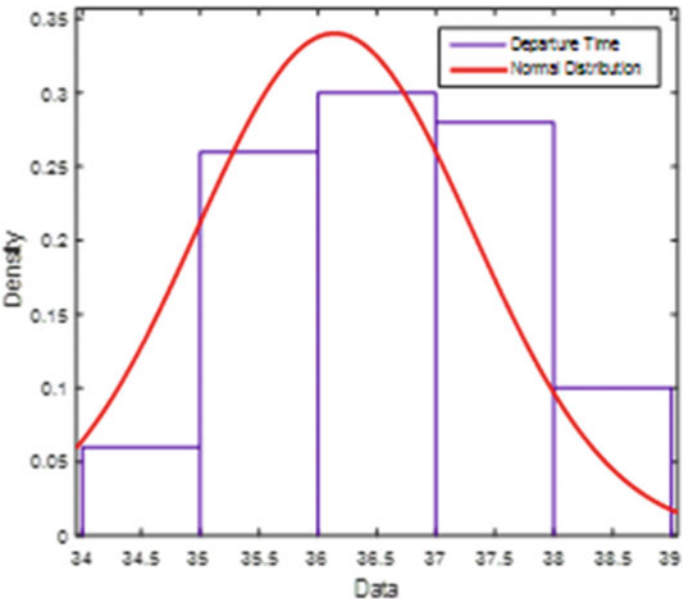

Fig. 4 Departure time

Table 1 Parameters of the duration time probability distribution

Time parameter	Arrival	Departure
μ	9	18
σ^2	1.2	1.2

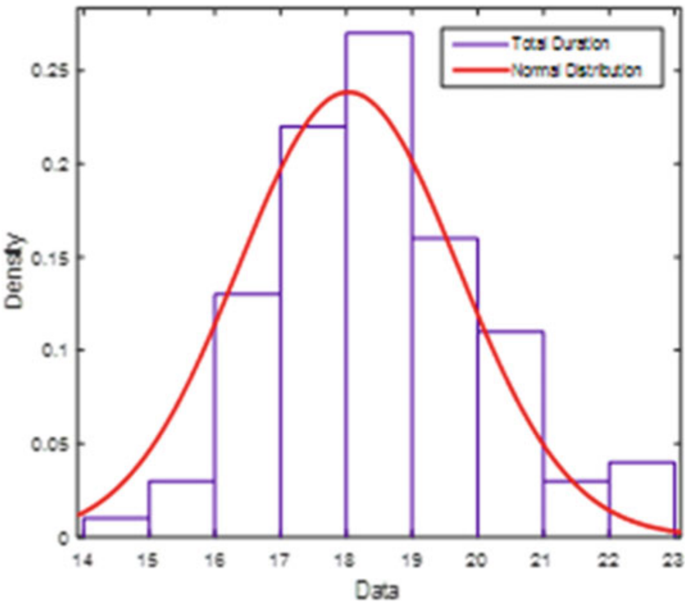

Fig. 5 Total duration

which is basically the total duration for which the PEV is parked daily. The daily parking duration time pdf is presented in Fig. 5.

3.2 *Initial SOC and Desired Departure Time SOC of PEVs*

The state of charge is a measurement of the amount of energy available in a PEV battery at a definite point in time. So as to increase the battery timespan, the base SOC of battery is taken to be 0.2 in this chapter. Starting SOC of PEVs at the hour of arrival in parking lot is calculated depending on the AER and first trip distance. SOC_A of a PEV ensuring an AER (all electric range) of d_R and d as its first trip distance can be determined by Eq. (1):

$$SOC_A = 1 - (d/d_R). \quad (1)$$

Similarly, STD and AER values are utilized to determine the desired SOC at departure time (SOC_D) of PEVs, as shown in Eq. (2):

$$SOC_D = (STD/d_R) + 0.2. \quad (2)$$

It is likewise noticed that the fundamental data with respect to the initial SOC, that is to be given to the charging facilitator, is legitimately accessible to the PEV proprietor (similar to the ordinary vehicle clients knowing the position of their fuel tank).

3.3 PEVs Energy Requirement

Depending on the arrival (SOC_A) and departure time SOC (SOC_D), the required energy of every individual PEVs (E_{req}) can be calculated by Eqs. (3) and (4):

$$SOC_{req} = \begin{cases} 1 - SOCA, & SOCD \geq 1 \\ (SOCD - SOCA), & SOCA < SOCD < 1 \\ 0, & SOCD = SOCA \\ -(SOCA - SOCD), & 0.2 < SOCD < SOCA \end{cases} \quad (3)$$

$$E_{req} = \left(SOC_{req} \cdot B_C\right)/\eta. \quad (4)$$

The efficiency coefficient (η) is shown as.

(1) η_c, $\eta_c = 0.9$ when PEVs are charging, and
(2) $1/\eta_D$, $\eta_D = 0.95$ when PEVs are discharging.

4 Problem Formulation

After the calculation of all the attributes and the energy requirement by PEVs, charging strategy vectors are generated. These vectors will ultimately be used in the smart charging strategy objectives. Therefore, the optimization of problem statement for the two brilliant charging methodologies that are discussed in this chapter is taken from [15]. The generation of a charging strategy vector for charging and discharging is represented by C_k and D_k, and their formulation is given in [15]. The time skyline vector is depicted by W = [1, ..., t, ..., T] and incorporates '48' equivalent half-hour time allotments. The quantity of PEVs showing up in car parking lot during a specific timespan t is shown by a vector Z = [1, .., k, ..., N].

At any time period *t,* the total industrial load demand after *N* PEVs which are integrated is calculated as

$$P^t_{\text{total}} = P^t_{\text{total}} + P^t_{PEV}, \quad \forall t \in W. \quad (5)$$

It is noticed that the total load demand in the industrial area *($P^t{}_{\text{total}}$)* before joining of any PEVs is identical to $P^t{}_{\text{base}}$. At any time period *t,* the industrial lateral has how much total power after the penetration of *N* number of PEVs is shown as

$$S_{\text{total}}^t = \sqrt{\left(P_{\text{total}}^t\right)^2 + \left(Q_{\text{base}}^t\right)^2}, \quad \forall t \in W. \tag{6}$$

Hereinafter, we have considered Sects. 4.1, 4.2, and 4.3 for discussing the different strategies for charging the EVs.

4.1 Charging Strategy A

The main agenda of this methodology is to optimize the total daily cost (TDC) acquired by the charging facilitator who is in charge of organizing the charging and discharging operation of PEVs in the car park. The TDC incurred by it is divided into two parts, i.e., the cost of charging ($\text{Cost}_{\text{charge}}$) and the cost of battery degradation (Cost_{bat}). The $\text{Cost}_{\text{charge}}$ is represented by Eq. (7), and it includes charging cost of PEV aside from the credits earned from PEV discharging

$$\text{Cost}_{\text{charge}} = \sum_{t=1}^{T} \left(\sum_{k=1}^{N} \left(C_k^t - D_k^t\right) * r_{PEV,k} \right) \cdot RTP(t). \tag{7}$$

Here, the Real Time Price (RTP) data needed for this charging technique is the predicted price information of the whole day that is made accessible by the distribution system operator to the charging facilitator, and $r_{PEV,k}$ is the rate at which a particular *k*th PEV is charged or discharged.

Due to the implementation of V2G technology, the EV batteries also degrade and their efficiency reduces. Thus, the battery degradation cost (Cost_{bat}) is represented by the following equation [15]:

$$\text{Cost}_{\text{bat}} = \sum_{k=1}^{N} \left(c_{b,k} E_{b,k} + c_L\right) \cdot E_{dis,k} / \left(L_c E_{b,k} DOD\right). \tag{8}$$

The TDC acquired by the charging facilitator is therefore given as the summation of these two costs:

$$\text{Cost}_{\text{total}} = \text{Cost}_{\text{charge}} + \text{Cost}_{\text{bat}}. \tag{9}$$

Therefore, the aim of Strategy A is shown as

$$\min\{\text{Cost}_{\text{total}}\}. \tag{10}$$

4.2 Charging Strategy B

The principle goal of this methodology is to limit the peak demand and straighten the demand. The aim of limiting the peak demand and straightening the overall load demand is accomplished by minimization of PAR [19], determined by the condition as demonstrated below (11)

$$PAR = \frac{\max\limits_{t \epsilon H} S_{\text{total}}^t}{\frac{\sum_{t=1}^T S_{\text{total}}^t}{T}}. \tag{11}$$

Therefore, the aim of Strategy B is shown as

$$\min\{PAR\}. \tag{12}$$

4.3 Smart Charging Strategy Constraints

Following constraints must be considered, for satisfying the PEVs energy requirement for both the strategies A and B.

$$\sum_{t=t_{in},k}^{t_{out},k} S_k^t . r_{PEV,k} = E_{req,k} \; \forall k \in Z. \tag{13}$$

Some other constraints like PEVs' battery SOC constraint and the charging framework constraint are shown by (14) and (15), respectively.

$$\text{SOC}_{\min} \leq \text{SOC}_k^t \leq \text{SOC}_{\max} \; \forall t \in H; k \in Z, \tag{14}$$

$$0 \leq r_{PEV,k} \leq P_{rated}, \quad \forall k \in Z. \tag{15}$$

$\text{SOC}_{\min}$ and $\text{SOC}_{\max}$ values are taken to be 0.2 and 1, respectively, for the purpose of this study. This is to be seen that for both the charging methodologies A and B, the optimization problem is evaluated for N PEVs incorporating at a specific timespan t, for example, N is the quantity of PEVs showing up at the car parking lot at a specific timespan t. For the optimal integration of the PEVs in the car parking lot, optimization is carried out each half-hour with the goal that we can adequately consider each PEV showing up at a specific timespan t. Additionally, the absolute PEV integration in the industrialized area is the sum total of each and every PEVs showing up in parking lots at every timespan t. The PEV integration in the grid is divided into 10 stages considering step size increases by 10%. Beginning from the least integration level, the smart charging system and the investigation technique decides most extreme conceivable penetration of PEV for which as far as possible loading and the voltage limits of the DT and distribution lines are not exceeded. The limitations identified with the distribution framework and voltage limits are as per the following.

$$V_i^{\min} \leq V_i \leq V_i^{\max}, \tag{16}$$

$$S_{\text{agg}}^t < T_{\text{rat}}, \quad \forall t \in H, \tag{17}$$

$$SP_i \leq SP_i^{\max}. \tag{18}$$

5 Implementation of Charging Strategies

The smart charging strategies are implemented using genetic algorithm. For the execution of the charging techniques, as the search space of the improvement issue for both the approaches is exceptionally huge, therefore it would be more feasible to employ heuristic initialization rather than going for random population initialization. Thus, heuristic initialization is used to tackle this complicated issue by lessening down the search space.

A. **Chromosome Representation**

For the motive of this work and to implement Genetic Algorithm, chromosome creation is the basic step to start with. Here, for representing a chromosome an (N × T) matrix is created, where N denotes the amount of PEVs reaching the car parking lot at a specific time span t and T indicates the overall time period. Also, every row of the chromosome is depicted by a strategy vector S for every PEV.

B. **Heuristic Initialization**

After the chromosome is created, we need to initialize the population in GA. For this purpose, as discussed above we are using heuristic initialization. In this, a possible strategy matrix (PSM) is created meant for every PEV entering the car parking lot that contains all the permissible strategy vectors S_k and also satisfies constraint (13) for corresponding PEVs.

C. **Implementation of GA**

After initializing the initial population, GA can be implemented using three operators as described below.

1. Selection operator: Roulette wheel selection is used.

2. Crossover operator: In this study, two-point row crossover is used for the crossover operation. In two-point row crossover, two parents are randomly selected and then two rows are randomly selected from it. The records in the two rows are then interchanged amid the 2 parents to produce the two offspring.
3. Mutation operator: Here, flip mutation is used with objective-specific amendments. Every row of each chromosome, i.e., the strategy vector Sk is flipped with a certain mutation probability, for a specific PEV with alternative strategy vector for the same PEV picked from its FSM.

6 Results and Discussion

The presented smart charging approaches are employed in the industrial nodes of an 11 kV 37-node distribution network for the purpose of optimum integration of PEVs in distribution infrastructure. The network and load attributes of 37-bus distribution network are taken from [20]. For the base load of the industrial area, i.e., non-PEV load, as presented in Fig. 7, power factor is supposed to be 0.85. Furthermore, rating of the DT providing the demand in the industrialized area is taken as 1 MVA. In this way, the base load curve for the modern parallel is likewise the load curve of the DT.

In this work, for the purpose of load flow studies on the distribution network, BFS (backward-forward sweep) technique is used. The loading and voltage limits of the DT and distribution lines are taken from [15].

In this chapter, PHEV-30 (numerical subscript represents the AER of the vehicle in miles) is considered for the integration in the lateral. It has a battery capacity of 13.8 kWh [15]. The annual average RTP information is acquired from the data taken from Energy Market Authority, Singapore as shown in Fig. 6 [21]. Depending on the base load profile of industrial (non-PEV) load as shown in Fig. 7, performance of both the proposed methodologies are compared and this analysis is carried out below. The charging slots installed in the car parking lots are assumed to have a power rating of 2 kW.

Figure 8 shows the optimized total cost incurred by the charging facilitator in strategy A at different penetration levels by running GA for 200 iterations. Similarly, Fig. 9 shows the optimized PAR values obtained corresponding to each penetration level.

Values of TDC and PAR at each penetration level are calculated for both the strategies as shown in Table 2. Along with that Table 2 also encapsulates the corresponding peak load of DT.

Table 3 gives the total peak load obtained at each penetration level for both the strategies and shows us that Strategy A runs feasibly up to 10% PEV penetration, while Strategy B runs feasibly up to 60% PEV penetration. Since the loading limit of the DT is 1 MVA, after 10% PEV penetration peak load for Strategy A exceeds the loading limits. Similarly, it was noted that after 60% PEV penetration for Strategy *B*, loading limits were exceeded of the DT. Thus, the maximum conceivable penetration of PEVs subject *Strategy A* is 10% and for *Strategy B* is 60%.

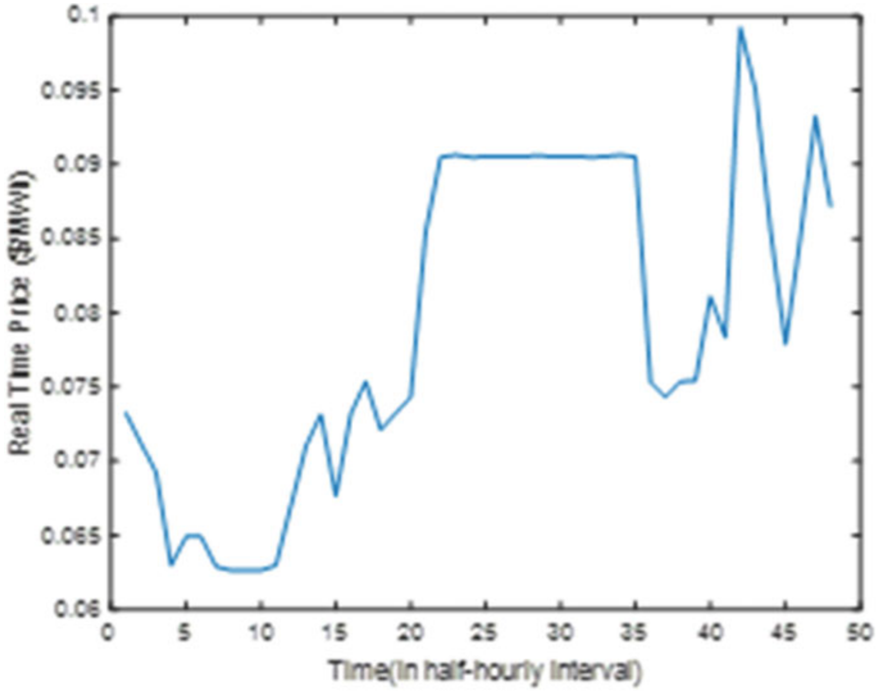

Fig. 6 Annual average real time pricing data

Load demand profile of the DT for various integration stages of PEV attained from Strategy A and B, respectively, is presented in Fig. 10a, b. It can be easily concluded from Fig. 10 that for Strategy A, the load limit of the DT, i.e., 1 MVA is exceeded by the peak load after 10% PEV penetration while in Strategy B it happens after 60% PEV penetration.

It can be noted from both the graphs shown in Fig. 10a, b that the load demand profiles of the DT are different from each other for the smart charging strategies proposed. This is the result of charging methodologies using different objective functions for optimization for both strategies used.

Strategy*A* focuses on TDC optimization/minimization as its target considering economic point of view. This results in multiple peaks and drops in the load profile generating due to charging and discharging operations while scheduling PEVs depending on the high and low pricing structure (RTP). Contrary to that, Strategy B focuses on the optimization of the peak-to-average (PAR) ratio as its objective which in turn results in the flattening of curve of the industrial load. This declaration can be backed up by Fig. 10b showing an almost flat profile of the load compared to that in Fig. 10a.

Thus, it can be concluded that Strategy A should be opted if the main target is to minimize the TDC that is acquired by the charging facilitator to minimize its expenses but its drawback will be that it will not be possible to penetrate vast number of PEVs

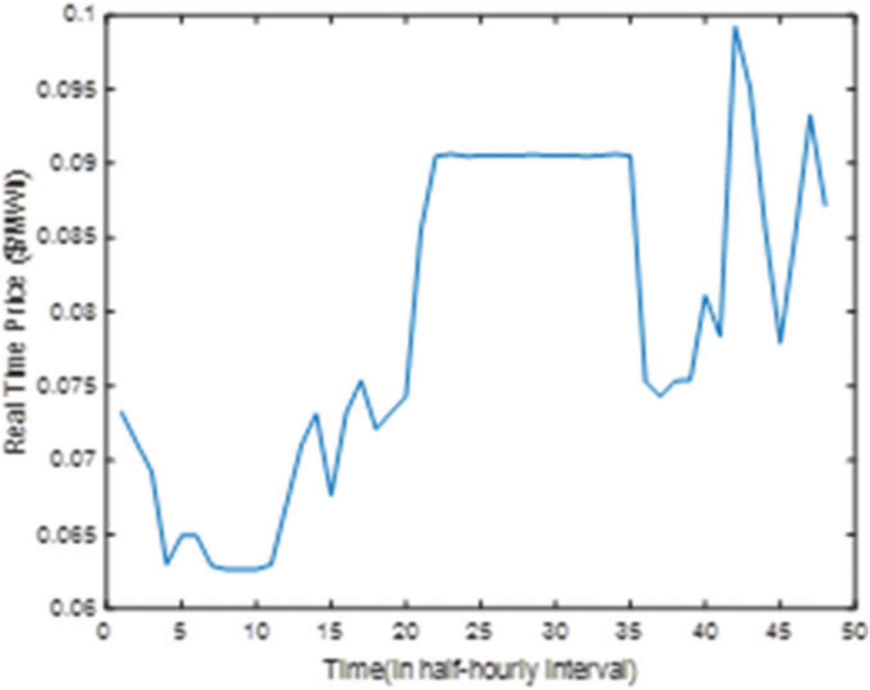

Fig. 7 Industrial based (non-PEV) power demand

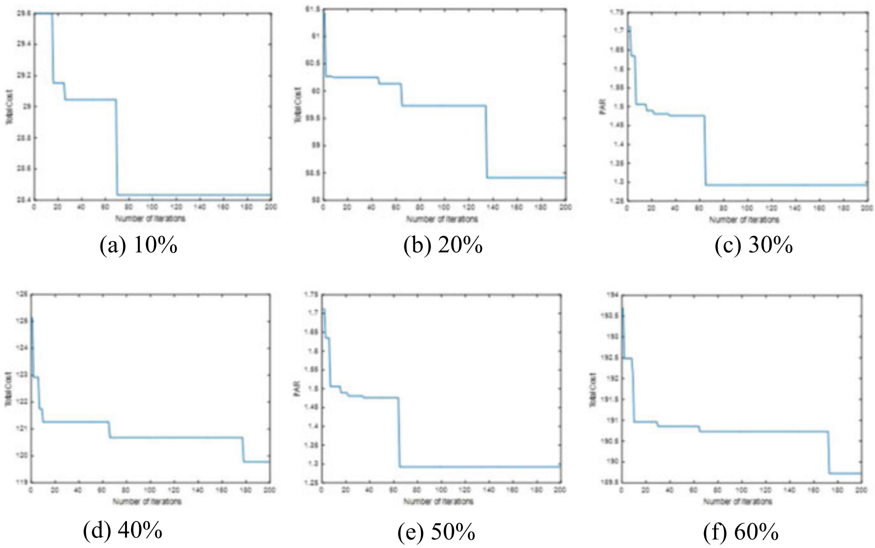

Fig. 8 Total daily cost (TDC) incurred at different penetration levels from

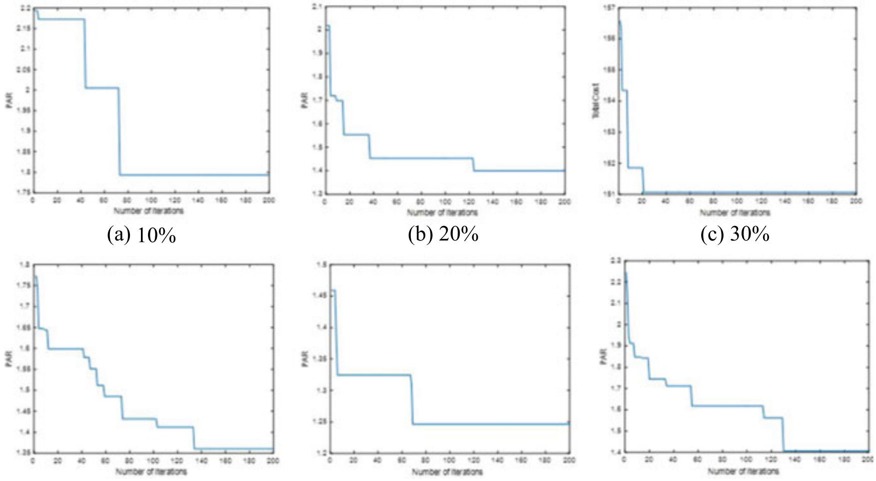

(a) 10% (b) 20% (c) 30%

(d) 40% (e) 50% (f) 60%

Fig. 9 PAR value obtained at different penetration levels from **a** to **f**

Table 2 Various attributes attained for both the charging schemes at different levels of PEV penetration

PEV penetration (%)	Strategy	TDC (S$)	PAR	Peak load increment (%)
10	A	$28.433	1.3541	3
	B	$30.584	1.2463	10
20	A	$58.413	1.3973	36
	B	$65.260	1.2924	−2
30	A	$89.376	1.4485	30
	B	$96.813	1.3600	−5
40	A	$119.777	1.4872	45
	B	$127.856	1.3994	5
50	A	$151.066	1.4995	44
	B	$159.715	1.4065	26
60	A	$189.727	1.8764	50
	B	$198.483	1.7933	−12

into the network without compromising on the grid stability. Whereas, Strategy B must be considered if the main purpose is to get the best out of the integration of EVs in the distribution framework without violating the limits.

Table 3 Peak load obtained at the industrial lateral for different PEV penetration levels

PEV penetration (%)	Strategy	Peak load (MVA)
0		0.051486819
10	A	0.974853927
	B	0.056553326
20	A	1.290157629
	B	0.050705634
30	A	1.230924103
	B	0.048882706
40	A	1.376803453
	B	0.054304671
50	A	1.367547258
	B	0.064735656
60	A	1.420574864
	B	0.045188597

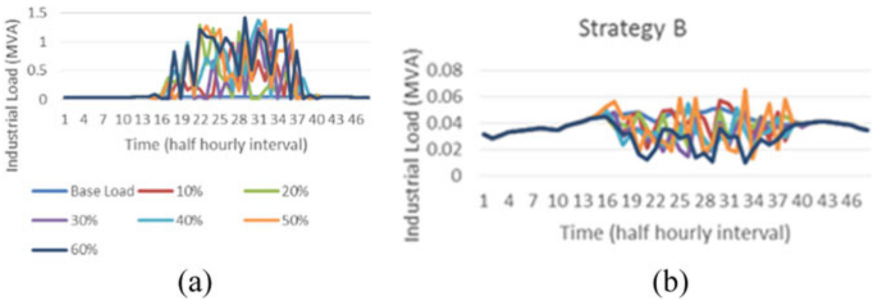

Fig. 10 Load profile of the DT at various penetration levels corresponding to **a** strategy A **b** strategy B

7 Conclusions

This chapter focuses on two smart charging strategies from both commercial and technical perspectives for the optimum charging of plug-in electric vehicle (PEVs) in workplace parking lots incorporating both vehicle to grid (V2G) and grid to vehicle (G2V) charging methodologies. The commercial objective was based on optimization of the total daily cost (TDC) which is acquired by the charging facilitator in that industrial area. The technical objective focuses on minimizing the peak-to-average (PAR) ratio for the purpose of straitening/flattening of the load curve. The strategies were designed to allow integration of PEVs having all kinds of energy requirements, i.e., positive, negative, or even zero. Also, the constraints concerning PEV batteries, distribution system framework, and charging framework are taken into consideration.

Based on the detailed analysis, after comparing both the smart charging strategies, it was observed that Strategy A (optimization of TDC) allows very less maximum PEV penetration into the distribution network as compared to that in Strategy B (PAR minimization). Apart from this, for every penetration level possible in both the methodologies, it was noticed that Strategy A gives more economical benefits on the other hand Strategy B gives more technical aids in relation to reducing peak load. Thus, it is valuable to note that each methodology has its own pros and cons and therefore, one needs to make a sound decision while selecting the strategy depending on his requirements.

References

1. Turker H, Bacha S (2018) Optimal minimization of plug-in electric vehicle charging cost with vehicle-to-home and vehicle-to-grid concepts. IEEE Trans Veh Technol 67(11):10281–10292
2. Wei Z, Li Y, Cai L (2018) Electric vehicle charging scheme for a park-and-charge system considering battery degradation costs. IEEE Trans Intell Veh 3(3):361–373
3. Vagropoulos SI, Kyriazidis DK, Bakirtzis AG (2015) Real-time charging management framework for electric vehicle aggregators in a market environment. IEEE Trans Smart Grid 7(2):948–957
4. Tan J, Wang L (2015) Real-time charging navigation of electric vehicles to fast charging stations: a hierarchical game approach. IEEE Trans Smart Grid 8(2):846–856
5. Jeong S et al (2018) Charging automation for electric vehicles: is a smaller battery good for the wireless charging electric vehicles? IEEE Trans Autom Sci Eng 16(1):486–497
6. Kong P-Y, Karagiannidis GK (2016) Charging schemes for plug-in hybrid electric vehicles in smart grid: a survey. IEEE Access 4:6846–6875. Central Electricity Regulatory Commission Indian Electricity Grid Code (2010)
7. Wu D et al (2017) Two-stage energy management for office buildings with workplace EV charging and renewable energy. IEEE Trans Transp Electr 3(1):225–237
8. Crow ML (2016) Cost-constrained dynamic optimal electric vehicle charging. IEEE Trans Sustain Energy 8(2):716–724
9. Zheng J et al (2013) Aggregation model-based optimization for electric vehicle charging strategy. IEEE Trans Smart Grid 4(2):1058–1066
10. Vaidya B, Mouftah HT (2020) Smart electric vehicle charging management for smart cities. IET Smart Cities 2(1):4–13
11. Wu D, Aliprantis DC, Ying L (2012) Load scheduling and dispatch for aggregators of plug- in electric vehicles. IEEE Trans Smart Grid 3(1):368–376
12. Huang J, Gupta V, Huang YF (2012) Scheduling algorithms for PHEV charging in shared parking lots. In: Proceedings of the American Control Conference (ACC), Montreal, QC, Canada, 2012, pp 276–281
13. Su W, Chow MY (2012) Performance evaluation of an EDA-based large scale plug-in hybrid electric vehicle charging algorithm. IEEE Trans Smart Grid 3(1):308–315
14. Sortomme E, Hindi MM, MacPherson SDJ, Venkata SS (2011) Coordinated charging of plug-in hybrid electric vehicles to minimize distribution system losses. IEEE Trans Smart Grid 2(1):198–205
15. Mehta R et al (2016) Smart charging strategies for optimal integration of plug-in electric vehicles within existing distribution system infrastructure. IEEE Trans Smart Grid 9(1):299–312
16. Land Transport Authority Singapore (2015) Singapore land transport statistics in brief [Online]. https://www.lta.gov.sg/. Accessed 10 Jan 2015

17. Mandal S, Biswas S, Balas VE, ShawRN, Ghosh A (2020) Motion prediction for autonomous vehicles from Lyft dataset using deep learning. In: 2020 IEEE 5th international conference on computing communication and automation (ICCCA), Greater Noida, India, 2020, pp 768–773. https://doi.org/10.1109/ICCCA49541.2020.9250790
18. Kumar KN, Sivaneasan B, Cheah PH, So PL, Wang DZW (2014) V2G capacity estimation using dynamic EV scheduling. IEEE Trans Smart Grid 5(2):1051–1060
19. Shaw RN, Walde P, Ghosh A (2020) IOT based MPPT for performance improvement of solar PV arrays operating under partial shade dispersion. In: 2020 IEEE 9th power india international conference (PIICON), SONEPAT, India, 2020, pp 1-4. https://doi.org/10.1109/PIICON49524.2020.9112952
20. Huber M, Trippe A, Kuhn P, Hamacher T (2012) Effects of large scale EV and PV integration on power supply systems in the context of Singapore. In Proceedings 3rd IEEE PES international conference and exhibition on innovative smart grid technologies (ISGT Europe), Berlin, Germany, pp 1–8
21. Wood AJ, Wollenberg BF (1996) Power generation, operation, and control. Wiley, Hoboken, NJ, USA

Chapter 7
Frequency Control of 5 kW Self-excited Induction Generator Using Gravitational Search Algorithm and Genetic Algorithm

Swati Paliwal, Sanjay Kumar Sinha, and Yogesh Kumar Chauhan

Abstract For harnessing the wind energy, self-excited induction generator is becoming more popular in today's scenario. Nonlinear loads lead to major drawbacks in self-excited induction generator such as poor voltage, frequency regulation and reactive power consumption. This poor voltage and frequency of SEIG depends on many factors like types of load, capacitance involved for reactive power compensation and prime mover speed. The improved performance of SEIG can be obtained by using steady-state analysis of equivalent circuit and usage of optimization techniques in SEIG machine. The main objective of this chapter to select the values of shunt and series capacitances at specified speed in order to achieve an optimum frequency regulation using gravitational search algorithm (GSA) and genetic algorithm (GA). GSA works on Newton's law of gravity, whereas GA follows the steps of selection, crossover and mutation. Both the techniques are based on heuristic approach of gbest and pbest. Therefore, this study is carried out on an objective function of relative mean error of frequency regulation. Correspondingly, the minimum fitness is calculated for resistive and resistive-inductive load. The improved performance validates both the optimization techniques.

S. Paliwal (✉) · S. K. Sinha
Department of Electrical and Electronics Engineering, Amity University, Noida, UP, India
e-mail: swatipaliwal03@gmail.com

S. K. Sinha
e-mail: sksinha6@amity.edu

Y. K. Chauhan
Department of Electrical Engineering, Kamla Nehru Institute of Technology, Sultanpur, India
e-mail: chauhanyk@yahoo.com

R. N. Shaw et al. (eds.), *AI and IOT in Renewable Energy*,
Studies in Infrastructure and Control,
https://doi.org/10.1007/978-981-16-1011-0_8

Nomenclature

Abbreviations

SEIG	Self-excited Induction Generator
STATCOM	Static synchronous compensator
ANFIS	Adaptive neuro-fuzzy inference system
VSC	Voltage source converter
SUMT	Sequential unconstrained minimization technique
GSA	Gravitational search algorithm
GA	Genetic algorithm

Symbols

Xro	Per unit blocked rotor reactance
R_1, R_2	Per phase stator and rotor resistance in per unit
X_1, X_2	Per phase stator and rotor leakage reactance in per unit
X_m, ${X_m}^{un}$	Per unit magnetizing and unsaturated magnetizing reactance
F, v	Per unit frequency and prime moverspeed
C_{sh}, C_s	Shunt and series capacitance in microfarad
${X_m}^{mn}$	Minimum value of magnetizing reactance in per unit
${X_m}^{mx}$	Maximum value of magnetizing reactance in per unit
Xc	Shunt capacitance in per unit
F^{mn}	Minimum value of frequency in per unit
F^{mx}	Maximum value of frequency in per unit
Is	Slip factor
Vs	Stator voltage in per unit
Vg_{en}	Air gap voltage in per unit
Is	Stator current in per unit
Il	Load current in per unit

1 Introduction

Per capita energy consumption of a country describes the standard of living of its citizens. Therefore, with the increase in demand of energy, the fuel consumption has also increased linearly. This fuel consumption has been a major concern for researchers in lieu of saving fossil fuel for future generation. The contribution of renewable energy resources towards the saving of fossil fuels and clean power generation would help in achieving milestones in the growth path of the world. Amongst renewable resources, India has the fourth highest installed capacity of wind in the world with total installed capacity of 37.50 GW (as on 31 December 2019) with 62.03 Billion Units were generated in the fiscal year of 2018–19 (MNRE annual report 2019–20 [1]). With the renewed interest in wind energy generation, the focal point is towards induction generators in comparison to synchronous generators which were used traditionally. In isolated areas, squirrel cage induction generators are very popular because of their several benefits. Nowadays, self-excited induction generator (SEIG) is used because of its various advantages like low cost, less maintenance over squirrel cage induction generator. SEIG also carries disadvantages like poor voltage regulation and consumption of reactive power under varying speeds. To overcome the drawbacks of SEIG, the capacitor bank plays an important role [2]. The placement of capacitor bank is either in short shunt or in long shunt. In paper [2], capacitive excitation compensation technique has been used for improvement in different profiles of voltage levels. Similarly, Swati et al. in paper [3] have computed an optimized capacitance value for initializing the voltage build up in three-phase self-excited induction generator. Apart from capacitive values, limits of different machine parameters are also a point of concern for improved performance of self-excited induction generator. In paper [4], S. S. Murthy et al. have designed 5 kW, 50 Hz, 230 V, 4 pole, single-phase AC generator by keeping the manufacturing constraints into view. The steady-state analysis of unbalanced load is done by using two-port equivalent networks for standalone conditions [4]. Further, the advancement in optimization techniques has helped to improve the performance of induction generators. In paper [5], adaptive neuro fuzzy-based inference system (ANFIS) with static compensator (STATCOM) has been used for controlling the voltage of SEIG during change in load conditions and also for balancing the harmonics.

In paper [6], intelligent neural network-based control algorithm employed on voltage source converter (VSC)-based battery energy storage system has been used for excellent dynamic and steady-state response of the system. In paper [7, 8], Mohamed A. Enany has investigated the voltage profile and power capability of series compensated self-excited induction generator for short shunt and long shunt compensation configurations using genetic algorithm-based assessment and ANFIS, respectively [9–11]. The proposed results have been compared with the experimental results which validate both. In paper [12], genetic algorithm has been used for short shunt SEIG for improving the two objectives of voltage regulation and optimum performance capability which depend upon voltage regulation as well as loadability. In paper [13–17], genetic algorithm has been used for assessing the different parameters of SEIG like speed, capacitance, leakage reactance, stator and rotor resistance.

In this chapter, 5 kW, 415 V, 10.1 A, Δ connected short shunt self-excited induction generator has been used. For improvement of frequency regulation, two optimizing techniques, gravitational search algorithm (GSA) and genetic algorithm (GA) have been implemented in order to get better performance. This chapter is outlined as introduction, machine modelling, problem formulation, results and discussion and conclusion.

2 Machine Modelling

In this section, machine modelling of SEIG has been explained using equivalent circuit diagram. The frequency regulation of SEIG can be improved by connecting series capacitance in combination with shunt capacitance. Depending upon the placement of series capacitance, a SEIG can be classified as short shunt and long shunt SEIG. Figure 1 shows a schematic diagram of short shunt SEIG. A capacitor bank is connected across the stator terminal of induction machine and load in order to supply reactive power to the induction generator for self-excitement. The value of capacitance at specified speed provides the optimum performance of SEIG.

The appropriate modelling is needed to improve the voltage and frequency regulation of SEIG for cost-effective utilization and improved performance. Therefore, to know the operation and design of SEIG machine the steady-state performance plays an important role. Modelling of short shunt SEIG includes the calculation of unknown variables from the steady-state model. In this chapter, the magnetizing reactance and unknown frequency can be calculated with the help of Newton–Raphson method in steady-state equivalent circuit of SEIG. Figure 2 represents the stator and

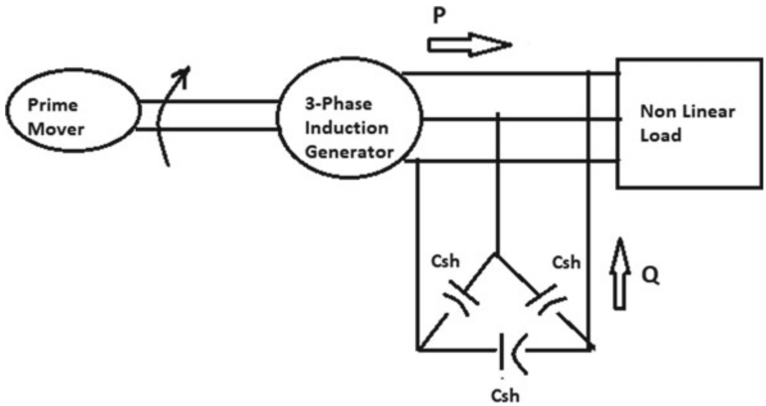

Fig. 1 Short shunt 3-Ø SEIG

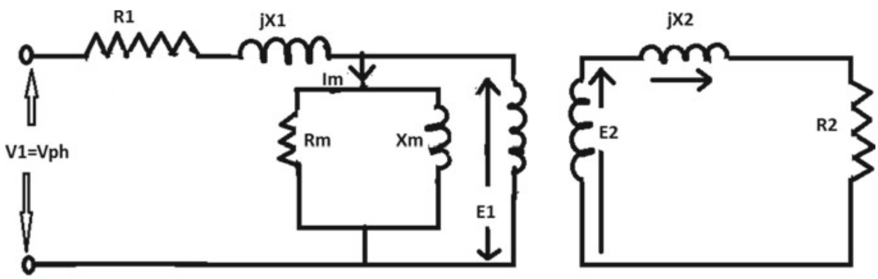

Fig. 2 Equivalent circuit of SEIG

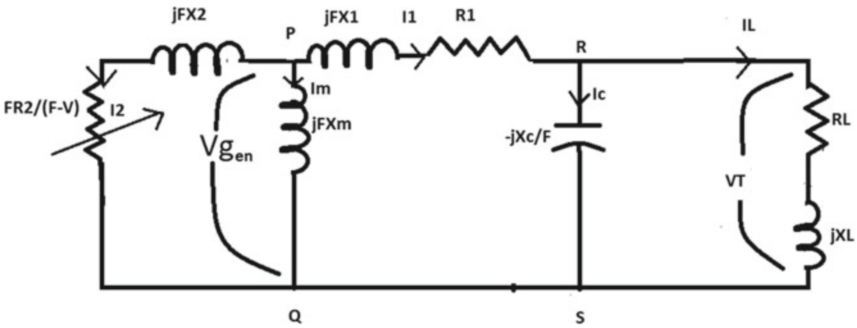

Fig. 3 Steady-state equivalent circuit

rotor side of SEIG.

$$E_r = sE_{ro} \tag{2.1}$$

where s is slip factor,

$$X_2 = sX_{ro} \tag{2.2}$$

where X_{ro} is Blocked rotor reactance.

For further calculation of machine parameters, the steady-state model is as shown in Fig. 3.

For steady state,

$$Z_{\text{total}} = Z_{PQ} + Z_{PR} + Z_{RS} \tag{2.3}$$

where

$$Z_{PQ} = \left\{ \left(\frac{R_2 F}{F - v} \right) + jFX_2 \right\} || jFX_m.$$
$$Z_{RS} = \left\{ \frac{jX_c}{F} || (R_L + jFX_L \right\}$$
$$Z_{PR} = R_1 + jX_1$$

For solving the two unknowns, magnetizing reactance (X_m) and generated frequency (F), the two nonlinear equations separated by real and imaginary parts are being solved using Newton-Rapson method.

$$f(X_m, F) = \left((P_1 X_m + P_2) F^2 + \cdots (P_5 X_m + P_6) + P_7 = 0 \right) \tag{2.4}$$

$$g(X_m, F) = \left((Q_1 X_m + Q_2)F^3 + \cdots (Q_7 X_m + Q_8) + Q_9 = 0\right) \tag{2.5}$$

Coefficients P and Q are expressed in Appendix 2. After the calculation of unknown variables, performance parameters are being solved using Eqs. 2.6–2.10.

$$I_s = Vg_{en} * F((Z_{PR} + Z_{RS})) \tag{2.6}$$

$$V_S = \{(Vg_{en} * F) - (I_s * Z_{PR})\} \tag{2.7}$$

$$I_c = \left\{ \frac{V_s}{(-j\frac{X_c}{F})} \right\} \tag{2.8}$$

$$I_L = I_s - I_c \tag{2.9}$$

$$Power = V_S * I_L \tag{2.10}$$

Steps to be involved in calculating unknown parameters by using Newton–Raphson method.

1. Read the input parameters of machine.
2. Apply loop impedance method for load calculation.
3. Select the initial values of magnetizing reactance and frequency.
4. With the help of Jacobian matrix, calculate ΔX_m and ΔF.
5. If elements are within permissible limits, print X_m and F. If not, repeat step 3.

3 Problem Formulation

In this section, the design parameters v, C_{sh}, C_s are computed for optimum frequency regulation using gravitational search algorithm and genetic algorithm. Therefore, the objective is optimized frequency regulation.

3.1 Objective Function

Mean Relative Error of frequency regulation is the objective function of SEIG which is defined as mean summation of frequency mismatch between load and rated conditions from no load point to 50 load points (for 5 kW machine). It depends on shunt capacitance, series capacitances and speed (C_{sh}, C_s, v) which is expressed in terms of F_{obj}.

$$F_{\text{obj}} = \frac{100\%}{n} \sum_{n=1}^{50} \left\{ \frac{[F_{Ln}(v, C_{sh}, C_s) - F_r]}{F_r} \right\} \tag{3.1}$$

The Fitness of this objective function is expressed in terms of

$$f = \frac{1}{(1 + F_{\text{obj}})} \tag{3.2}$$

This objective function is subjected to various constraints and bound on variables which are described as

Equality constraints: It is expressed in Eq. (3.3) and is used to solve X_m and F using Newton-Rapson method and inequality constraints which are expressed in terms of X_m, F is shown in Eqs. (3.4a, 3.4b). Both are required in order to express the equations of steady-state equivalent circuit of SEIG.

Z_1 and Z_2 at nth load point are solved using Eqs. (2.4) and (2.5).

$$Z = Z_1(v, C_{sh}, C_s, X_m, F) + jZ_2(v, C_{sh}, C_s, X_m, F) \tag{3.3}$$

$$X_m^{mn} \le X_m \le X_m^{mx} \tag{3.4a}$$

$$F^{mn} \le F \le F^{mx} \tag{3.4b}$$

For deep saturation of SEIG operation, $X_m{}^{mn}$ and $X_m{}^{mx}$ are taken as 0.1 pu and $X_m{}^{uns}$, respectively. F^{mn} and F^{mx} are considered as v pu and 0.90 v pu, respectively, from viewpoint of quality.

Bound limits: For covering the solutions, limits are important parameter which include

$$15\,\mu\text{F} \le C_{sh} 35\,\mu\text{F} \tag{3.5a}$$

$$50\,\mu\text{F} \le C_s 300\,\mu\text{F} \tag{3.5b}$$

$$0.88\,\text{pu} \le v \le 1.16\,\text{pu}. \tag{3.5c}$$

3.2 *Flowchart of Algorithm Used*

As mentioned earlier, GSA works on the principle of Newton law of gravity where each particle attracts the other via gravitational force. In GSA, agents act as objects and their performance is being measured in terms of their masses. The gravity force pushes the objects globally towards heavy masses of objects which will provide better solutions in terms of gbest and pbest. The flowchart of GSA methodology shows the following steps: Initialization of GSA parameter, selection of constraints and identification of pbest and gbest values as shown in Fig. 4. In flowchart, G(t) is a function of initial value and time, whereas best(t) and worst(t) of population are defined as minimum fitness value of agents at time 't'. Figure 5 represents the

Fig. 4 Flowchart of GSA technique

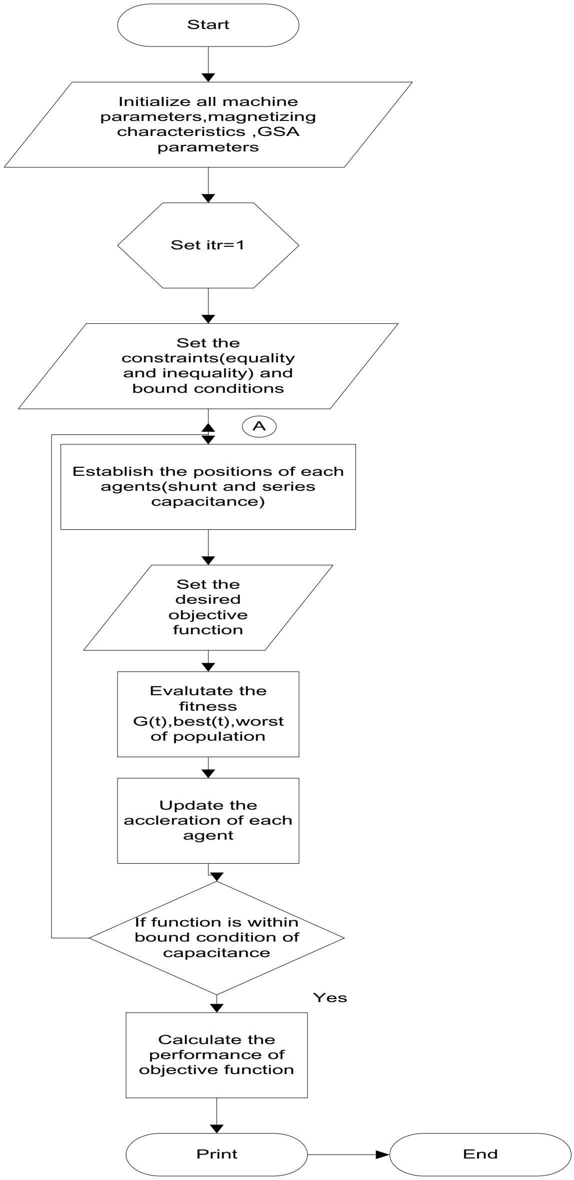

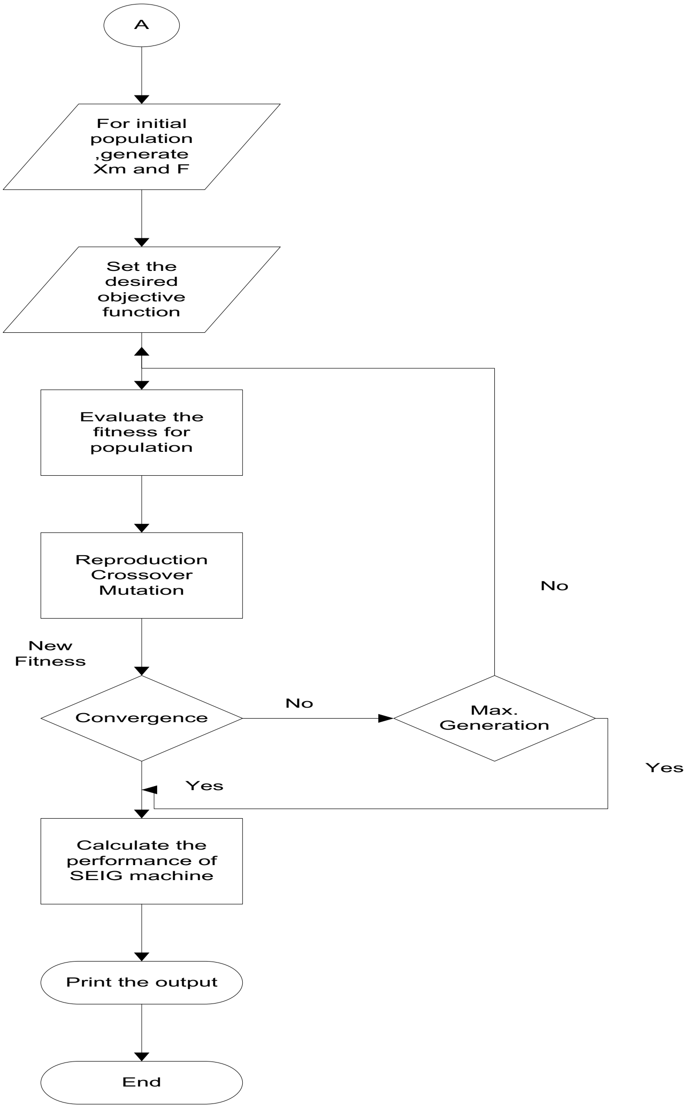

Fig. 5 Flowchart of GA technique

flowchart of GA steps involved in SEIG machine. GA technique includes the steps of reproduction, crossover and mutation.

4 Results and Discussion

In this section, relative mean error for frequency regulation of different loading conditions has been compared. Correspondingly, the minimum fitness required for 5 kW, 415 V Induction motor operated as SEIG has been validated by using optimization techniques of GSA and GA. The rated capacity at rated voltage is represented as 50 load points, i.e. from no load to rated load for 5 kW machine.

Comparison between GSA and GA results

In Table 1, optimized frequency regulation is investigated for 50 load points (Resistive load). It is observed that the highest fitness and power output of 0.61 pu is achieved above the rated speed at 1.03 pu in case of GSA technique as compared to GA. The increase in capacitance supplies the excitation VARs at reduced speed and thus maintains the terminal voltage and frequency.

Whereas Table 2 represents the optimum frequency regulation for R-L load with unequal series capacitances. Tables 1 and 2 also show the comparison of two optimization technique. In case of resistive load, root mean square error of frequency regulation gives a power output of 0.6158 pu in GSA and 0.6078 pu in GA, respectively. In case of R-L load, mean relative error of frequency regulation gives a power output of 0.5990 pu in GSA and 0.5935 pu in GA, respectively. Therefore, the power output of resistive load is better than resistive-inductive load.

Figure 6 show the droop in frequency at rated speed for R load using two optimization technique named GSA and GA. The figure shows that GSA technique is better than GA techniques as the frequency is better in case of GSA optimization technique.

Figure 7 represents the fitness of resistive load for different parameters like shunt capacitance, series capacitance and speed of prime mover. This fitness is based on bound limits for covering the solutions within specified range.

Figure 8 indicates the maximum loading point condition and rated speed point for R-L load conditions. The maximum loading point occurs above the rated speed for GSA.

Table 1 GSA versus GA for resistive load

v	C_s	C_{sh}	Pl	Technique
1.03	203.49	16.51	0.6158	GSA
1.03	199.34	15.98	0.6078	GA

Table 2 GSA versus GA for resistive-inductive load

v	C_s	C_{sh}	Pl	Technique
0.99	189.48	17.42	0.5992	GSA
0.99	181.00	18.62	0.5935	GA

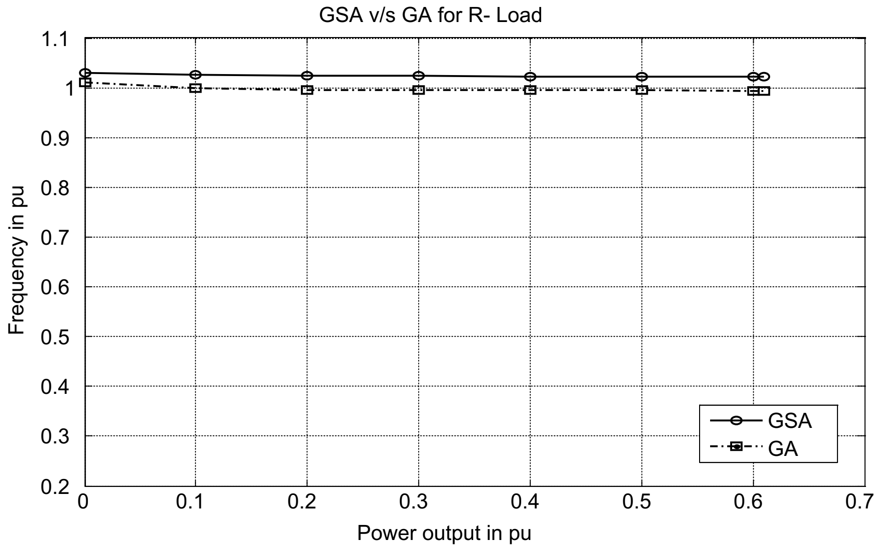

Fig. 6 GSA versus GA for R-load

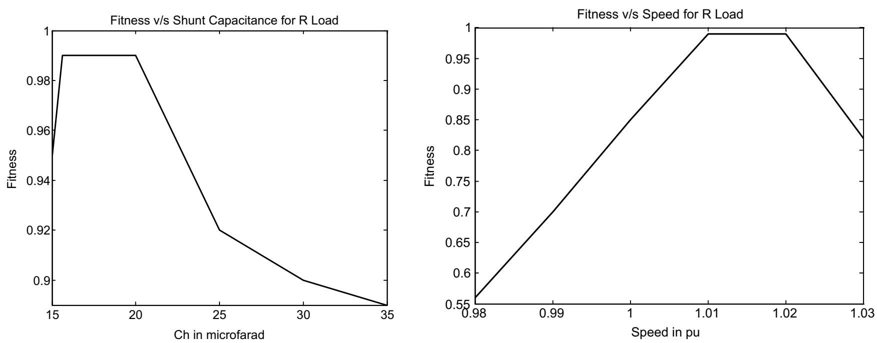

Fig. 7 Fitness w.r.t to various parameters for optimum FR in R-load

Figure 9 represents the fitness for optimum frequency regulation in case of R- L load during different parameters constraints.

Conclusion: This chapter represents the 5 kW, 415 V, 10.1 A, Δ connected short shunt SEIG. The relative mean error of frequency regulation is optimized with the help of GSA and GA optimization technique. The required optimized value of capacitance and speed are being selected by these heuristic approaches. The simulated results of both GSA and GA are in proximity and validated the results in table [1, 2]. The validated results concluded that the GSA technique gives better performance in terms of frequency regulation for both R and R-L load. It provides good

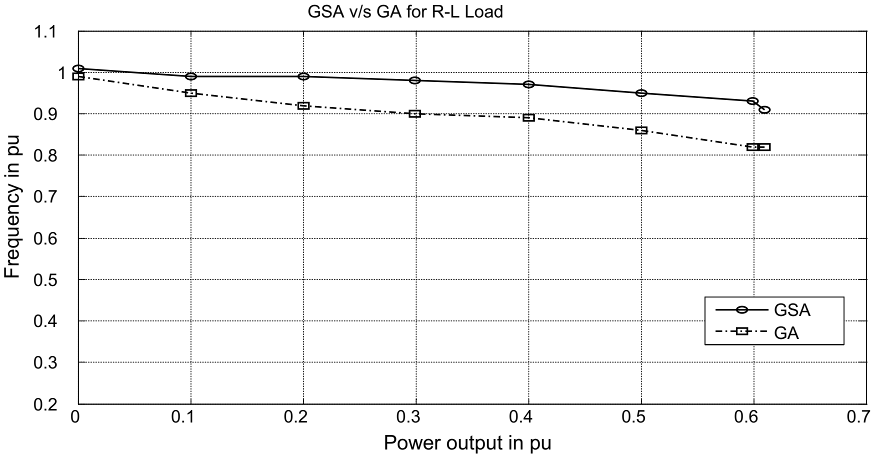

Fig. 8 GSA versus GA for R-L load

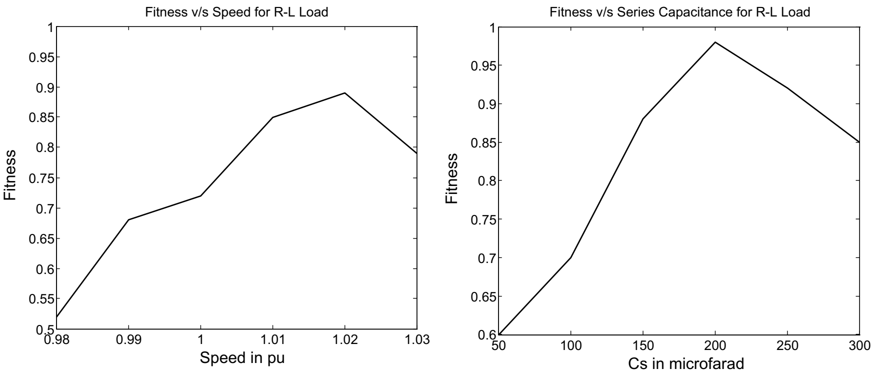

Fig. 9 Fitness w.r.t to various parameters for optimum FR in R- L load

scope of research in an area of self-excited induction generator for better performance in terms of voltage and loadability by using different optimization techniques.

Appendix 1: Specification of Self-excited Induction Generator

5 kW, 415 V, 10.1 A line, Δ connected, 4 pole, 50 Hz $R_s = 0.0532$ pu, $R_r = 0.0337$ pu, $X_s = 0.0533$ pu, $X_r = 0.0733$ pu, $X_m{}^{uns} = 3.48$ pu.

Appendix 2: Coefficients of Z_{total}

The coefficients P and Q are defined as

$$
\begin{aligned}
P_1 &= -X_1 * R_L * (X_2 + Xm) - X_2 * R_L * Xm \\
P_2 &= X_1 * R_L * v * (X_2 + Xm) + X_2 * R_L * Xm * v \\
P_3 &= R_1 * R_2 * R_L + X_1 * X_c * R_2 + (R_1 * X_c + R_L * X_c) * (X_2 + Xm) \\
&\quad + R_2 * X_m * X_c \\
P_4 &= ((-v * R_1 * X_c) - v * R_L * X_c) * (X_2 + Xm)
\end{aligned}
$$

$$
\begin{aligned}
Q_1 &= 0 \\
Q_2 &= X_1 * R_L * R_2 + (X_2 + Xm) * (R_1 * X_c + R_L * X_c) + Xm * R_2 * R_L \\
&\quad + Xm * X_c * X_2 \\
Q_3 &= (X_2 + Xm) * (-R_1 * R_L * v - X_1 * X_c * v) * Xm * X_c * X_2 * v \\
Q_4 &= -R_L * Xc * R_2 - R_1 * R_2 * Xc
\end{aligned}
$$

References

1. https://mnre.gov.in/img/documents/uploads/file_f-1597797108502.pdf
2. Kumar S, Kumar S, Yadav PA (2013) Effect of capacitive excitation on voltage stability of three phase self-excited induction generator. Int J Electr Electron Eng Res 3(1):87–96
3. Devabhatuni S, Jayaram Kumar SV (2011) Design of excitation capacitance for self-excited induction generator. Int J Comput Sci Commun Netw 1(3):264–269
4. Murthy SS, Singh B, Sandeep V (2016) Experience in developing a single phase two winding 5 kW self excited induction generator for off-grid renewable energy based power generation. J Inst Eng (India) Ser B 97(2):127–137
5. Das M, Giribabu D (2016) ANFIS controller based STATCOM regulator for SEIG. IEEE 2016. Kalla UK, Singh B, Murthy SS (2016) Intelligent neural network based controller for single phase WECS using two winding self-excited induction generator. IEEE Trans Ind Inform 12(6):1986–1997
6. Enany A (2017) Series compensation assessment of self-excited induction generator using genetic algorithm. Eur Power Electron Drives 27(1):1–11
7. Singaravelu S, Sasikumar S (2019) Steady state modeling and analysis of three phase self-excited induction generator with series compensation. Int J Adv Eng Technol (IJAET) 3(2):371–380
8. Kumar S, Pradhan SK, Yadav A (2013) Effect of capacitive excitation on voltage stability of three phase self-excited induction generator. Int J Electr Electron Eng Res 3(1):87–96
9. Dalei J (2016) Fault classification in SEIG system using Hilbert–Huang transform and least square support vector machine. Elsevier Electr Power Energy Syst 76:11–22
10. Ibrahim H, Metwaly M (2011) Genetic algorithm based performance analysis of self-excited induction generator. Sci Res Eng 3:859–864
11. Chauhan YK, Jain SK, Singh B (2011) Genetic algorithm-based optimum performance of compensated self-excited induction generator. Int J Model Simul 31(4):263–270

12. Chaturvedi Y, Kumar S, Gupta V (2020) Capacitance requirement for rated current and rated voltage operation of SEIG using whale optimization algorithm. In: International conference on computational intelligence and data science (ICCIDS), vol 167, pp 2581–2589
13. Vadhera S, Sandhu K (2010) Genetic algorithm toolbox based investigation of terminal voltage and frequency of self excited induction generator. Int J Adv Eng Appl 1(1):243–250
14. Faisal Khan M, Rizwan Khan M, Iqbal A (2017) Modeling, implementation and analysis of a high (six) phase self-excited induction generator. J ElectrSyst Inf Technol 156:1–18
15. Chatterjee A, Roy K, Chatterjee D (2014) A gravitational search algorithm (GSA) based photo-voltaic (PV) excitation control strategy for single phase operation of three phase wind turbine coupled Induction generator. Energy 1–12. Elsevier
16. Cheu G, Liu L, Huang S (2015) Enhanced GSA-based optimization for minimization of power losses in power system. Math Problems Eng Hindawi
17. Enany A (2014) Steady state modelling and ANFIS based analysis of self excited induction generator. Wind Eng 38(3):349–358

Chapter 8
Cloud Based Real-Time Vibration and Temperature Monitoring System for Wind Turbine

Subharshi Roy, Barnali Kundu, and Debanjan Chatterjee

Abstract In the present scenario, Renewable Energy requires real-time condition monitoring for their uninterrupted performance. Wind turbines are often subjected to huge mechanical, and thermal stresses which in turn result in causing faults. In this paper, a Cloud-based Real-time Monitoring System (CRMS) has been developed for the early detection of a problem and identify the need for maintenance before a wind turbine fails. CRMS associated with vibration sensor and temperature sensor can easily detect the fault and alarming system indicates the operator personnel about the abnormal state of the motors in the industrial plant. With real-time data monitoring system and LabVIEW, it enables the detailed spectral analysis of the system. A wireless sensor networks are included in this research work for a real-time condition monitoring. Therefore, the authors of this paper have developed a prototype which can provide smart maintenance to elongate the life of wind turbine and prevent the harm of nearby equipments.

Keywords Real-time condition monitoring micro-electromechanical system · Wind turbine

1 Introduction

Technological advancements and social awareness in the climatic health are promoting the use of renewable energy in an increasing proportion. In particular, wind farm are capable to produce 10.4% of total renewable energy. The installation of wind energy throws vast challenges for operations and maintenance. Rough environmental characteristics and implementation of large wind turbines lead to relatively high breakdown rates for wind turbines. Increased product maintenance has a significant role to keep system healthy so as to obtain safe and smooth operation efficiently and cost effectively. The best maintenance strategy involves condition monitoring where overall operational cost of periodic maintenance and plant shutdown time can

S. Roy · B. Kundu (✉) · D. Chatterjee
Guru Nanak Institute of Technology, Sodepur, Kolkata, India
e-mail: barnali.kundu@gnit.a.in

R. N. Shaw et al. (eds.), *AI and IOT in Renewable Energy*,
Studies in Infrastructure and Control,
https://doi.org/10.1007/978-981-16-1011-0_9

be minimized [1]. So, proper condition monitoring and diagnostics are vital for such machinery due to the continual extended use. Condition monitoring is a graphical trend of the machine parameters for the purpose of detection, analysis, and correction of the machine problems much before the failure takes place [2, 3].

Vibrations are inevitable phenomenon that leads to various types of malfunctions in the machine. In some scenarios, the vibrations originated from a machine can cause damage to the nearby machinery. Rotor faults are mainly caused by pulsating mechanical loads such as reciprocating compressors or coal crushers, etc., and due to imperfections in the manufacturing process of the rotor cage which cause high mechanical and thermal stress [4]. Analysis associated with bearing faults are overwhelmingly used in the induction motors and motors reliability studies show that bearing problems amount to over 40% of all machine failures [5]. A vibration sensor is able to sense mechanical vibration of each component that occurred with increased noise. Temperature will also increase above the limiting value which is prescribed by the manufacturer of the particular motor. In [6], the researcher has mentioned the two possible positions for sensor placement. In order to detect the failures promptly or the arisen malfunctions, it is important to identify the manifestations of the faults occurred. The researchers have claimed that an Internet of Things (IOT) based real time monitoring system can save the maintenance cost approximately 10–40% per year [7]. In [8], the authors have mentioned the two possible positions for sensor placement. So, proper condition monitoring and diagnostics are vital for such machinery due to the continual extended use. Condition monitoring is a graphical trend of the machine parameters for the purpose of detection, analysis and correction of the machine problems much before the failure takes place [9, 10]. Vibrations are inevitable phenomenon that leads to various types of malfunctions in the machine. In some scenarios, the vibrations originated from a machine can cause damage to the nearby machinery. Rotor faults mainly caused by pulsating mechanical loads such as reciprocating compressors or coal crushers etc., and due to imperfections in the manufacturing process of the rotor cage which cause high mechanical and thermal stress [11]. Analysis associated with bearing faults are overwhelmingly used in the induction motors and motors reliability studies show that bearing problems amount for over 40 % of all machine failures [12]. A vibration sensor is able to sense mechanical vibration of each component occurred with increased noise. Temperature will also increase above the limiting value which is prescribed by the manufacturer of the particular motor. In order to detect the failures promptly or the arisen malfunctions, it is important to identify the manifestations of the faults occurred. Vibration analysis of electrical machines is used to monitor the characteristics frequency in order to determine the motor faults. .

In this paper, a Cloud-based Real-time Monitoring System (CRMS) has been developed for the early detection of a problem and to identify the need for maintenance before a motor fails. CRMS associated with vibration sensor and temperature sensor can easily detect the faulty motors, and alarming system indicates the operator personnel about the abnormal state of the motors in the industrial plant. Considering the present scenario of Wind plants and existing issues of real-time monitoring system, an integrated communication system using wireless sensor nodes is proposed.

Table 1 Specifications of test system

	Specifications
Manufacturer (MODEL No.)	GE (190906 T)
Type and class	TDC & B
Power rating	1 kW
Volts (V)	230 V
Rated current (A)	12 A
Frequency (Hz)	50
Rated speed (RPM)	1425
Rated current (A)	1.9 A
Insulation temp rise	80 °C

Therefore, the authors of this paper have developed a prototype which can provide smart maintenance to elongate the life of motors and prevent the harm of nearby equipments (Fig. 1).

2 Analysis of Electromagnetic Vibration Effects

Analysis of electromagnetic vibration effects modern motors/generators does not involve variable elements of electromotive forces, but due to internal and external motor faults, such as nominal power supply quality and load and electromagnetic vibration might deviate from the normal operation of the generator. Excessive amount of electromagnetic vibration of generators results in a resonance condition on the structural aspects of the motor. There are two prior sources of EM vibrations in induction motors: radial and tangential electromagnetic forces. Simulation has been performed using COMSOL Multiphysics software and results of magnetic Flux Density distribution and current Density distribution shown in Fig. 2a, b.

The magnetic waves in co-ordinance with Maxwell's law (1) develop a radial EM force-wave with doubled line frequency. The prior vibration is developed at the frequencies of radial electromagnetic forces [13]:

$$f_{rotor} = \frac{f_{line}\mathrm{kzrt}(1 - \mathrm{s})}{\mathrm{p}} \tag{1}$$

where p is no. of pole pair, s is the slip, $z_{rt\ is}$ no. rotor teeth, k = 1, 2, 3….

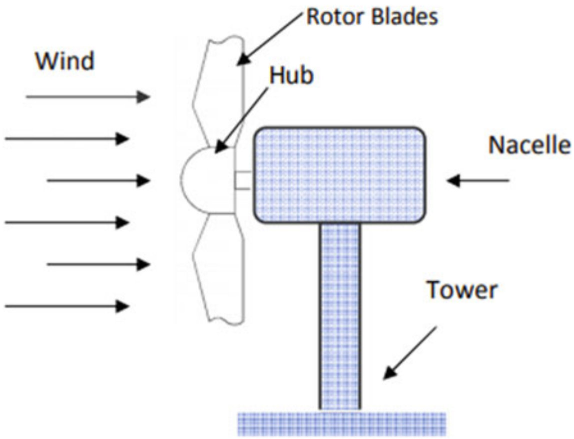

Fig. 1 Schematic view of wind turbine

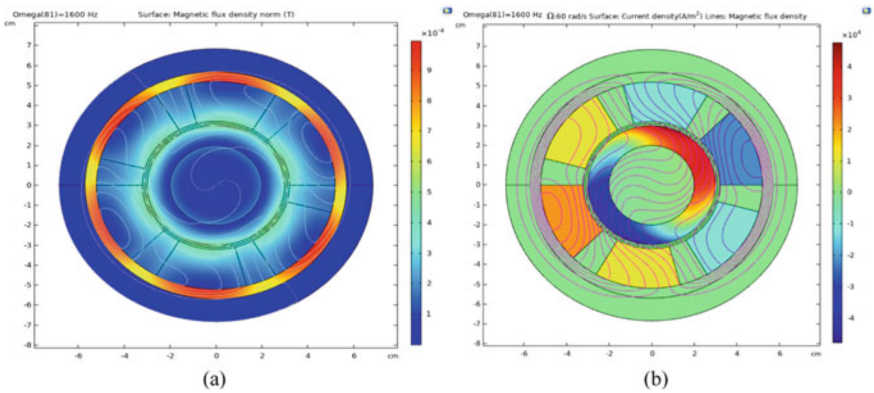

Fig. 2 **a** Magnetic flux density **b** current density using COMSOL multiphysics

3 Prototype Description

In this paper, a prototype is developed which is implemented on an induction generator as shown in Fig. 3 and the specifications are given in Table 1.

A. Vibration Sensors

MPU-6050 tri-axial accelerometer is aligned to the generator surface with sensitivity of 100 mV/g. Samples are recorded with signals of duration 2 s where sampling rate is 20 kS/s. The spectrum was recorded through tri-axial accelerometers aligned on the induction generator. The combination of 3-axis accelerometer and gyroscope on the similar silicon die processes Motion Fusion 6-axis algorithms. The device nodes access external magnetometers through an auxiliary I2C master bus which allows

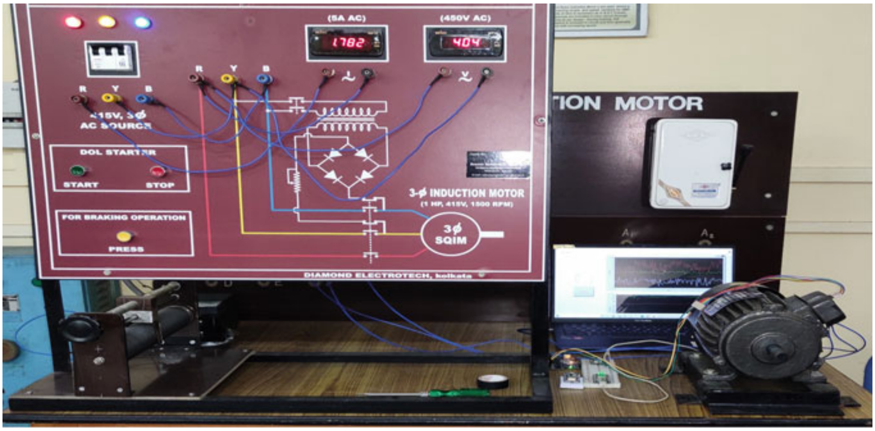

Fig. 3 Experimental Setup with prototype implementation

the other device nodes to gather external data without interruption from the system processor.

B. Temperature Sensors

DHT22 has been interfaced with the microcontroller. It employs digital signal collection technique where the sensors are connected with 8-bit single-chip computer. The sensors of this model are pre-compensated and pre-calibrated in the high precision calibration chamber. The coefficient is saved in the OTP memory where the sensor detection cites coefficient from the memory. The analog input of the microcontroller receives sensors data and projected into human–machine interface of temperature monitoring system.

C. Wireless Sensor Node (WSN)

A wireless sensor network is formed for transmission of data from sensors to microcontroller or monitoring devices using ESP-NOW protocol developed by Espressif. This protocol enables data transmission in between nodes via Master–Slave communication without the use of WiFi. Individual NODEMCU ESP8266 are connected to MPU6050 and DHT22 forming two separate Master nodes. Initially, the sensor nodes are paired and an encrypted peer-to-peer connection is formed without the requirement of TLS Handshake protocol.

The vibration data derived requires constant flow to the monitoring systems. The flow of data is made through self-configured wireless networks to pass the data through the network to a specified main location where the data can be monitored and analyzed. NodeMCU Client–Server communication is done via ESP-NOW communication protocol. The hardware model of prototype and PCB of the Tri-axal accelerometer connection is shown in Fig. 4a, b, respectively.

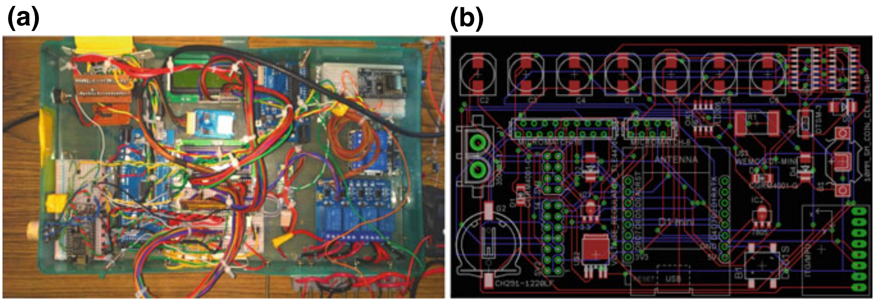

Fig. 4 **a** Hardware model of prototype **b** PCB of the tri-axial accelerometer connection

D. Cloud Storage

The data retrieved through the microcontroller is transferred wirelessly to a Time Series Database (TSDB) optimized for storing and serving series of data points indexed in time order through associated pair of time(s) and value(s). The functional block diagram of Wireless sensor node is shown in Fig. 5. The cloud server accepts data via protocols such as HTTP, TCP, and UDP. The microcontroller program has

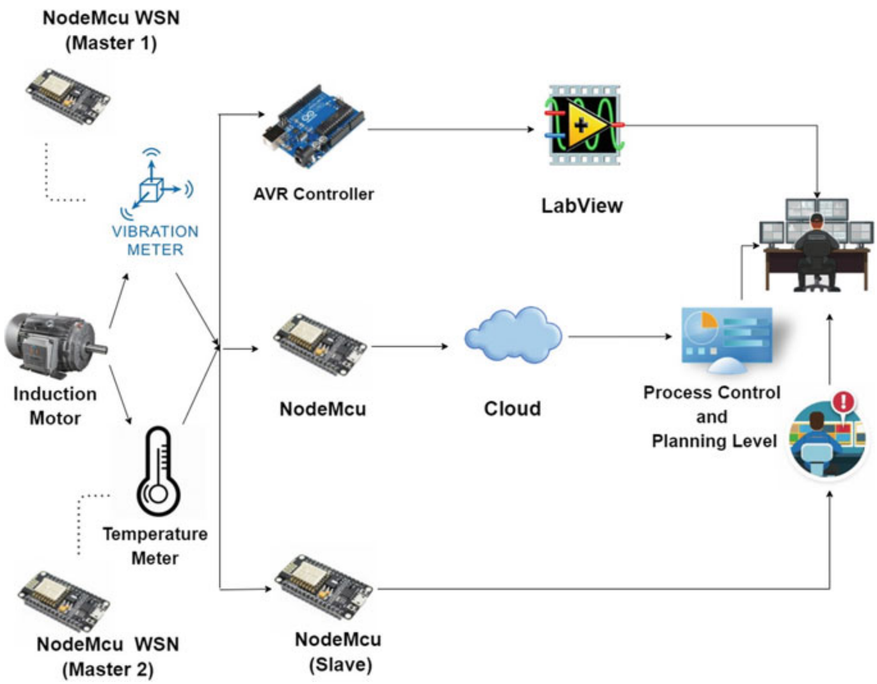

Fig. 5 Wireless sensor node functional block diagram

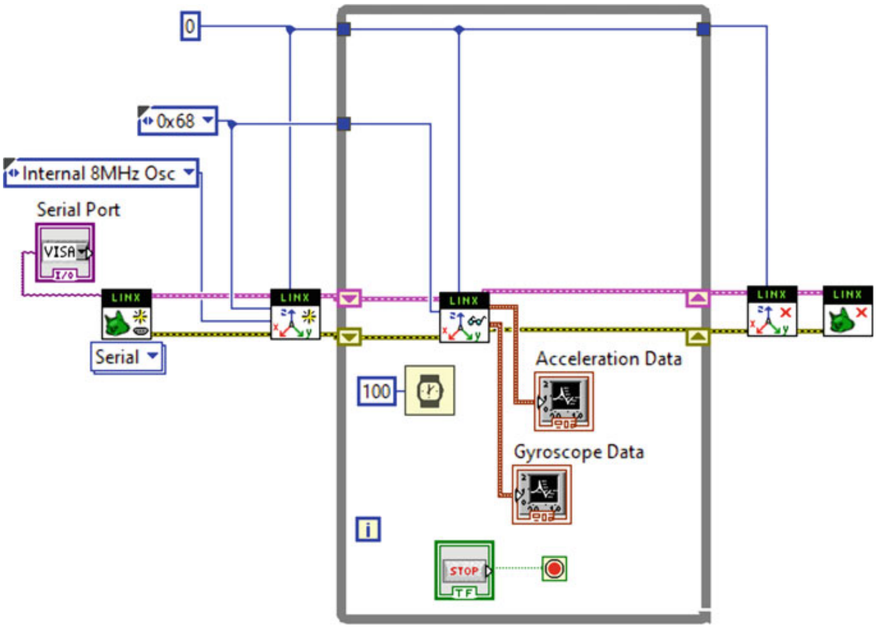

Fig. 6 LABVIE model for vibration monitoring

been set to process and regulate real-time data from the sensors and store it to the cloud with InfluxDB Cloud, a high accessible storage and time series data retrieval with Graphite protocol support.

4 Experimental Results

This section deals with the experimental methodology that was performed by the prototype under real-time operating conditions to verify sensitivity of the measurement, reliability in data transmission between sensor nodes and cloud-base server, system stability and efficiency, and results are retrieved (Fig. 7).

Data from accelerometer in Fig. 7a, b and from gyroscopic in Fig. 8a, b are necessary for fault detection. The MPU6050 sensitivity level is enough to detect anomalies that are harmful to the generator. Figures show the amplitude-time level recorded for healthy and unhealthy generator condition, i.e., failure in ball bearing. It clearly elaborates the difference between healthy and generator with bearing fault with respect to their amplitudes. With frequency of 50 Hz at running condition, the data clearly indicates the increase in vibration in motor with bearing failure.

A. Temperature sensor results

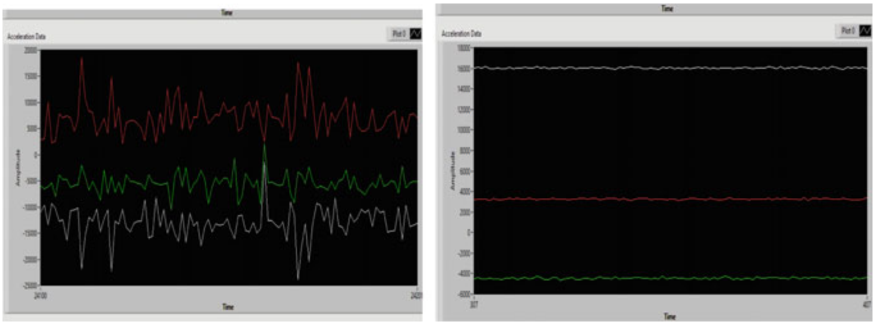

(a) (b)

Fig. 7 Waveform of **(a)** unhealthy and **(b)** healthy generator obtained from accelerometer

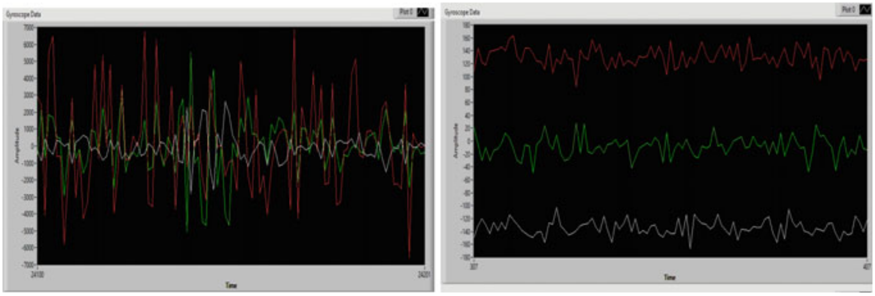

(a) (b)

Fig. 8 Waveform of **(a)** unhealthy and **(b)** healthy generator obtained from gyroscope

The normal working condition in healthy generator and abnormal increase in temperature in the unhealthy generator is detected by the sensor updating the fluctuations at LabView and cloud-server, respectively. LabView model has been developed in Fig. 9. The sensor was placed on the motor's front-rear ball bearing areas and casing. Compared to the healthy generator, the rise in temperature at the unhealthy motor (faulty ball bared motor) raised much rapidly and settled around 43 °C. Figure 10 shows the Human–Machine Interface (HMI) of temperature monitoring panel. Increase in temperature has been properly updated at the LabView user interface, sensor nodes, and cloud server.

A. Cloud server result

Figure 11 shows the data is updated successfully in the cloud server in case of healthy and unhealthy motors. The fluctuations in the data clarify the increase in vibrations as per the health of the generators. The data is stored in the data logger system with respect to time span. Also, the data can be downloaded as Comma-Separated Value (CSV) files for further analysis or machine learning algorithms.

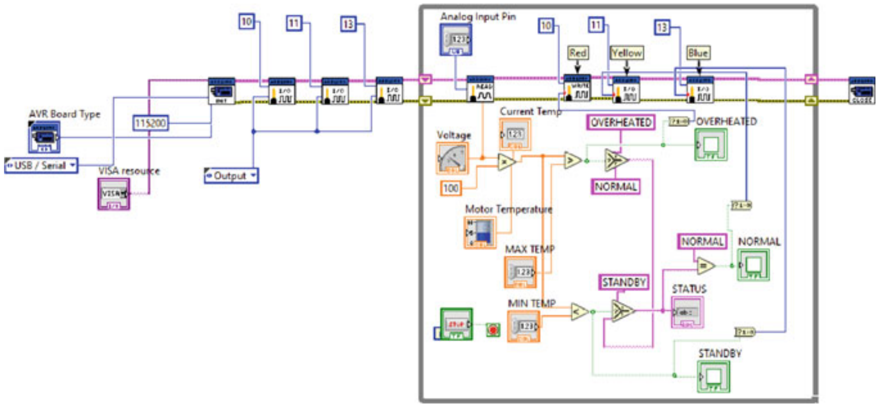

Fig. 9 LABVIEW model of temperature monitoring system

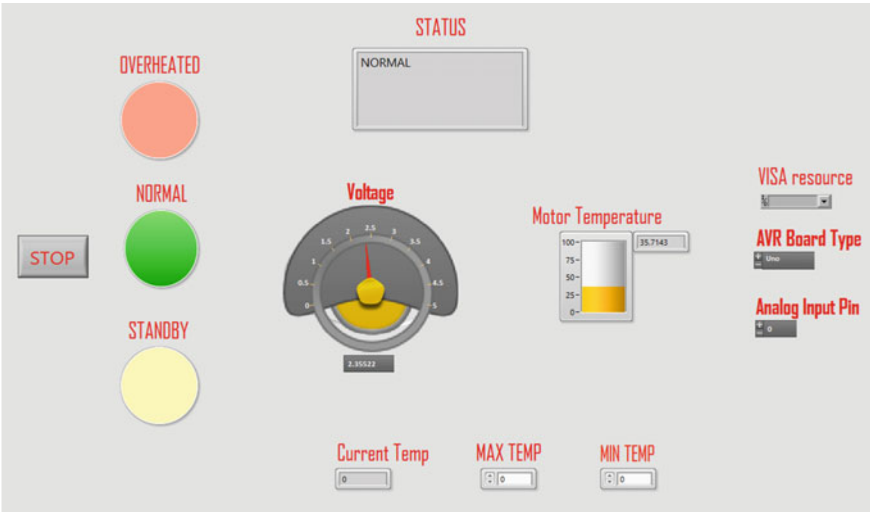

Fig. 10 Human–Machine Interface (HMI) of temperature monitoring panel

5 Conclusion

A clear understanding of the motor phenomena that causes vibrations at such frequencies is a major factor for diagnosing of induction generator-based wind turbine. Condition monitoring using vibration analysis is a very reliable diagnostic method compared to other methods for both electrical and mechanical faults in the AC generator. In the upcoming generations, periodic manned inspections of renewable power plant will be obsolete. In this current era of real-time data monitoring and predictive maintenance, the improvisation of condition monitoring of industrial equipment

(a) (b)

Fig. 11 Waveform of **a** unhealthy and **b** healthy generator from InfluxDB

is necessary. With the help of IoT, wireless sensor node and cloud computing, the longevity of wind power plant and safe operations are achieved. The sensor data can be used further used for machine learning algorithms for predictive maintenance of the induction generators-based wind turbine. The vibration and anomaly detection accuracy can be improved using various other methods such as Wavelet transform, Short-Time Fast Fourier (STFT) Transform, or Power Spectrum Density (PSD).

References

1. Goyal D, Chaudhary A, Dang RK, Pabla BS, Dhami SS (2018) Condition monitoring of rotating machines: a review. Wold Sci News 98–108
2. Dorrell DG, Thomson WT, Roach S (1997) Analysis of airgap flux, current, and vibration signals as a function of the combination of static and dynamic airgap eccentricity in 3-phase induction motors. Ind Appl IEEE Trans 33(1):24–34
3. Shuting W, Zhaofeng X, Yonggang L, Zili H, Heming L (2003) Analysis of generator vibration characteristic on rotor winding interturn short circuit fault. In: ICEMS 2003 sixth international conference on electrical machines and systems, vol 2
4. Guo P, Infield D, Yang X (2012) Wind turbine generator condition-monitoring using temperature trend analysis. Sustain Energy IEEE Trans 3(1)
5. Wang L, Zhang Z (2017) Automatic detection of wind turbine blade surface cracks based on UAV-taken Images. IEEE Trans Ind Electron 46
6. Hodge VJ, O' Keefe S, Weeks M, Moulds A (2014) Wireless sensor networks for condition monitoring in the railway industry: a survey. IEEE Trans Intell Transp Syst 1088–1106 (2014)
7. Manyika J, Chui M, Bisson P, Woetzel J, Dobbs JR, Aharon BAD (2011) Unlocking the potential of the Internet of Things. McKinsey Global Institute, New York
8. Lamim Filho PCM, Pederiva R, Brito JN (2014) Detection of stator winding faults in induction machines using flux and vibration analysis. Mech Syst Signal Process 42(1):377–387
9. McInerny SA, Dai Y (2003) Basic vibration signal processing for bearing fault detection. IEEE Trans Educ 149–156

10. Nandi S, Toliyat HA, Li X (2005) Condition monitoring and fault diagnosis of electrical motors—a review. IEEE Trans Energy Convers 719–729
11. Bergasa LM, Nuevo J, Sotelo MA, Barea R, Lopez ME (2006) Real-time system for monitoring driver vigilance. IEEE Trans Intell Transp Syst 63–77
12. Yang W, Tavner PJ, Crabtree CJ, Wilkinson M (2009) Cost-effective condition monitoring for wind turbines. IEEE Trans Ind Electron 263–271
13. Tsypkin M (2017) Induction motor condition monitoring: Vibration analysis technique — diagnosis of electromagnetic anomalies. IEEE AUTOTESTCON 2017, Sept 11–14

Chapter 9
Smart Solar-Powered Smart Agricultural Monitoring System Using Internet of Things Devices

Paras Patel, Anand Kishor, and Gitanjali Mehta

Abstract India is the fastest-growing big financial system in the world, with a massive population, useful demographics, and excessive catch-up potential. In India, agriculture is a primary activity, around two-third of India's population remains dependent upon agriculture. In developing nations, farmers aren't using smart agricultural technique but if they begin the use of smart agricultural technique with the assist of this technique, they can produce good yield crops, wide range of development on the agriculture, and can make superior amount of profit. To reduce long-time expenditure in agriculture, use of renewable energy is important for that smart solar is the primary energy which may be used.

Keywords Smart solar system · GSM module · Internet of things

1 Introduction

India is the speediest growing enormous economy on the planet, with a huge populace, helpful demographics, and excessive catch-up potential. In essential area of economy, exercises are attempted through on double utilizing common assets. Farming, fishing, dairy, and other normal items are alluded to as so in light of the fact that they shape the base of all particular item. Since limit of the characteristic time we get is from farming, dairy, fishing, it is likewise called agriculture and unified area [1–3]. Agriculture plays a fundamental capacity inside the Indian monetary framework. More than 70% of the rustic families rely on farming. Agriculture is a significant

P. Patel · A. Kishor · G. Mehta (✉)
School of Electrical, Electronics and Communication Engineering, Galgotias University, Greater Noida, India
e-mail: gitanjali.iitr@gmail.com

P. Patel
e-mail: patelparas9473714518@gmail.com

A. Kishor
e-mail: anandkishor7747@gmail.com

R. N. Shaw et al. (eds.), *AI and IOT in Renewable Energy*,
Studies in Infrastructure and Control,
https://doi.org/10.1007/978-981-16-1011-0_10

Fig. 1 Smart solar system

area of Indian monetary framework since it makes commitments around 17% and large GDP and gives work to more than 60% of the populace [4–6]. Agriculture is the technology & artwork of cultivation of plants & domestic animal. Farming was the evolution for development of mankind. For example,—Punjab, Haryana, Uttar Pradesh. Figure 1 shows a smart solar system with the following specifications:

- Area—200 square feet
- Cost—2–3 Lakh
- Output—2.5 kw
- Average annual energy output—5000kwh
- Size of solar cell—156 mm by 156 mm
- Diameter—16 feet
- No. of slides—12
- Weight—400–450 kg.

2 Proposed System Design and Working Principle

Present-day farming is another and rising idea utilized in developing the yield of a harvest with the aid of using advanced technology to help in conventional cultivating rehearses. Ideas, for example, exactness in Agriculture (PA), Internet of Things (IoT), Wireless Sensor Networks (WSN), and many other techniques are utilized with conventional framing to help in the profit of harvests, growing efficiency, and controlling of expenses. The purpose of the execution is to exhibit the smart and brilliant

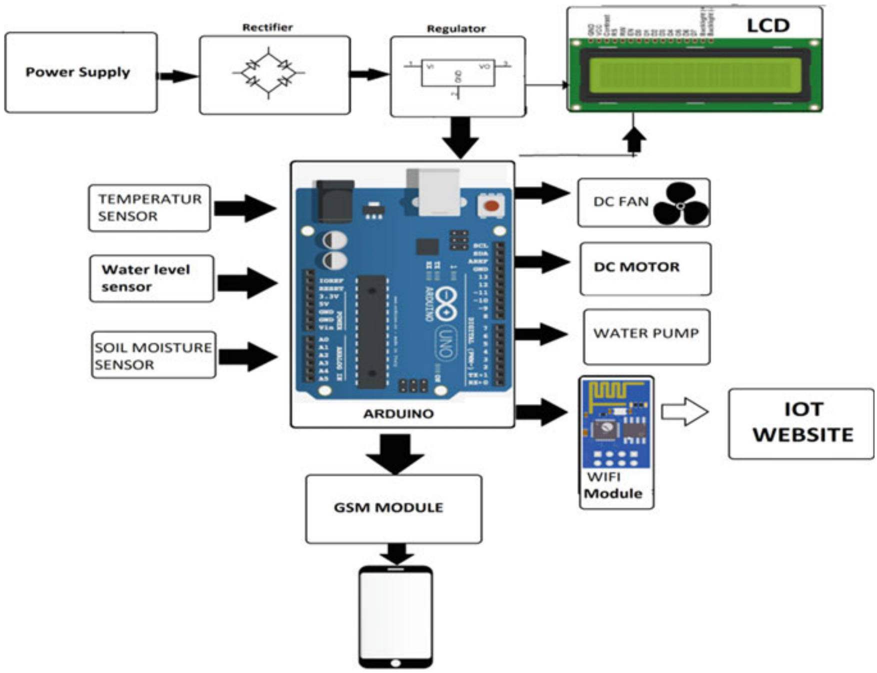

Fig. 2 System design

abilities of the microprocessor to permit the choices to be taken on irrigation of the vegetation, checking the temperature of fields, soil moisture, and many more based on the non-stop tracking of the ecological conditions in the field [7, 8].

Figure 2 shows the designed system. There are many different types of sensors which are used in our system. These sensors are constantly observing the parameters & forward it to the Arduino board for additional handling which goes about as an IoT gateway. "This passage has been given the wireless service by putting in a GSM module which will be updating the records to the cloud". With the help of GSM module, we can also able to operate our device over 2G and 4G networks.

The frameworks have been diverse in that the sensor hubs planned, utilized explicit detecting units for tracking surroundings. In sensor hubs comprised of soil wetness, temperature, air humidity, and laser sensors. In sensor hubs, the best effective is to acquire a soil wetness sensor. In most of the gadget planned, hubs didn't contain any energy gathering gadgets, and as such could best effective capacity for a specific time period earlier than the hub's energy flexibility could need to be supplanted. In this work, we expand on top of these recently published works, and furthermore exploit the segments that take lead of the element present in the blueprint of a remote IoT organization [9, 10].

Sensors networks have been geared up with photovoltaic panels for power harvest to be able to rise the overall run-time of the network. When sensor information was

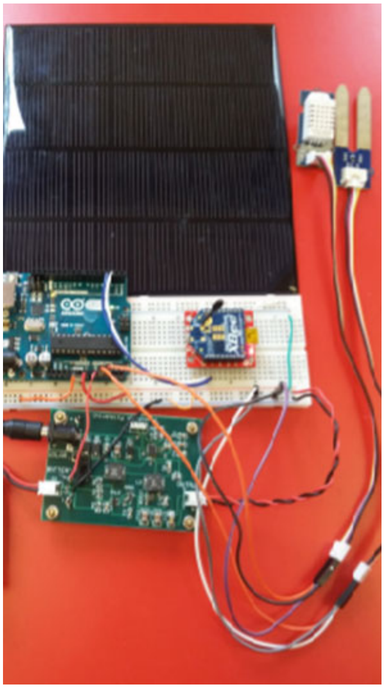

Fig. 3 Assembled system with components

estimated and conveyed to the objective, time stamps were set on the bundles and stock, which would then be able to be explored later to decide any potential activities that are expected to additional consideration of the yields [11, 12]. Figure 3 shows the assembled system with different components.

3 Sensor Description

To gauge the particular ecological conditions needed in an agricultural positioning framework, two kinds of sensors have been used:

(1) **Soil wetness sensors**

The Grove Soil Wetness Sensor is fit for estimating the dampness content material inside the soil. This sensor was chosen as it can properly check the volumetrically water contendent material inside the dirt in a roundabout way by utilizing the electrical obstruction among the two pushes. This is helpful in rural frameworks, for the explanation that through realizing the dampness levels inside the dirt, fields could best need to be flooded when needed and will restrict the expansion of microorganisms [2]. Figure 4 shows the assembled soil moisture sensors with equipment.

(2) **Humidity and Temperature sensors**

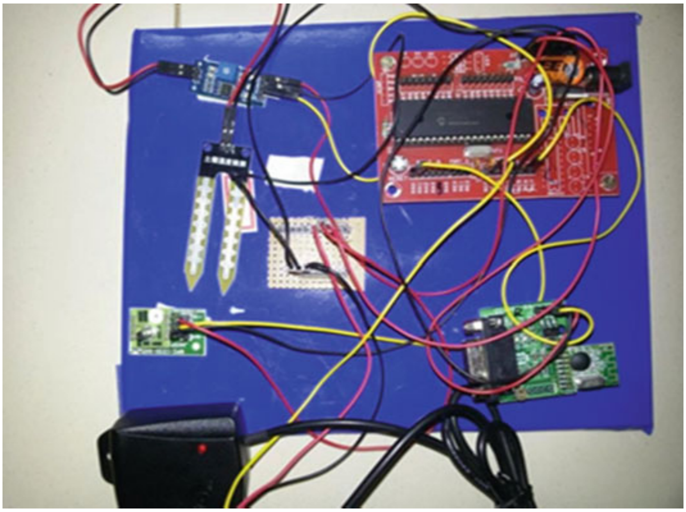

Fig. 4 Assembled soil moisture sensors with other equipment

Figure 5 shows the assembled humidity and temperature sensor. Temperature and mositure sensor can estimate the natural data with skimming point precision, up to 0.4° for temperature and 2% for comparable dampness. This sensor was chosen as most extreme harvests will create the best yield while the temperature and dampness are inside an ideal range. These estimations end up being fundamental in nurseries as

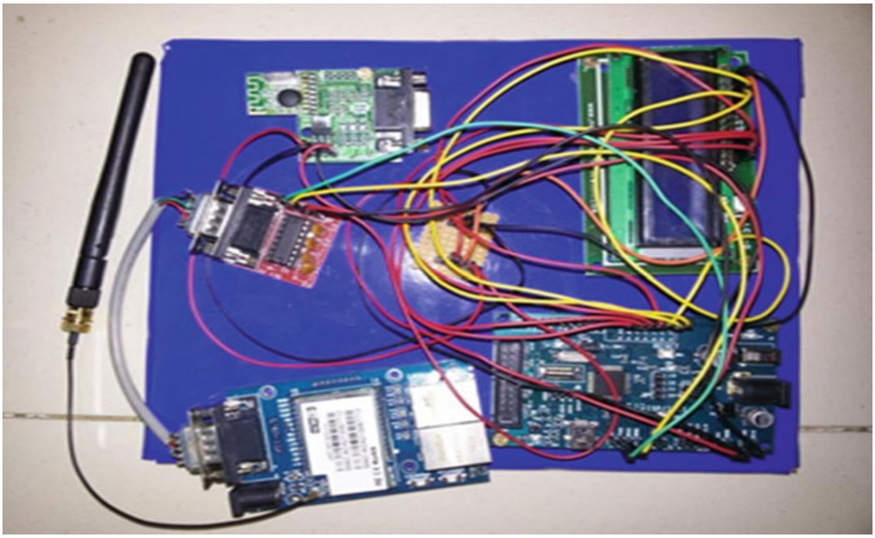

Fig. 5 Assembled humidity and temperature sensor

Fig. 6 Connected router with model

open-air circumstances can altogether influence those inside the nursery. The ability to control the circumstances can altogether help with inside the improvement of the plants itself as most required definite temperature and mugginess stages at some point of the different levels of growth [3–14]. Figure 6 shows the connected router with model.

(3) **Obstacle sensor**

This sensor can work at the standard of sound waves and their appearance property. It has two sections such as supersonic transmitter and supersonic recipient. Transmitter communicates the 40 kHz sound wave and, on its gathering, it imparts the electric sign to the miniature regulators. The speed of sound in air is now known.

Subsequently from time needed to get again the sent sound wave, the hole of hindrance is determined. Here, it is utilized for impediment location if there should be an occurrence of cell robot and as a development finder in product habitation for halting burglaries. The supersonic sensor permits the robot to find and avoid hindrances and furthermore to gauge the hole from the deterrent. The scope of activity of supersonic sensor is 10–30 cm.

4 Software Used

(1) Arduino IDE

When operating with the InduinoR3 Board, select the board as Arduino UNO from the Tools Boards sequence and choose the Appropriate Com Port.

(2) AVR Studio Version 4

It is utilized to compose, manufacture, compile, and troubleshoot the implanted C program codes that have been consumed in the miniature regulator to have the option to perform wanted tasks. This software program promptly gives.hex file that can be effortlessly consumed into the miniature regulator.

Proteus 8 Simulator

Proteus 8 is single of the extraordinary reenactment programming program for different circuit designs of miniature regulator. It has virtually all miniature regulators and computerized segments that are promptly accessible in it and along these lines it far generally utilized test system. It might be utilized to check program and embedded drawing for gadgets before genuine equipment examination. The simulation of programming of micro-controller likewise can be completed in Proteus. Simulation avoids the opportunity of harming apparatus because of inaccurate plan. Figure 7 shows the program codes.

The advantages and disadvantages of the proposed system are as

Advantages

- Actual-Time Data & Productivity Insight
- Low Operation Expenses
- Increased Quality of Productivity
- Accurate Farming and Field Rating
- Third eye Monitoring
- Water Conservation
- Increasing renewable energy.

Disadvantages

- The Cost Involved in Smart Agriculture
- There could be wrong Analysis of Weather Conditions
- Reliability
- Increased channel maintenance.

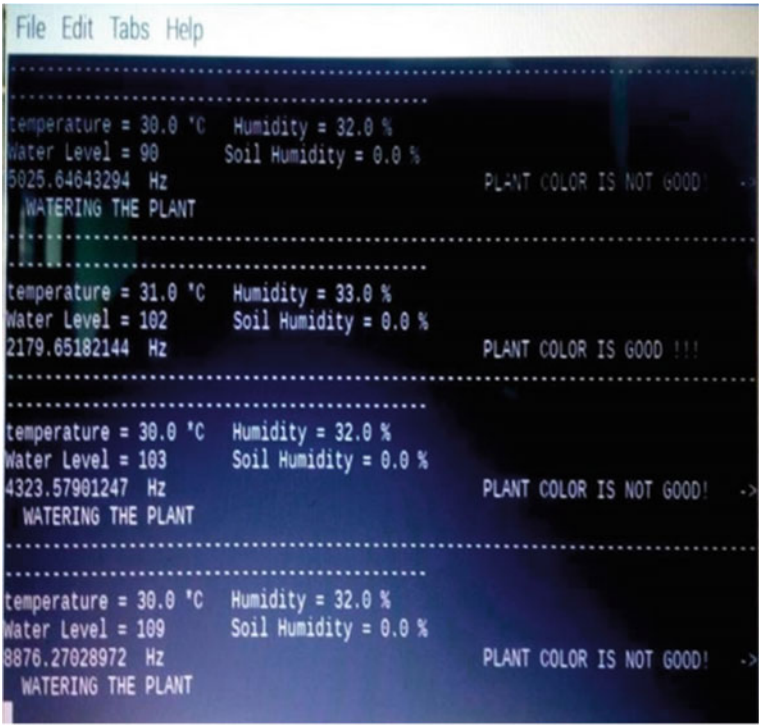

Fig. 7 Program codes

5 Conclusions

Smart Agricultural Field observing framework can assume a significant function in Agricultural countries. Through this framework, soil condition can be monitored. This framework can assist with continuing cultivation and accurately. This framework forestalls the misuse of water. Some more sensors with more information investigation should be possible as future work of this chapter. IoT sensors have high efficiency and accuracy, so it is easy to obtain the direct data of ground wateriness and warmth in agriculture field. The water stages indicator is used, so prevents the waste of water and saves water; it helps the farmers to expand their production. By forcing this framework, farming, plant lands, parks, gardens, golf courses can be irrigated. Thus, this device is more affordable and proficient when contrasted with various types of mechanization gadget. In huge scope applications, high sensitivity sensors can be applied for huge regions of agricultural grounds.

References

1. Navulur S, Giri Prasad MN (2017) Agricultural management through wireless sensors and Internet of Things. Int J Elect Comput Eng 7, 3492–3499
2. Zhang L, Dabipi IK, Brown WL (2018) Internet of things applications for agriculture. In: Internet of things A to Z: technologies and applications
3. Khanna A, Kaur S (2019) Evolution of internet of things (IoT) and its significant impact in the field of precision agriculture. Comput Electron Agricult 157:218–231
4. Tzounis A, Katsoulas N, Bartzanas T, Kittas C Internet of things in agriculture recent advances and future challenges. Biosyst Eng 164
5. Chetan Dwarkani M, Ganesh Ram R, Jagannathan S, Priyatharshini R (2015) Smart agriculture system using sensors for agricultural task automation. In: 2015 IEEE international conference on technological innovations in ICT for agriculture and rural development (TIAR 2015)
6. Dhanasekar N, Kayalvizhi R Accidental navigation and rescue system using GSM and GPS technology. Asian J Res Soc Sci HumIties 6(11):158–166
7. G. Mehta, G. Mittra and V. K. Yadav, "Application of IoT to optimize Data Center operations," in proceedings of International Conference on Computing, Power And Communication Technologies 2018, Greater Noida, pp. 738–742.
8. Shaw RN, Walde P, Ghosh A (2020) IOT based MPPT for performance improvement of solar PV arrays operating under partial shade dispersion. In: 2020 IEEE 9th power India international conference (PIICON), SONEPAT, India, pp 1–4. https://doi.org/10.1109/PIICON49524.2020.9112952
9. Lalitha CVNS, Aditya M, Panda M (2019) Smart irrigation alert system usingmultihop wireless local area networks. In: International Conference on Inventive Computation Technologies. Springer, Cham
10. Garg H, Dave M (2019) Securing IoT devices and securely connecting the dots using REST API and middle-ware. In: 2019 4th international conference on internet of things: smart innovation and usages (IoT-SIU). IEEE
11. Fox J, Donnellan A, Doumen L (2019) The deployment of an IoT network infrastructure, as a localised regional service. In: 2019 IEEE 5th world forum on internet of things (WF-IoT). IEEE
12. Navulur S, Giri Prasad MN (2017) Agricultural management through wireless sensors and internet of things. Int J Elect Comput Eng 7, 3492–3499
13. Tzounis A, Katsoulas N, Bartzanas T, Kittas C (2017) Internet of things in agriculture recent advances and future challenges. Biosyst Eng 164:31–48
14. Sadowski S, Spachos P (2018) Solar-powered smart agricultural monitoring system using internet of things devices. In: 2018 IEEE 9th annual information technology, electronics and mobile communication conferenc (IEMCON)